Generation of Downstream Vorticity Through the Use of Modified Trailing Edge Configurations

Benjamin Worrall

Thesis submitted to the faculty of the Virginia Polytechnic Institute and State University in partial fulfillment of the requirements for the degree of

Master of Science
In
Aerospace Engineering

Committee Members:
William Devenport, chair
Aurelien Borgoltz
Ricardo Burdisso
Trevor Wood

5 May 2010
Blacksburg, Virginia

Keywords: Trailing Edges, Vortex Generators, Vorticity, Cascade

Generation of Downstream Vorticity Through the Use of Modified Trailing Edge Configurations

Benjamin Worrall

ABSTRACT

Detailed measurements were taken downstream of several modified trailing edge configurations designed to impart streamwise velocity into the flow behind a cascade of GE Rotor B fan blades. These measurements were conducted in the Virginia Tech Low Speed Linear Cascade wind tunnel. The trailing edge configurations tested utilized passive techniques for producing streamwise vorticity, which in turn causes downstream wake diffusion and increased mixing. A more diffuse wake, when it impinges on the downstream stator, will produce lower noise levels as a result of this rotor-stator interaction. Furthermore, increased mixing in the flow will reduce the levels of turbulence kinetic energy observed downstream of the blade trailing edge. Thus, this project seeks to identify which passive techniques of imparting streamwise vorticity are most effective at improving the flow characteristics responsible for some of the noise production in modern jet aircraft.

The three trailing edge configurations tested in detail for this project showed significant ability to widen and stretch the downstream wake by utilizing vorticity generation techniques. The TE-8 configuration was the most effective at increasing the wake width downstream of the trailing edge. Additionally, each configuration was able to successfully reduce some of the turbulence kinetic energy levels observed downstream when compared to the baseline blade, the most effective configuration being TE-8. Finally, the momentum thickness of each configuration was measured. When compared to the baseline, the TE-1 configuration showed an increased momentum thickness, TE-8 showed little change, and TE-7 actually showed an improved momentum thickness value.

Acknowledgements

This project was made possible through the generous support of GE Global Research. On that topic, I would specifically like to thank Trevor Wood for all of the work, guidance, and effort he put into ensuring that this project was a success.

I would also like to thank everyone in the Lab 7 group. Most importantly, I want to thank my advisor Dr. William Devenport for all of the help and motivation he gave throughout my time working on this project at Virginia Tech. Without his mentoring and guidance, I wouldn't have been able to accomplish everything I needed. Also, I'd like to thank Dr. Aurelien Borgoltz for all of his help throughout this project. Aurelien was always there to show how to use the equipment, help with setup, and anything else that I needed help. He was a fantastic asset to the successful completion of this project. Matt, Ryan, Nathan, Jon, and Rachel – thanks for keeping the lab fun.

To my committee members: thanks for all of the support in completing my project, and the valuable feedback that you provided. I appreciate your focus on ensuring I have a successful and informative final product for my thesis.

Finally, I'd like to thank my family for their support in everything I do. I would also like to thank The U.S. Air Force for providing me with a fantastic opportunity to pursue my Master's degree, but the views expressed in this article are those of the author and do not reflect the official policy or position of the United States Air Force, Department of Defense, or the U.S. Government.

Table of Contents

List of Figures

List of Tables

1 Introduction

1.1 Project Motivation

In modern jet engines, the interaction between the rotor and stator components is a significant cause of both tonal and broadband noise. When the fan blade interacts with the incoming airflow, a wake is produced that propagates downstream of the trailing edge. It is this wake that, when it impinges on the downstream stator, produces a significant portion of the noise generated in jet engines. The wake produced by the upstream rotor produces downstream turbulence, which in turn causes the production of unsteady lift on the downstream stator. This unsteady lift creates random lift fluctuations on the stator vanes. Additionally, any periodic variations in the flow result in the production of tonal noise as the wake collides with the downstream stator.

An extremely promising method for reducing this rotor-stator interaction noise is to diffuse the wake produced by the upstream rotor. As it diffuses downstream, the wake mixes with the freestream flow resulting in lower turbulence levels as it interacts with the stator. Thus, diffusion causes the wake velocity deficits and turbulence levels seen by the stator to be reduced, resulting in lower sound levels. Previous research has identified several means by which this wake diffusion can be obtained, and has shown promise for generating enhanced flow mixing and reduced rotor-stator interaction noise.

One of the most effective methods of diffusing the downstream wake involves the introduction of the mass flow at the trailing edge of a fan blade through the use of trailing edge blowing, which reduces the wake deficit produced by the upstream rotor. This active method of controlling the wake behind an airfoil not only shows potential for reducing the momentum thickness and wake depth, but also decreases peak unsteadiness in the trailing edge flow. This benefits not only the performance of the fan blade airfoil, but also has potential to decrease both tonal and broadband noise produced by the airfoil and wake-stator interaction. In his Master's thesis, Sell (1997) studied the effects of mass modification on the wake of a first-stage fan rotor in a linear cascade wind tunnel. Measurements were taken at low speed, and each of the fan blades were outfitted with a slot capable of producing both blowing and suction immediately at the trailing edge of the blade. Sell's research showed that mass addition at the trailing edge was the best method for reducing the wake, and he produced results indicating momentum thickness was reduced by 100%, wake depth by 67%, wake width by 6.85%, and peak unsteadiness by 44.5% when mass was injected with 1.08% rate of fan flow through.

The concept of trailing edge blowing has also been investigated more in depth as a means for minimizing and controlling the tonal noise interaction between the rotor and stator on a turbofan engine. In a similar fashion as Sell, further research was conducted by Brookfield (1998) regarding the specific wake harmonic reductions capable through trailing edge blowing. For this research, air was injected at the trailing edge of a high-bypass ration fan stage ($1/6^{th}$ scale) with mass flow rates between 1.8% to 2% of the fan throughflow. Brookfield was able to show that significant wake harmonic amplitude reduction was found at 0.1 and 1.5 chords downstream. This research suggests that controlled blowing can cause significant noise reductions without modifying the existing rotor-stator spacing of the engine. Additionally, work conducted by Craig, 2005 and Borgoltz, 2007 showed that

trailing edge blowing is successful in reducing wake deficit and noise sources with as little as 2% mass flow from the trailing edge.

As well as showing direct acoustic benefits, Brookfield was able to show that wake skew and freestream swirl caused by the blowing mechanism could increase mixing in the wake, making it wider and shallower. This widening and shallowing was observed by Envia (2002), who was able to show in his research, "The viscous wake is essentially filled at a blowing rate of 1.8% of the fan mass flow rate." Additionally, Envia was able to show that at the 2^{nd} and 3^{rd} harmonics, blowing showed a significant impact at reducing the rotor-stator interaction modes and showed significant tonal reductions as a result of filling the viscous wake behind the rotor.

In addition to tone noise, the broadband noise resulting from the rotor-stator interaction was investigated more thoroughly by Sutliff (2005), who was able to show a substantial reduction in the rotor wake turbulent velocity and the stator vane unsteady surface pressures as a result of blowing. The primary noise source from the stator is a result of the unsteady surface pressure that causes unsteady lift on the stator. By using trailing edge blowing flow control, Sutliff was able to show turbulence levels downstream reduce by 25-50%. Thus, with less unsteady lift acting on the stator, the broadband sound pressure level integrated over the stator vane showed a 2-3 dB reduction from the blowing technique.

Despite the successful noise reduction resulting from the use of trailing edge blowing, proper implementation requires a very large amount of engine core flow to be extracted. Clearly, this presents a problem in directly affecting the performance of the engine itself. In order to reduce this penalty, research has been conducted to develop more strategic methods of trailing edge blowing which utilize a smaller mass flow. One such study was conducted by Halasz et al (2005) who adapted the technique using circumferentially varying and alternating methods of blowing. For this test, air was not injected into every fan blade which reduced the total mass flow required from the trailing edge. As expected, the circumferentially varying methods tested provided a lesser amount of noise reduction. As some reductions in the original tones occur, new tones are introduced as a direct result of the alternating blowing configurations. Because this interaction produces a broader noise band as a result of the varying blowing, the tonal spectral shape is modified and expanded, so acoustic liner effectiveness is improved. Thus, Halasz et al (2005) were able to show that this method of circumferentially varying and alternating forcing is effective at increasing the efficiency of trailing edge blowing.

A study conducted by Winkler et al (2009) further identified the introduction of competing sound sources that exist as a result of trailing edge blowing. Their study found that farfield sound was raised at medium to high frequencies as a result of the interaction between the blowing jet and the trailing edge of the blade. As identified before, however, Winkler et al showed significant potential for reducing the wake turbulence kinetic energy from blowing. Therefore, this study showed that trailing edge blowing has competing mechanisms between sound generation from the blowing itself, and sound attenuation from the decreased unsteady lift on the stator. It is also interesting to note that this study showed that trailing edge blowing not only affects the downstream characteristics of the blade, but also causes an *upstream* modification and boundary layer reduction through a changed transition point on the suction side of the blade.

Another method of strategic trailing edge blowing was applied to jet nozzles to attain similar effects. Henderson et al (2005) used a jet $1/9^{th}$ scale core jet with slots cut near the nozzle lip to allow for air injection into the core stream. These slots followed an alternating pattern around the core nozzle. For analyzing the characteristics of these fluidic chevrons, Henderson et al used a 28 element microphone array for acoustic measurements. This study concluded that enhanced mixing can be achieved through fluidic injection; however, although some of the nozzles did improve the mixing, some did elevate high frequency noise as a result of the jet configuration. This research was able to conclude that mimicking alternating chevrons through discrete air injection produced good mixing results and the improved acoustic suppression at aft observation angle. Despite this success, this technique did show an increase in high frequency noise, perhaps as a result of high frequency turbulence that results from the injectors.

This concept of using discrete jets was also researched by Langford et al (2005) by utilizing discrete pressure jets on the suction and pressure surfaces of the blade. By utilizing discrete jets instead of a constant spanwise slot across the trailing edge, Langford et al could effectively reduce the wake deficit with a smaller amount of air. They tested several different configurations, and determined that placing these discrete jets at approximately 80% of the chord seemed to show the best and most efficient wake-filling results. In addition to the wake deficit improvements possible through discrete jets, Langford et al (2005A) analyzed the noise reduction capabilities of discrete surface jets on the fan rotor. They discovered that the best noise reduction was obtained by a non-uniformly filled wake using surface jets. Furthermore, this strategic forcing using surface jets required about half the mass flow as required by complete trailing edge slots, but demonstrated similar noise attenuation. Through their research, Langford et al concluded that perhaps some of the overfilled sections resulting from the discrete jets act as a noise source out of phase with the wake impingement noise, resulting in greater cancellation. Although half the mass flow was necessary for noise attenuation with these discrete jets, the same blowing *momentum* was required to achieve the same attenuation in their studies. This suggests that even strategic methods of momentum injection require significantly large amounts of core flow from the engine.

Although the use of trailing edge blowing has shown tremendous effect in reducing the tonal noise generation resulting from the rotor-stator interaction, this active concept is entirely impractical to implement. In order to achieve the desired results, even while utilizing strategic forcing methods, too much mass flow must be extracted from the engine core flow. To overcome this downfall of trailing edge blowing, it is apparent that passive means of reducing the fan noise must be pursued. One such passive noise control method that has been researched is the utilization of flow techniques to generate enhanced mixing downstream of the trailing edge.

Some of the first steps into this passive means of noise reduction was researched by Weygandt and Mehta (1995) on a split flow wind tunnel. In this configuration, two flow streams are separated by a splitter plate, and then allowed to mix of the trailing edge into one continuous flow. Weygandt and Mehta attached a corrugated extension to the splitter plate trailing edge, which produced a relatively strong array of counter-rotating pairs of streamwise vortices. The wavelength of the corrugation was picked to match the natural streamwise vorticity studied on the flat splitter plate with an unmodified

trailing edge. The injected vorticity produced large spanwise variations in the mean velocity and Reynolds stress contours, even into the farfield. However, the mean streamwise vorticity rapidly dropped off, and was not detectable in the farfield. Additionally, this research concluded that the injected vortices did not spread out spanwise with an increase in streamwise distance like the naturally shed vortices did with an unmodified trailing edge.

Similar research was conducted by Yu et al (1995), but they instead used a lobe shaped mixer with 3 trailing edge configurations (square wave, circular wave, triangular wave) on a split stream tunnel. These lobed trailing edges effectively give out of plane modifications to the trailing edge of the splitter plate. Yu et al concluded that the "enhanced mixing of lobed mixers is believed to be directly attributable to the large mixing scales generated by the streamwise vortices." The out of plane lobes resulted in the near elimination of high turbulence regions beyond 6 wavelengths downstream of all lobed mixers investigated. Moreover, the turbulence showed trends of decay and homogeneity at downstream locations. For 1:1 velocity ratios between the two primary streams, secondary flow strength shed by the lobe was higher for straight parallel walls. This would suggest that for a particular lobed mixer, the strength of vorticity shed was more dependent on geometrical conditions than inflow conditions. This research also identified that the high turbulence kinetic energy produced by square and circular lobes is fundamental in improving mixing downstream of the trailing edge.

The research conducted on the two-stream mixing wind tunnels was further expanded by Yu and Yip (1997) to include three more advanced trailing edge configurations. This research utilized a straight, lobed forced mixer, and scalloped forced mixer. The scalloped forced mixer in this research was essentially designed to allow both upturn and downturn in the flow as it passes the shaped trailing edge. The geometry of the lobes causes large scale streamwise vorticity to shed at the trailing edge, and in the case of the scalloped force mixer this shedding could be seen out of plane with the trailing edge. The scalloped lobes produced the highest streamwise vorticity downstream of the trailing edge, and showed a significantly more rapid decay rate than the other two configurations tested. The scalloped lobes can not only shed a higher strength of streamwise vorticity, it can provide a relatively lower induced drag when compared to lobed or straight trailing edge configurations.

This research on split flow trailing edges can be directly applied to the use on airfoil trailing edges. Some such earlier research was conducted by Howe (1990) who investigated low Mach number turbulent flow over the serrated trailing edge of a flat plate airfoil at no angle of attack. Howe concluded that fluctuating vorticity at the edge of the trailing edge is ultimately responsible for the production of sound, and this fluctuation is generated by boundary layer instability upstream. Howe's initial research concluded that "trailing edge serrations can reduce low Mach number trailing edge noise, provided that the edges are inclined at an angle less than about 45° to the mean flow direction over a significant portion of the edge." Howe was also able to develop an equation for predicting the noise reduction based on the wavelength, frequency, and streamwise length of the chevrons, indicating that the primary mechanism of noise reduction is primarily based upon the geometry of the chevrons. According to FFowcs-Williams and Hall, noise depends on angle of mean flow with the trailing edge; therefore, it can be concluded that a parallel trailing produces no additional noise. Therefore, by

introducing serrations, the effective span of the trailing edge that is perpendicular to the flow can be reduced.

Further research into this phenomenon was presented by Guidati et al (2000), who focused on the noise produced by wind turbine blades. A phased array of microphones was used to conduct some of the trailing edge acoustic testing reviewed in this compilation, which presented some of the major concepts behind the use of trailing edge serrations. The research analyzed in this paper suggests that chevrons should be aligned with the pressure side of the blade in order to achieve the highest noise attenuation. It is also interesting to note another driving mechanism in the sound reduction caused by trailing edge serration. In their research, Doty et al[11] (2004) used particle image velocimetry to measure the flow behind chevrons on the trailing edge of a core nozzle. This research was able to conclude that although chevrons produced a slightly higher turbulence kinetic energy just aft of the nozzle, they showed a quicker dissipation rate with significantly lower turbulence kinetic energy measured further downstream of the nozzle.

In a study conducted by Geiger (2004), the performance and characteristics of trailing edge serrations on fan rotor blades was thoroughly examined. Using Pitot measurements in the wake region, Geiger was able to visualize the individual trailing edge serration tips and valleys effect on the flow field. The chevron geometries examined in this study were able to introduce significant streamwise vorticity into the wake behind the trailing edge. Furthermore, the turbulence kinetic energy downstream of the serrated trailing edges was decreased in comparison to the baseline blades, which should cause a decrease in the unsteady pressures on the stator which is a major contributor to the fan noise.

Despite these successes, however, serrations continue to have significant downfalls. The use of traditional trailing edge serrations, as shown in Geiger (2004), cause significant declines in the performance of the airfoil. Trailing edge serrations result in an increase in the wake deficit behind the airfoil, as well as an increase in the momentum thickness. However, as Geiger's work helps to show, the momentum thickness expected from the geometry of the chevrons used should have been significantly higher than the actual increase in observed momentum thickness. This conclusion suggests that there is perhaps something intrinsic to vortex injection (generated through chevrons in this case) that is beneficial to the flow. Thus, it can be concluded that proper design of vortex injection can significantly decrease the noise produced from a fan blade while minimizing negative effects seen by using chevrons as a means of producing vorticity in the flow.

1.2 Project Objectives

The primary objective of the research completed in this project is to identify and test new passive techniques for diffusing the wake downstream of the blade trailing edges. The principal mechanism utilized to achieve this downstream wake diffusion is the injection of streamwise vorticity into the flow behind the trailing edge. Through proper application of vorticity generation, the wake profile seen by the stator can essentially be widened, which improves the resulting rotor-stator interaction noise.

In addition to wake spreading, introduction of streamwise vorticity causes the flow behind the trailing edge of the upstream rotor to more rapidly mix with the freestream. In turn, this causes reduced variations and turbulence levels at the site of the downstream stator. Thus, the second primary

objective of the research conducted in this project is to develop trailing edge configurations which effectively reduce the levels of turbulence kinetic energy downstream of the rotor blades.

Finally, the secondary objective of this project is to determine and changes in rotor blade performance that might result from the modified trailing edge configurations tested. It is desirable to achieve both primary objectives of wake diffusion and turbulence reduction without producing negative impacts on the blades performance. The measure of success for this objective will be the momentum thickness curves that result from each trailing edge configuration tested. By seeking negligible change in momentum thickness across the blade, the overall aerodynamic performance of each trailing edge configuration can be compared.

2 Apparatus and Instrumentation

2.1 Cascade Tunnel

For the completion of this research, the Virginia Tech Low-Speed Linear Cascade wind tunnel was used exclusively. This facility is able to replicate the principle flow characteristics found in the rotating reference frame of a typical low speed compressor blade, in a linear setting. The following section identifies in detail the specifics of this cascade tunnel that allow for proper analysis of the research conducted for this project. The general configuration of the tunnel, which is explained in further detail, can be seen in Figure 2.1.

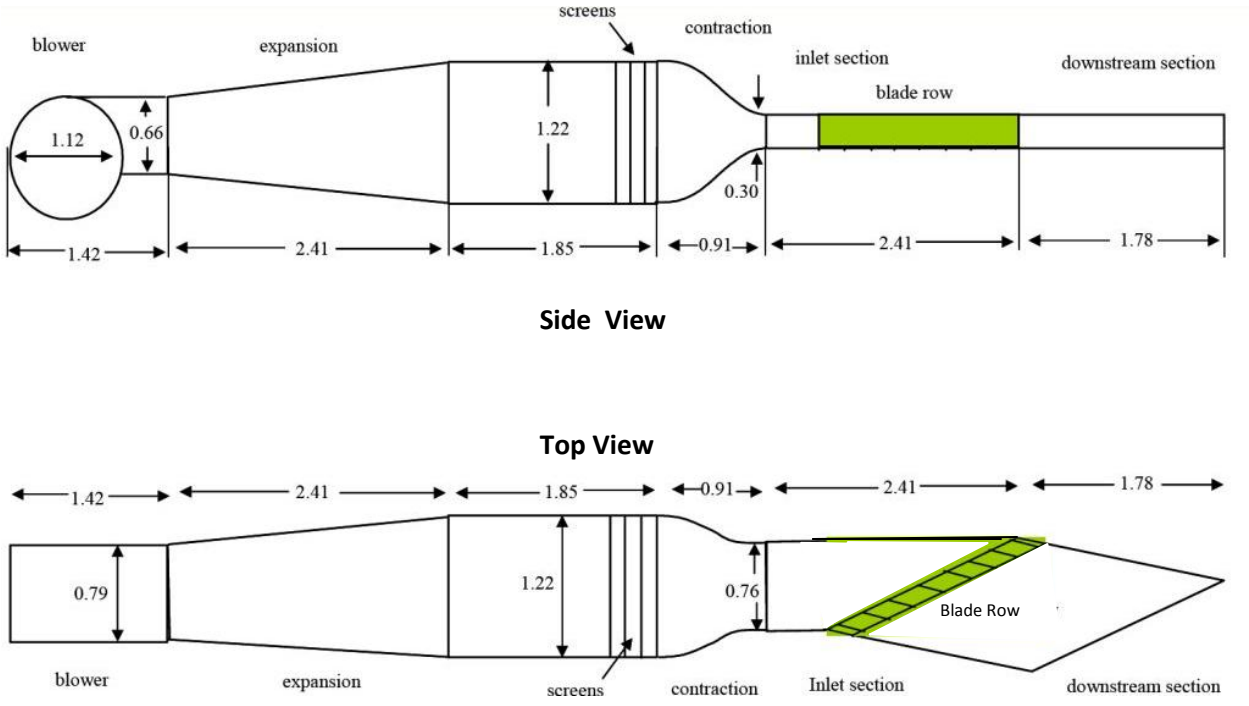

Figure 2.1 Layout of the Virginia Tech Low-Speed Linear Cascade Wind Tunnel (Dimensions in meters). From Borgoltz 2007

2.1.1 Upstream Configuration

In the upstream section of the cascade wind tunnel, the flow is supplied by means of a 15 horsepower AC motor attached to a centrifugal fan. The exit area of the fan blower is measured at 0.521 m^2. After exiting the blower, the diffuser section slows the flow by means of a 1:2.86 expansion ratio. The flow is then conditioned by a series of screens designed to reduce the turbulence levels of the flow. Finally, a 2-dimensional rectangular contraction accelerates the flow to conditions necessary for proper testing by utilizing a 6.43:1 contraction ratio over this section which is 0.91 meters long.

2.1.2 Test Section Configuration

The test section of the linear cascade consists of three primary components in order to ensure proper flow characteristics for measurements and analysis. The first of these three sections is the inlet, which performs additional flow conditioning and boundary layer control; the next is the blade row,

where the actual testing and measurement takes place; and the final component is the downstream section, which must be adjusted to ensure blade-to-blade periodicity across the entire blade row. The test section configuration can be seen in Figure 2.2.

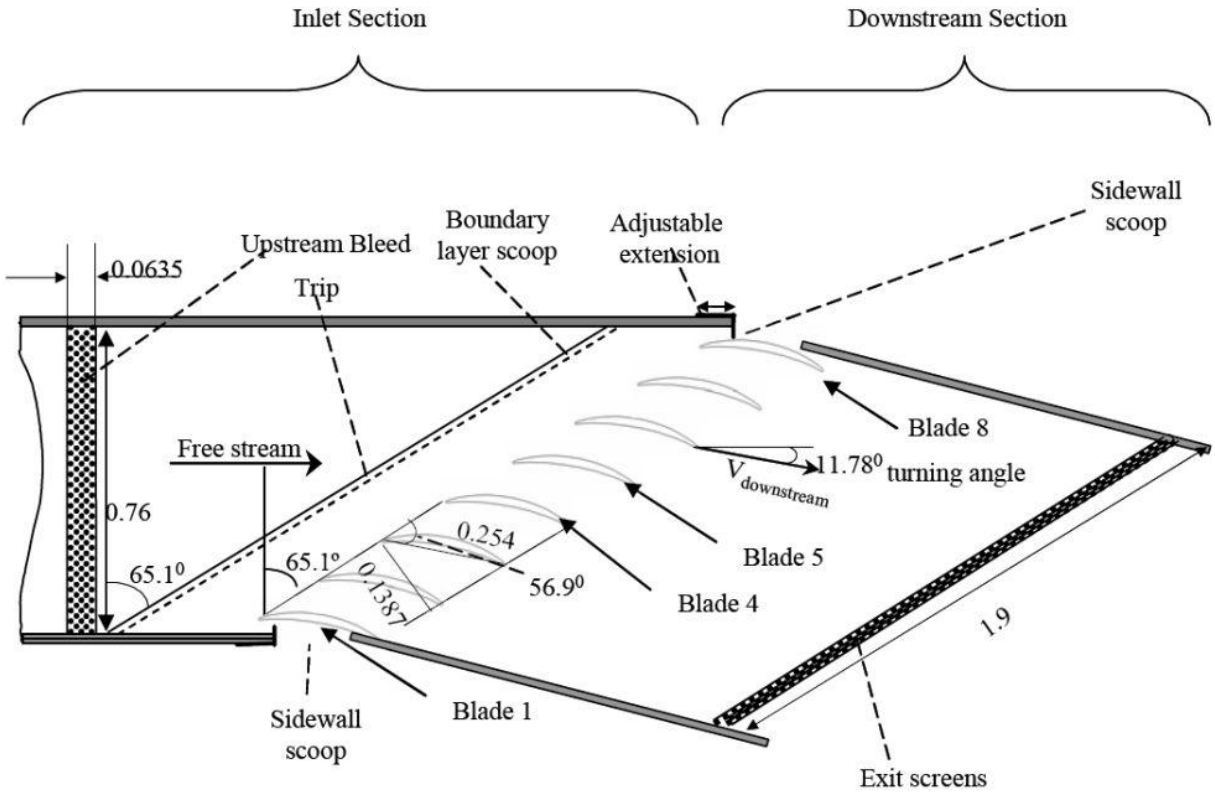

Figure 2.2 Top View of the Virginia Tech Linear Cascade Wind Tunnel Test Section (Dimensions in meters). From Borgoltz 2007.

2.1.2.1 Test Section Inlet Configuration

Prior to entering the blade row, the inlet section further conditions the incoming flow. After the contraction, the flow enters the inlet section through a rectangular area that is 0.305m in height and 0.762m in width. This rectangular cross section has constant dimensions prior to entering the blade row section. The leading edge of the blade row section has an angle of 65.1° measured normal to the free stream direction (Figure 2.2). This blade staggering is required to replicate the rotating reference frame of an axial compressor in a stationary frame. As a result, the inlet test section consists of a short-wall measured at 0.85m and a long-wall measured at 1.81m.

As the flow exits the inlet section, further conditioning takes place by means of the 25.4mm high boundary layer scoops. These flow conditioners are positioned parallel to the leading edges of the blade row, and are located on both the test section floor and ceiling. These boundary layer scoops are designed to ensure a thin, uniform boundary layer with a thickness of approximately 15mm at the leading edge of the blade row. The specific configuration of the boundary layer bleed sections is shown in Figure 2.3.

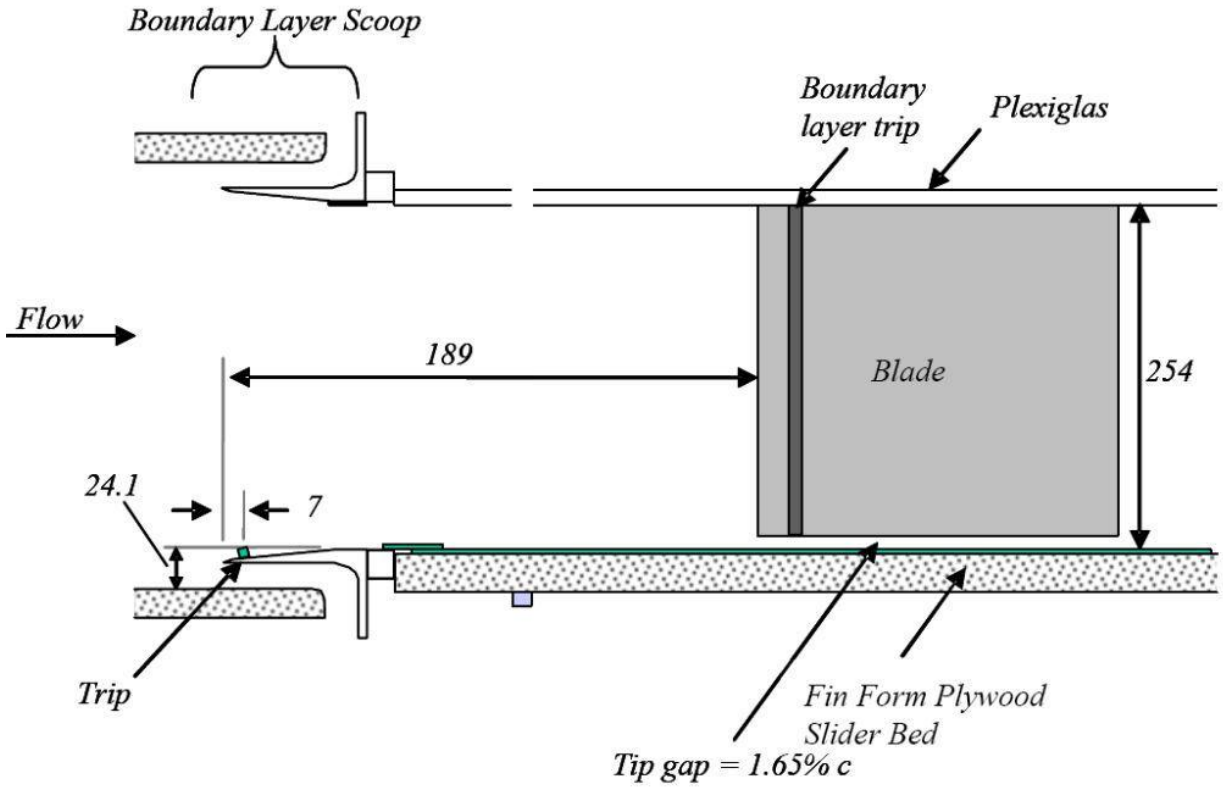

Figure 2.3 Side View Cross-section of the Boundary Layer Scoops and Blade Row. (Dimensions in mm). From Borgoltz 2007.

As identified in Muthanna (2002), the height of the boundary layer was estimated using a 1/7 velocity distribution, and the boundary layer scoops were designed accordingly. As a further insurance that the entire boundary layer was removed from both the floor and ceiling of the test section, metal scoops are installed which allow adjustment to the amount of air that is bled from the incoming flow. As a result of the boundary layer removal, the incoming flow sees a sudden change in the cross sectional area. In order to ensure uniform flow as a result of this occurrence, the test section is reduced in height to 254 mm. To further condition the flow, a boundary layer bleed is located 48.3 cm downstream of the contraction exit. This upstream bleed section on the floor of the inlet consists of a sheet of perforated steel 76.2 cm wide and 6.35 cm long.

2.1.2.2 Blade Row Configuration

The Virginia Tech Linear Cascade wind tunnel has a total of 8 blades with 7 passages in a blow-down configuration, which is detailed in Geiger (2005), Intaratep (2006), and Borgoltz (2007). A study conducted by Moore *et al* (1996) concluded that a linear cascade configuration with 5 or more passages is necessary to simulate an infinite cascade. Thus, the Virginia Tech facility is an adequate representation of an infinite cascade.

Each airfoil in the blade row is spaced 23.6cm apart from the adjacent airfoil, measured at the leading edge. In order to properly simulate the rotating reference frame of an axial compressor, each blade is staggered at an angle of 56.9 degrees and has an inlet angle of 65.1 degrees,as seen in Figure 2.2. A boundary layer trip strip with a width of 6.35mm is applied to each blade at a distance of 2.54 cm

from the leading edge. The trip strip was manufactured using 0.5mm diameter glass beads on an adhesive surface.

On the outside of the blade row, side scoops form the intersection between the blade surface and the walls of the test section inlet. These side scoops are another means by which the boundary layer is conditioned prior to the test section blade row, and help ensure blade-to-blade periodicity and uniformity. The side scoop of the long-wall side can be seen in Figure 2.4.

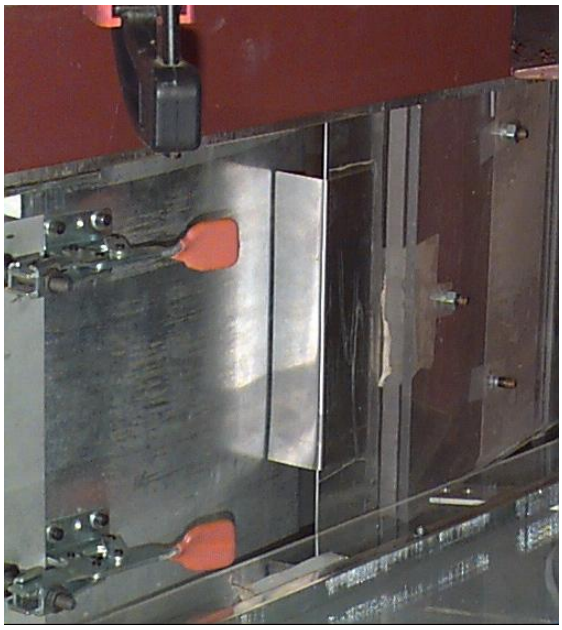

Figure 2.4 Side Scoop at the Long-Wall and Blade 8 Intersection

The entire blade row is attached to an aluminum superstructure that is fixed above the test section. The superstructure is designed to allow independent adjustment of pitch and tip gap for each blade in the cascade. In this configuration, the span of the blades inside the test section is maintained at 254mm minus the tip gap setting of 0.165 inches for this configuration. This ensures identical flow conditions across all aspects of the test section. At the ceiling of the test section, each blade has a custom fitted slot which is designed to maintain a 1mm gap around each blade where it passes through the 6.3mm thick Plexiglas ceiling. This blade gap at the ceiling intersection is to ensure consistency with CFD simulations performed by Daniel Tweedt (private communication). The edge spacing is created by using 0.5mm steel skirts with a slightly enlarged Rotor B profile cut-out. These skirts can be removed to ensure proper adjustment of the blades, and the proper edge spacing helps reduce the development of a corner stall at the blade root.

2.1.2.3 Blade Configuration

Each of the eight core compressor blades has a total chord (c) of 25.4 cm, an axial chord (c_a) of 13.89 cm, and an aspect ratio of 1. The spacing between the blades is measured at 23.6 cm along the leading edge line of the blade row. The blades profiles are modeled after the GE Core Compressor Rotor

B blades which comprise of a modified circular arc section with 4% thickness. The specific coordinates and measurements of the GE Rotor B blades used for this researcn are shown in Table 2-1. The x-coordinate is measured in the chordwise direction with its origin at the blade tip, and the y-coordinate is measured perpendicular to x in the pitchwise direction. Despite the fact that these are by definition compressor blades, they are quantitatively comparable to the blade loading characteristics found in a subsonic aircraft engine in takeoff conditions. For further information on this phenomenon, see Muthanna and Devenport (2004).

Table 2-1 GE Rotor B Airfoil Coordinates

Suction Side		**Pressure Side**	
x/c	y/c	x/c	y/c
0	0	0	0
0.00006	-0.00149	0.00044	0.0006
0.00092	-0.00317	0.00141	0.00105
0.0026	-0.00501	0.00293	0.00132
0.00509	-0.00697	0.00497	0.00139
0.00841	-0.00902	0.00752	0.00121
0.01258	-0.0111	0.0106	0.00078
0.0176	-0.01318	0.0142	0.00014
0.02347	-0.01524	0.01905	-0.00075
0.03019	-0.01729	0.02912	-0.00255
0.03775	-0.0194	0.03918	-0.0043
0.04586	-0.02159	0.04923	-0.006
0.09315	-0.03348	0.09696	-0.01342
0.14059	-0.04394	0.14456	-0.01978
0.18816	-0.05303	0.19206	-0.02516
0.23582	-0.06079	0.23947	-0.0296
0.28357	-0.06728	0.28681	-0.03317
0.33139	-0.07255	0.3341	-0.03593
0.37925	-0.07664	0.38136	-0.03793
0.42716	-0.07961	0.42859	-0.03922
0.4751	-0.08149	0.47579	-0.03983
0.52307	-0.08226	0.52298	-0.03975
0.57106	-0.08194	0.57017	-0.03899
0.61906	-0.08049	0.61735	-0.03757
0.6671	-0.07767	0.66452	-0.0356
0.71515	-0.07328	0.71168	-0.033
0.76318	-0.06716	0.75889	-0.0296
0.81113	-0.05916	0.80619	-0.02524
0.85895	-0.04914	0.85365	-0.01977
0.90656	-0.03696	0.90134	-0.01301
0.95391	-0.02246	0.94933	-0.00478
0.96383	-0.01911	0.95946	-0.00284

0.97373	-0.01565	0.96962	-0.00083
0.98361	-0.01207	0.97979	0.00125
0.99348	-0.00839	0.98998	0.00342
0.99644	-0.00726	0.99305	0.00409
0.99947	-0.00467	0.99704	0.00356
1	0	1	0

Blades 4 and 5 of the cascade blade row have been modified to allow for the trailing edge section to be easily interchangeable. In order to achieve this, the baseline blade was cut at the 80% chord line to allow for the last 20% of the blade chord to be replaced with various configurations. The removable trailing edges are affixed to the blade section by means of a hole and pin configuration. Set screws were installed into the main blade section to secure the removable trailing edge during testing, and a sealant was used at the intersection point to assure no flow can pass between the suction and pressure sides of the blade. **Figure 2.5** shows the configuration of the baseline removable trailing edge.

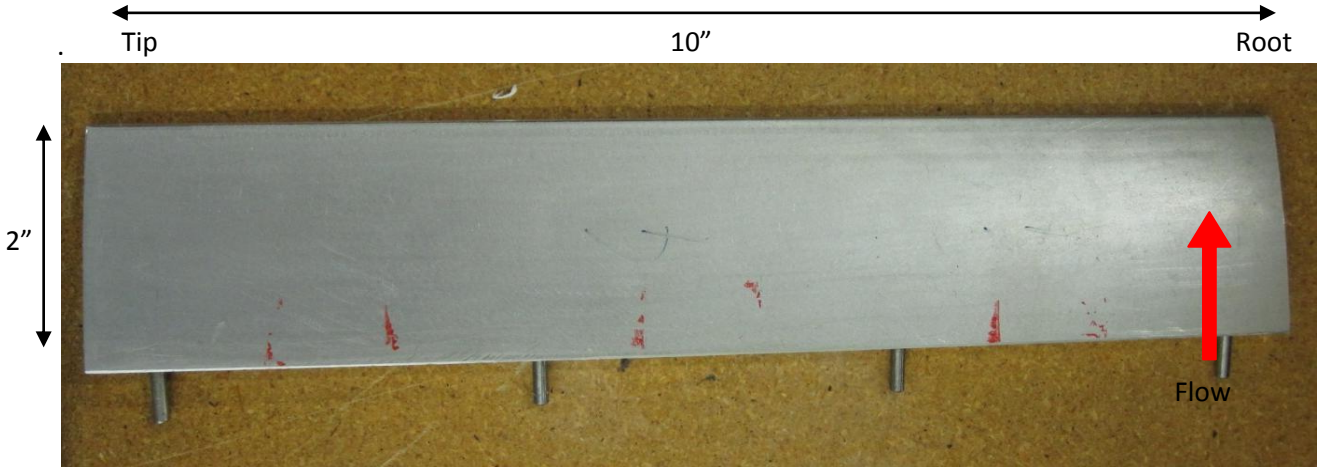

Figure 2.5 Removable Trailing Edge Section of the Baseline Blade (Suction side pictured)

2.1.2.4 Trailing Edge Configurations

Several differing trailing edge configurations were utilized in this study to induce changes to the flow downstream. The non-proprietary trailing edge designs were created by attaching surface mounted delta wing vortex generators directly to the surface of the removable trailing edge. Two sizes of vortex generators were used, the large size measured 10 mm in height, and the small vortex generators measured 6 mm in height. These vortex generators were placed on the trailing edge with an angle of attack of 18 degrees to the freestream flow. The size comparisons of these two surface mounted vortex generators are shown in **Figure 2.6**.

Figure 2.6 Side profile of the large (left) and small (right) surface mounted vortex generators

The first four trailing edge configurations tested are shown below in **Figure 2.7** through **Figure 2.10**. The black arrows in these diagrams indicate the direction of flow over the trailing edge segment. It should be noted that these designs utilized only the large surface mounted vortex generators. Two more trailing edge configurations were tested that were identical to the TE1 and TE2 configurations, but utilized only small surface mounted vortex generators (TE5 and TE6, respectively).

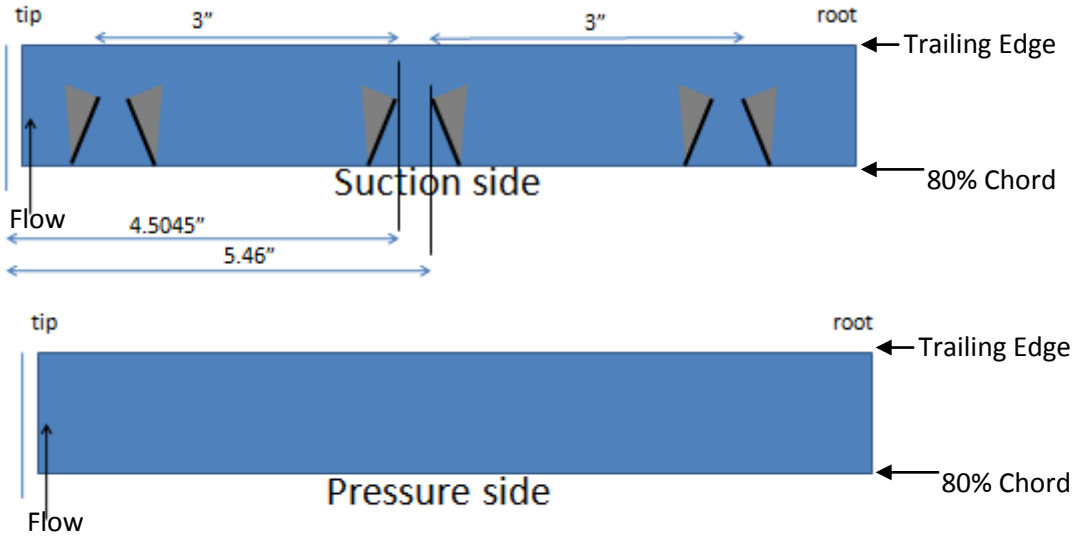

Figure 2.7 Layout of the TE1 Vortex Generator Configuration

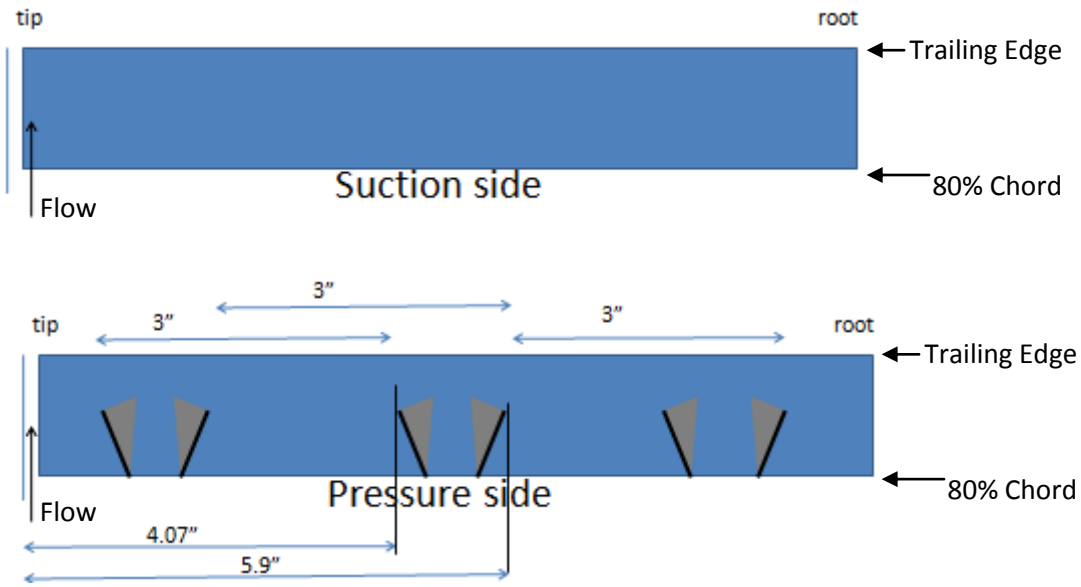

Figure 2.8 Layout of the TE2 Vortex Generator Configuration

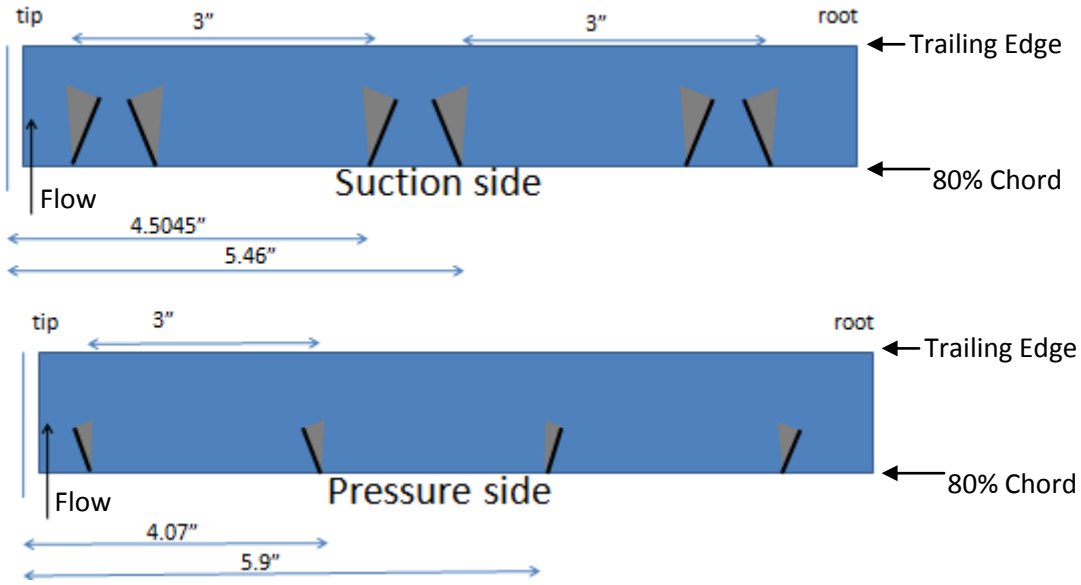

Figure 2.9 Layout of the TE3 Vortex Generator Configuration

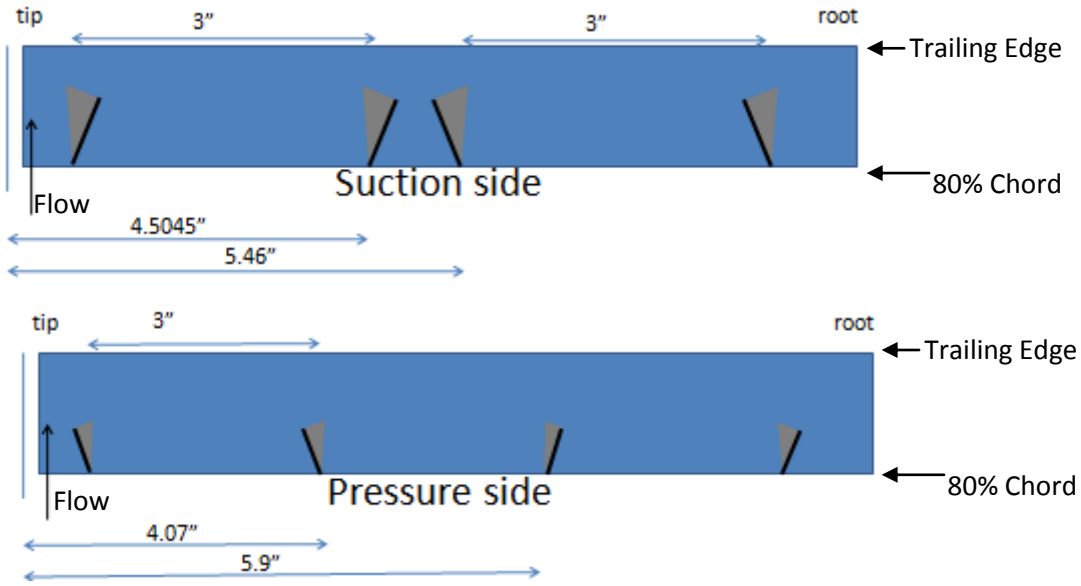

Figure 2.10 Layout of the TE4 Vortex Generator Configuration

2.1.2.5 Downstream Section Configuration

After departing the blade row the flow enters the downstream section of the facility which measures 1.81m wide and maintains a height of 25.4 cm. The walls of this section are parallel to the flow after the turning provided by the blades, as seen in Figure 2.2. These edge walls of the test section are adjustable by hinges attached to blades 1 and 8 of the blade row. Proper adjustment assures that the blades produce the required turning angle of 11.8° without any pressure gradient across the blade row. The individual adjustment of each sidewall is an important part of the tunnel calibration, which is detailed in the following section.

The ceiling of the downstream section consists of two separate parts. The furthest upstream ceiling is manufactured using foam board with a thickness of 6.34mm. The foam ceiling allows for easy modifications to permit full control of the 3-dimensional traverse that is used for wake measurements downstream of the blade row. By using foam board for the section that will be traversed, significant flexibility is allowed due to the fact that new traverse slots can be cut at any point. The ceiling downstream of the foam board traverse section consists of 6.34mm thick Plexiglas.

At the exit of the downstream section, a set of two steel mesh screens are used to ensure proper back pressure of the entire tunnel facility. The mesh used in these screens has a 69.5% open ratio. This mesh, in combination with vertical and horizontal blocking strips (made of adhesive tape), allow for flexibility in adjusting the back pressure of the facility. The back pressure can be monitored using aluminum static pressure ports with a diameter of 0.762 mm which are installed in the floor of the downstream section. These ports are positioned 127mm upstream of the exit plane, and are another important aspect to the facility calibration process identified in the following section.

2.1.3 Linear Cascade Tunnel Coordinate Systems

For the purposes of this project, three different coordinate systems are used to present the data acquired, and can be defined as either flow aligned or cascade aligned. These two classifications define the reference frame used for the system, where cascade aligned is referenced to the blade row, and flow aligned is referenced to the flow direction downstream of the cascade section. A visual depiction of the coordinate systems utilized can be seen in Figure 2.11.

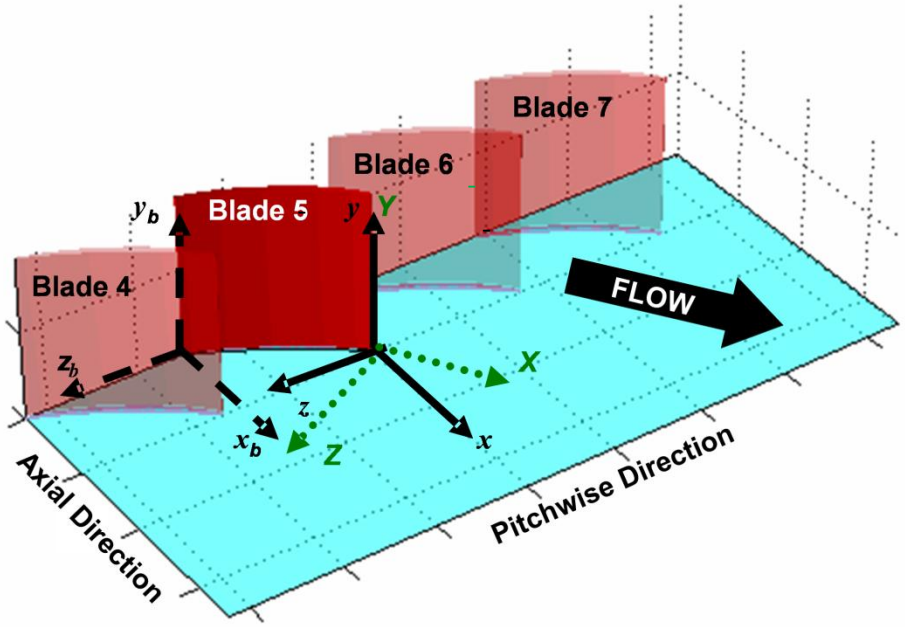

Figure 2.11 Description of the Coordinate Systems Used. From Borgoltz 2007.

The primary coordinates used to present data for this project is the axial-pitchwise cascade aligned coordinate system (seen in solid black in Figure 2.11). This system places the *z*-axis collinear with the line connecting the baseline trailing edges of the blade row. This axis follows the pitchwise direction of the blade row and is referenced to the trailing edge of blade 5. The *x*-axis of this coordinate system is placed perpendicular to the line connecting the baseline trailing edges and is also referenced to the trailing edge of blade 5 at the floor of the test section. Finally, the *y*-axis completes the right-hand-rule and is thus placed parallel to the blade span. This coordinate system is notated through the use of lowercase *x*-, *y*-, and *z*-, and the blade leading edges are located at $x/c_a = -1$.

Another coordinate system used for data presentation is the flow aligned coordinate system shown in green in Figure 2.11. This system aligns the *X*-axis with the spanwise average flow direction behind the trailing edge of the blade row. Based on the configuration of this cascade tunnel, the *X*-axis is inclined 53.3° from the cascade aligned *x*-axis. As with the cascade aligned system, the *Y*-axis of the flow aligned coordinate system is perpendicular to the span of the blades, and the *Z*-axis completes the right hand rule. The flow direction associated with the X-axis is referred to as Streamwise (*U*), and the Y- and Z- flow directions are referred to as Spanwise (*V*) and Lateral (*W*), respectively. Each axis in this

system is referenced to the trailing edge of blade 5 at the floor of the cascade. This coordinate system is notated through the use of uppercase *X*-, *Y*-, and *Z*-.

The final coordinate system used in this study is a variant of the previous cascade aligned system. The axes of this system are identical in direction; however, the reference point has been moved to the leading edge of blade 5. This system of axes is used primarily to present blade loading data. In Figure 2.11, this coordinate system is shown as the dashed axes, and is denoted as x_b, y_b, and z_b. For this system, the leading edge of the blade is located at $x_b = 0$, and the trailing edge is located at $x_b/c_a = 1$.

2.1.4 Linear Cascade Tunnel Calibration

In order to assure optimal flow characteristics inside the test section of the linear cascade tunnel, the entire facility must be calibrated. Adjustments must be made to ensure the following flow conditions:

1. Uniform flow without acceleration or deceleration entering the blade row
2. No pitchwise pressure gradients upstream or downstream of the blade row
3. Constant back pressure throughout the entire configuration
4. Periodic wake deficits downstream of the blade row

When these requirements are met the tunnel is considered calibrated, and for the purpose of this research calibration was measured at the midspan height of the test section (127 mm above the floor of the test section). These measurements were taken using the Pitot-static system and measured on Setra pressure transducers as detailed in the Pitot measurements section of this report. For the downstream measurements, the 3-dimensional traverse was located at a distance of approximately 1.8 axial chords downstream of the trailing edge of the blade row, and traversed pitchwise across the wake between blades 3 and 7 at the mid-span location of the blade. Results from these Pitot-static measurements are reported using the total pressure and static pressure coefficients, which can be calculated as

$$C_{p0} = \frac{(P_0 - P_\infty)}{P_{0\infty} - P_\infty} \quad \textbf{(2-1)}$$

$$C_p = \frac{(P - P_\infty)}{P_{0\infty} - P_\infty} \quad \textbf{(2-2)}$$

where P_0 is the local total pressure, P is the local static pressure, and ∞ denotes the free stream conditions measured upstream of the blade row.

A typical plot verifying tunnel calibration can be seen in Figure 2.12. This specific figure only shows the wake profiles of blades 4 and 5. The data presented in this plot was obtained immediately prior to proceeding with further tests of the cascade tunnel system, and shows tunnel calibration for the measurements to follow in this report The horizontal axis represents the pitchwise location of the probe measured in axial chords, and the vertical axis represents the downstream pressure coefficients C_p and C_{p0} as well as the normalized velocity component U/U_∞, which is calculated as

$$\frac{U}{U_\infty} = \sqrt{C_{p0} - C_p}. \quad \textbf{(2-3)}$$

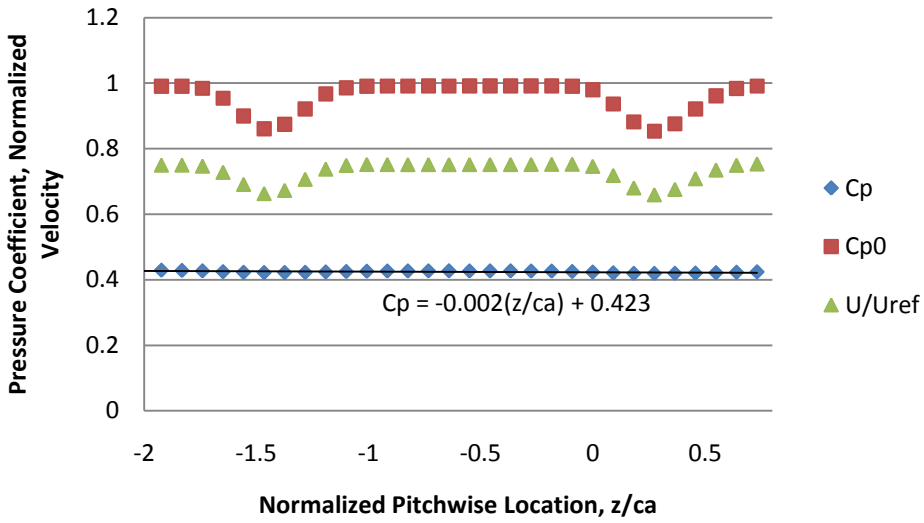

Figure 2.12 Typical Tunnel Calibration Plot across Blades 4 and 5

As shown in Figure 2.12, there is a consistent static pressure coefficient across the entire test section, as identified by the negligible slope in the linear regression equation. Additionally, the average value of the downstream static pressure measurement is $0.423U_{\infty}$, which is consistent with previous calibrations and the values recorded on subsequent tests. It is also important to note that there is a consistent and periodic wake deficit across the test section, which can be seen from the pressure coefficients. Such results indicate proper calibration of the Linear Cascade Tunnel test section, and shows that further testing can continue.

2.2 Measurement and Acquisition Equipment

2.2.1 Hotwire Anemometry Measurements

In order to obtain the 3 velocity components of the wake behind the blades tested, quadwire hotwire anemometry was used. These hotwire anemometers, as well as the data acquisition system used for this research are described in the following sections.

2.2.1.1 Hot-Wire Probe Systems

Three component velocity and turbulence measurements were obtained using four-sensor hotwire probes, manufactured by the Auspex Corporation. Each of these probes consists of two pairs of X-wire arrays situated orthogonally. Each sensor in the X-wire array is made from a tungsten filament with a total diameter of 5 µm, and has a total length of approximately 1mm. Each sensor is inclined at a 45° angle measured from the probe axis (which is aligned with the axial direction of the cascade aligned coordinate system for measurement purposes). The probe configuration is presented in Figure 2.13. These hotwire probes were connected to the traverse system using an adjustable probe stem. These stems afforded adjustment in the axial direction, and allowed for rotation about the z-axis of the traverse.

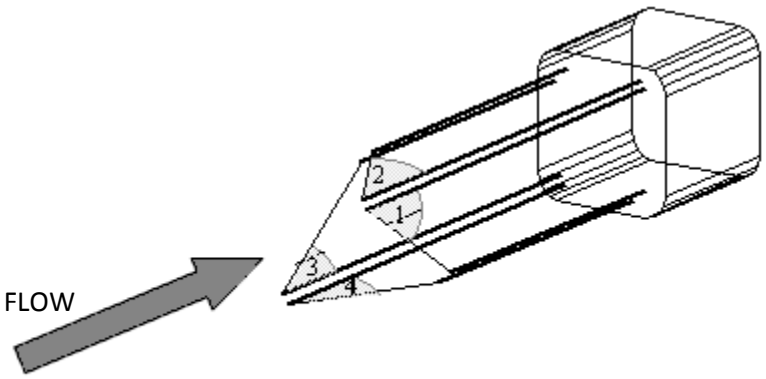

Figure 2.13 Quadwire Hotwire Probe Diagram. From Devenport, private communication.

2.2.1.2 Constant Temperature Anemometer System

The hotwire probes were operated for this research using a Dantec Dynamics StreamLine Constant Temperature Anemometry (CTA) system, model number 90C10. This system was controlled using the Dantec Dynamics Streamware 2.08 software. This StreamLine system utilizes built in signal conditioners to ensure proper frequency response throughout the measurement range. These conditioners consist of high-pass filters, low-pass filters, and amplifiers. The overheat ratio used on this system was set to 1.7, and the signal conditioner was controlled to yield the best response, which dictated an output gain of 16 and a DC-offset of 1.5 volts. This system is designed to produce a flat frequency response up to 18kHz, a value which is well above the expected frequencies to be observed in this study. To ensure consistent results in this study, no conditioning was necessary prior to signal acquisition.

2.2.2 Quadwire System Calibration Methods

In order to properly measure the flow, hotwire systems must be calibrated for expected flow conditions. This process was completed by using a controlled open jet tunnel with an external traverse capable of controlling both pitch and yaw of the probe. One source of concern with using hotwire systems is the fact that during use the velocity readings can drift. In order to reduce this error, velocity calibrations were conducted immediately prior and immediately following data acquisition. The measurement signals were then reprocessed to extrapolate between these two calibration points using a software program written by Dr. William Devenport. The calibration method used for this system is based upon the calibration scheme detailed by Wittmer *et al*, 1998.

2.2.2.1 Velocity Calibration

The first step in ensuring proper readings from the hotwire system is to conduct a velocity calibration of each probe. This is completed by subjecting the hotwire probe to a stream of air with a known velocity. This process involves the use of King's law, which relates heat transfer as a function of measured velocity. The probe's longitudinal axis is aligned with the flow direction, and the velocity of this jet is varied to include all of the expected velocity ranges of the measurement. The output voltage

from each sensor is recorded in order to determine the probe's response to a change in velocity. For this study, the sensor output voltages were recorded for velocities ranging from approximately 8m/s to 25 m/s. This range encompasses the typical reference velocity found downstream of the blade row of approximately 18 m/s.

2.2.2.2 Angle Calibration

The next aspect of calibrating quadwire hotwire probes involves determining the probes response to changes in pitch and yaw. For the angle calibration, the probe is placed in the same air jet, but the velocity is held at a constant value (typically the expected mean velocity of the measured flow). Next, a traverse system is used to vary the probe angle in both pitch and yaw, and the corresponding changes in voltage are measured and recorded for each sensor. Angle calibrations of each quadwire probe are significantly less affected by drift, so the angle calibrations only need to be conducted every 3 to 6 months. For this study, the probe was traversed from -45° to 45° in both pitch and yaw while subjected to a flow velocity of approximately 18 m/s (the expected freestream flow velocity downstream of the blade row).

2.2.2.3 Quadwire Velocity Gradient Errors

Previous studies which utilized the Virginia Tech Cascade Wind tunnel and four-sensor hot-wire probe data have shown the existence of errors resulting from the velocity gradients measured across the probes. In theory, the velocity cross-sections produced by the trailing edge configurations should be symmetrical as a result of the construction process used for these designs. After close inspection of the velocity fields, it was determined that large enough pitchwise and spanwise velocity variations were strong enough to produce a noticeable gradient across the measurement volume of the hotwire probe. When two of the opposing sensors on the hotwire probe measure differing velocities, the data acquisition system treats this as a result of a non-existent velocity component, thus producing inaccurate results.

When the data acquisition system observes a velocity gradient across the sensor, it produces a spurious velocity component in the direction normal to the direction of the individual sensor wire. As can be seen in Figure 2.13, opposing sensors (such as 1 and 3), are positioned at right angles to each other. One method to remove the gradient error would be to take a complete second set of data with the probe rolled 180 degrees. This would cause the spurious velocity components to be interpreted exactly opposite by the data acquisition system. However, due to the symmetric nature of the Auspex hotwire probes used for analysis, this error can be corrected more simply by using the expected spanwise symmetry of the blade. If the data obtained is mirrored across a center axis, this creates the same effect as rotating the probe and taking a second set of measurements. This reflection method causes the spurious velocity component to be eliminated, producing more accurate results. Further details of this correction can be found in Borgoltz and Devenport, 2007.

2.2.3 Pitot Static Measurements

Pitot static measurements were used throughout this study to determine the freestream velocity upstream of the blade row, pitchwise wake profiles in the wake of the airfoils, and the calibration profiles (See section 2.1.4).

The inlet freestream velocity was obtained using a standard Airflow Development Systems Pitot-static probe. This probe was located 0.91 meters downstream of the contraction exit and 0.15 meters inboard of the long wall at approximately mid-height of the test section. The pressure data from this probe was measured using a Setra Systems model 261 pressure transducer with a range of 0 to ±2.5 in. of water.

Downstream of the blade row in the measurement section, a Dwyer Instruments model 166-12 Pitot-static probe was utilized. This probe was attached to the 3-D traverse (see section 2.3) to allow for full control over the measurement location. The pressure data was measured from this probe using a Setra Systems model 239 pressure transducer with a range of 0 to 2.5 in. of water.

2.2.4 Surface Pressure Measurements

The blade loadings of the airfoils in the test section were determined using surface pressure measurements by means of static ports drilled on both the suction and pressure sides of the blade. These ports were connected to a pressure scanner using lengths of Tygon tubing. The pressure scanner utilized for this study is an Esterline Netscanner system model 98RK. This system is able to simultaneously measure 16 pressure ports per installed module. For this study a total of three modules were used (model number 9816), each with a range of 10 in. of water. This system has an accuracy of 0.1% of the measurement range.

2.3 Three-Axis Traverse System

To obtain the necessary hotwire and Pitot-static measurements of the wake behind the blades, a computer controlled three-axis traverse system was used. This traverse system is aligned with the cascade blade row, so measurements are made using the primary cascade aligned axis system identified in section 2.1.3. The primary 2-axis traverse rail system allows for movement both pitchwise across the wake and spanwise in the cascade aligned axis system. This 2-axis traverse is mounted to an aluminum I-Beam which is affixed to a secondary traverse system which allows for motion in the axial direction. The complete configuration of the traverse can be seen in **Figure 2.14** and **Figure 2.15**. Each axis of this traverse is powered by Compumotor stepper motors, model S-57-83-MO, which are in turn controlled through corresponding Parker PDX13 single-axis mini-step drives. As a result of the configuration of this traverse, the final resolution is 0.025 mm along any axis.

Figure 2.14 Downstream 2-D traverse for pitchwise and spanwise probe motion

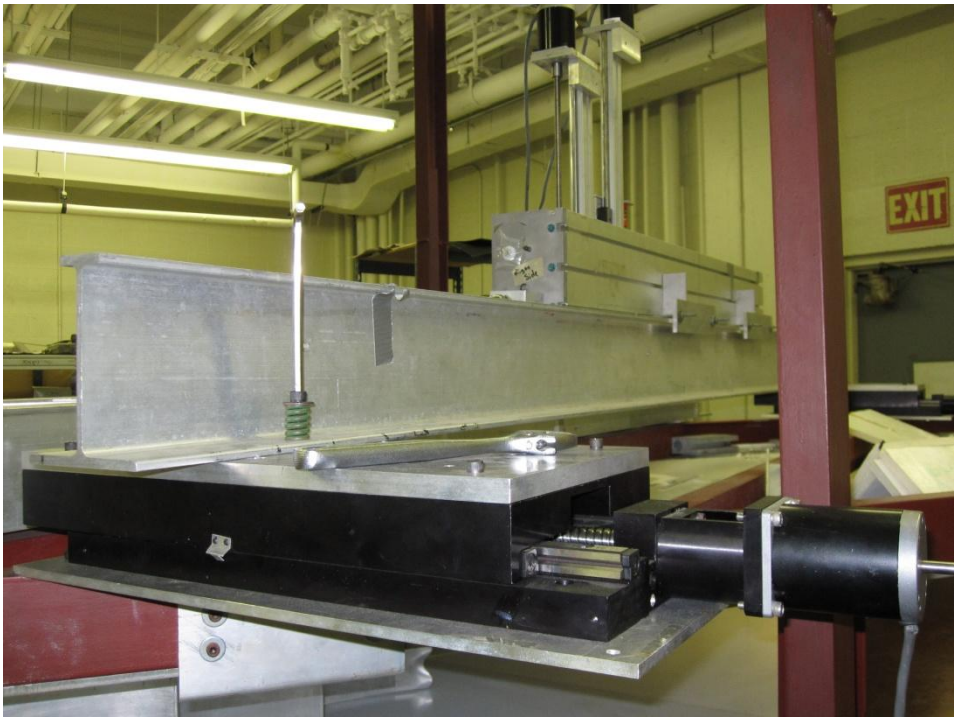

Figure 2.15 Downstream traverse providing motion in the axial direction

3 Results and Discussion

The purpose of this section is to provide the results analysis necessary to understand the flow characteristics resulting from the various methods of vorticity generation implemented for this project. Each subsection will begin with a description of the generation technique analyzed before discussing the results of the tests conducted. This section will begin with an initial analysis of six delta-wing surface mounted vortex generator configurations. Their effectiveness at diffusing the wake will be compared to determine which configuration provides the most substantial wake widening with minimal momentum thickness penalties.

Following this initial analysis, one delta-wing surface mounted vortex generator configuration will be selected for detailed analysis using the four-sensor hotwire anemometry. This configuration will be compared with the detailed analysis of two proprietary trailing edge configurations. These measurement of success for each of these blades will be the amount by which each configuration is able to effectively diffuse the wake by means of wake dispersion. The drag penalties or improvements of each configuration will be tested, as well as the configurations effectiveness at reducing the levels of turbulence kinetic energy downstream to determine which method of wake diffusion is most effective at reducing the overall noise produced by the rotor-stator interaction.

Each vorticity generation technique will be analyzed from data collected primarily from four-sensor hotwire measurements taken in the Low-Speed Linear Cascade Wind Tunnel at Virginia Tech. The inlet freestream was determined using a Pitot-static probe located upstream of the test section as described in Section 2.1.1 of this report. The inlet velocity for each measurement was set to an average velocity of 24.88 m/s, with an uncertainty of ±0.171% of this freestream value. This inlet velocity is referred to as U_∞. Each measurement of velocity is normalized by U_∞ at the time of measurement.

Measurement profiles were taken at several locations downstream of the trailing edge configurations analyzed. The downstream measurement locations are normalized on the axial chord, c_a, of the baseline blade which measures 5.46 inches. The zero reference point for the downstream location is anchored at the cascade-aligned location of the baseline trailing edge. The three-axis traverse system measures data points using the cascade aligned coordinate system. In order to clearly present the data acquired, these measurements are rotated into the flow-aligned coordinate system which aligns the streamwise velocity with the x-axis of the coordinate system. In this flow-aligned coordinate system, the streamwise velocity component is defined as *U*-, the velocity component along the spanwise direction of the blade is the *V* –component, and the *W*- component of velocity completes the right hand rule for this system. Further details of these coordinate systems can be found in Section 2.1.3 of this report.

As previous studies involving the use of trailing edge chevrons have indicated, the presence of streamwise vorticity has significant promise for diffusing the wake by means of enhancing mixing as the flow propagates downstream. Thus, the mean streamwise vorticity was extracted from the four-sensor hotwire measurements taken at each downstream location for each of the vortex generator configurations studied. To ensure consistency, the velocity measurements are normalized on c_a, and the

coordinates are presented in the same fashion as the velocity cross-sections which are normalized on λ_{TE1}, the spanwise period of the placement of the vortex generators.

The data for the streamwise vorticity was extracted directly from the mean velocity field measured by the four-sensor hotwire probe, based upon the equation,

$$\Omega_x = \frac{\delta W}{\delta Y} - \frac{\delta V}{\delta Z}. \quad \textbf{(3-1)}$$

This vorticity field is presented in flow aligned coordinates, so the cascade aligned measurements must be rotated to the flow-aligned direction after the computation takes place. The streamwise gradients in these calculations are assumed to be small, so are neglected in the calculations. To approximate the derivatives, the central difference method combined with the forward and backwards difference methods were used across the range of measurements. This analysis technique was compared with previous data to ensure consistency and validity of the results.

3.1 Baseline Trailing Edge Configuration

To serve as an initial point of comparison for the follow on measurements, specifically those of the surface mounted vortex generators, Pitot-static measurements were taken downstream of the baseline trailing edge configuration. This also had the benefit of verifying the consistency of the data with measurements and results taken from previous studies taken in the Virginia Tech Low-Speed Linear Cascade wind tunnel.

The wake profile seen in **Figure 3.1** is measured from 1.6 axial chords downstream of the trailing edge. The horizontal axis shows the pitchwise location across the wake of the blade. This horizontal axis is centered on the mean wake centerline of the baseline configuration, and is normalized on c_a. The vertical axis of this graph shows the spanwise position, and is also normalized on c_a. The color scale presented on the right hand of the graph shows the normalized velocity contours. As can be seen, the velocity of the potential core, U_{core}, outside of the wake of the blade is 74% of the measured inlet freestream velocity. This indicates a consistent turning angle when compared to previous studies done on the baseline trailing edges. The tip leakage vortex extends from the floor of the test section to a spanwise location 0.5 axial chords. The size of this tip leakage vortex is consistent with previous data (see Geiger 2005) and further verifies proper calibration of the linear cascade tunnel for the remaining measurements.

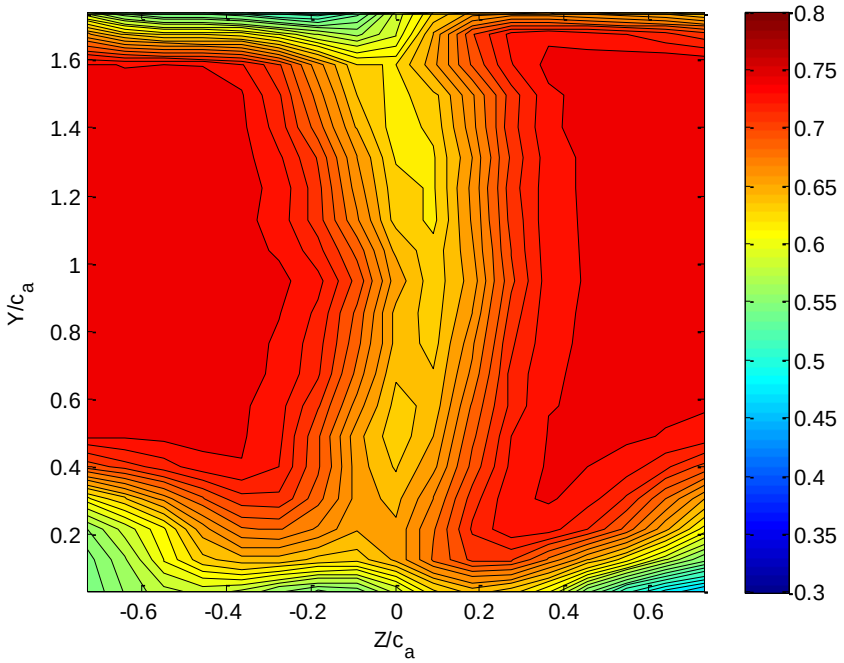

Figure 3.1 Normalized streamwise velocity measurement of the Baseline Blade

In addition to this Pitot-static measurement, four-sensor hotwire data measured for the baseline was used for comparing the methods of vorticity production for this study. Because numerous previous studies have been conducted on the performance of the baseline blades, this report will not go into the details of this configuration. Instead, downstream four-sensor hotwire measurements previously taken by Geiger et al (2005) will be used as the basis for comparison in the following sections. This quadwire data was taken at axial locations of 0.6, 1.2, and 1.8 axial chords downstream of the baseline trailing edge at the midspan location of the blade.

In order to obtain a comparison of the drag created by each of the trailing edges, the momentum thickness was calculated based upon the wake profiles measured at 1.6 axial chords downstream. The momentum thickness values were normalized on the freestream velocity, U_∞, and the baseline blade axial chord, c_a. Momentum thickness can be used as a proportional relationship to the drag on an airfoil. For each trailing edge, the momentum thickness was obtained by integrating the streamwise velocity deficit both pitchwise and spanwise across the wake of the trailing edge. The velocity deficit was normalized on the edge velocity, U_e, for each of the individual cases analyzed. The momentum thickness of the wake is calculated using the equation

$$Momentum\ Thickness = \int\int \frac{(U_e - U_i)U_i}{U_e^2} dZdY. \quad \textbf{(3-2)}$$

To evaluate these integrals, the trapezoidal method was utilized. Performing the first integral in the pitchwise direction provides the spanwise variation in momentum thickness across the wake of each trailing edge. To obtain the overall momentum thickness, the average of the spanwise values was taken for each downstream location. Because a pitchwise profile was measured across the flow aligned wake,

the values presented must be multiplied by the cosine of the angle between the flow aligned and cascade aligned coordinate system, as described in Section 2.1.3. As can be seen in **Figure 3.2**, the momentum thickness calculated using this method varies across the span of the blade, especially in the endwall regions.

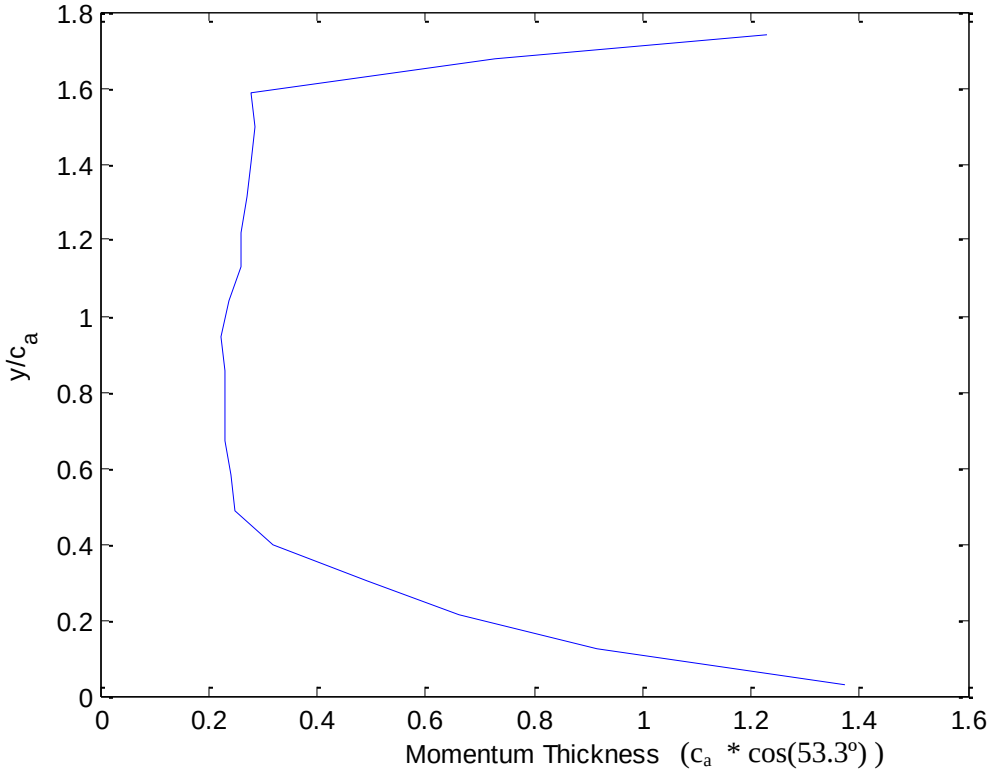

Figure 3.2 Pitchwise Integrated Momentum Thickness Across the Span of the Baseline Trailing Edge

3.2 Surface Mounted Vortex Generators

The following vortex generator configurations were set up as identified in the Apparatus and Instrumentation section of this report. Several configurations of surface-mounted vortex generators were analyzed to determine which method provides the best results for deeper analysis. The TE1 configuration detailed below was determined to be most effective at altering the flow, and was selected for further hotwire analysis.

3.2.1 Surface Vortex Generator Configuration Comparisons

Each of the six surface mounted vortex generator configurations was first analyzed using downstream Pitot-static measurements to give an overall view of the resulting flow characteristics. These initial Pitot measurements were taken at a location of 1.6 axial chord lengths downstream of the trailing edge of the baseline blade. The criteria for selecting the best configuration for further analysis are its ability to diffuse the wake downstream without a large increase in wake deficit. Ultimately, the best vortex generator configuration would utilize the induced vorticity to diffuse the wake by stretching portions of it in the pitchwise direction downstream of the trailing edge. This results in the stator seeing

a wider spanwise average wake profile, which reduces the average velocity fluctuations seen in this intereaction.

The first configuration tested was the TE1 configuration which included spanwise placement of surface mounted vortex generators only on the suction side of the trailing edge. As can be seen in **Figure 3.3**, the application of large vortex generators to the suction side of the blade is quite effective at modifying the structure of the wake. This configuration produces two lobes of velocity deficit along the span of the blade. These lobes correspond with the spanwise placement of the vortex generators on the trailing edge, and appear at 0.85 and 1.3 axial chords from the floor of the test section. The vorticity induced by the generator placement appears to be the cause of the desired stretching of the wake in the pitchwise direction. Additionally, this configuration does not show a substantial change in velocity deficit when compared to the baseline blade results.

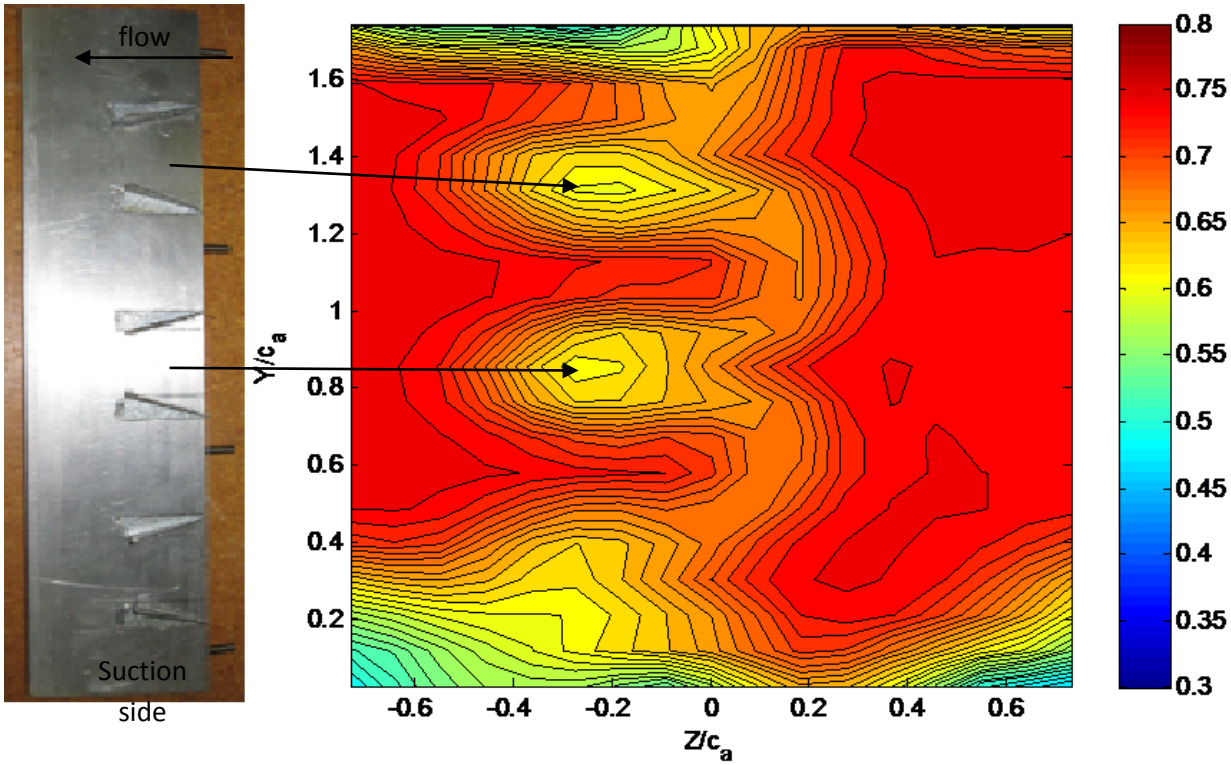

Figure 3.3 Normalized streamwise velocity measurements of Vortex Generator Configuration TE1

In a fashion identical to that for the baseline blade, the momentum thickness was calculated across the span of the TE1 configuration, and is presented in **Figure 3.4**. It is interesting to see the spanwise variation in momentum thickness that is produced by the TE1 configuration. When compared to the streamwise velocity profile (**Figure 3.3**), it can be seen that the lobes of velocity deficit correspond to regions of high momentum thickness across the span. This suggests that although they are effective at stretching the wake width, the placement of the vortex generators inherently increases the drag at their location.

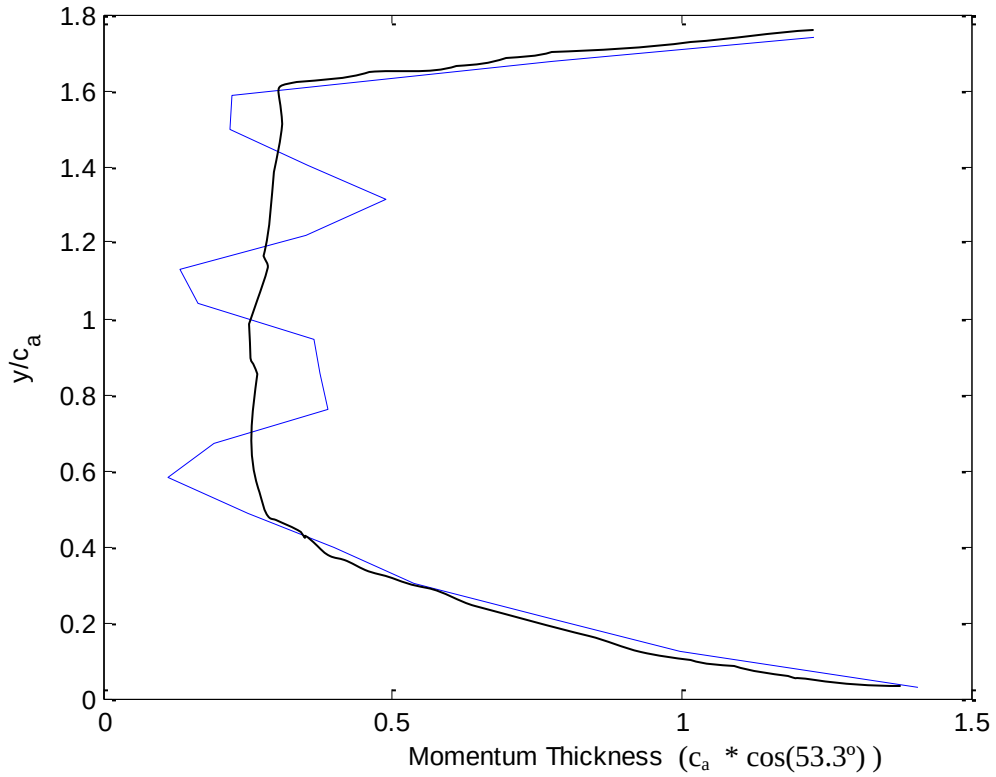

Figure 3.4 Pitchwise Integrated Momentum Thickness Across the Span of the TE1 Configuration (Baseline shown in black)

After testing the effects of vortex generators only on the suction side of the trailing edge, configuration TE2 was developed to measure the effect of placing periodic vortex generators on the pressure side of the blade. These vortex generators were placed in a fully periodic fashion similar to configuration TE1, but only on the pressure side of the trailing edge. The wake results of configuration TE2 are presented in

Figure 3.5. In a manner similar to the TE1 configuration, the pressure side vortex generators of TE2 add two lobes of higher velocity deficit to the wake at spanwise locations of 0.6 and 1.2 axial chords. However, the induced vorticity is ineffective at altering the overall shape of the wake behind the trailing edge, and the overall profile does not demonstrate any noticeable wake stretching.

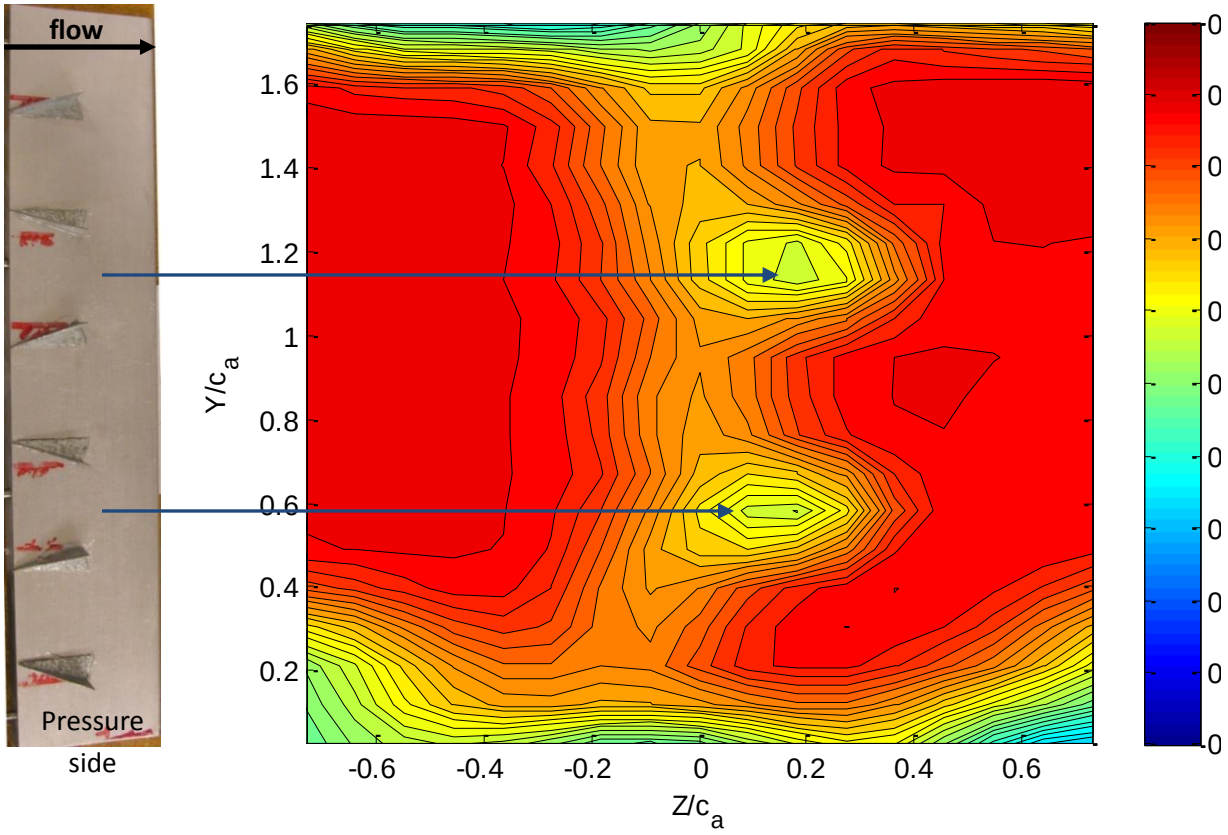

Figure 3.5 Normalized streamwise velocity measurements of Vortex Generator Configuration TE2

The resulting momentum thickness produced by the TE2 configuration is presented in **Figure 3.6**. As with the previous TE1 configuration, TE2 also shows some dramatic spanwise variation in the momentum thickness produced. When compared to the TE1 configuration (**Figure 3.4**), the TE2 configuration appears to show smoother, but equally substantial variations across the span of the blade.

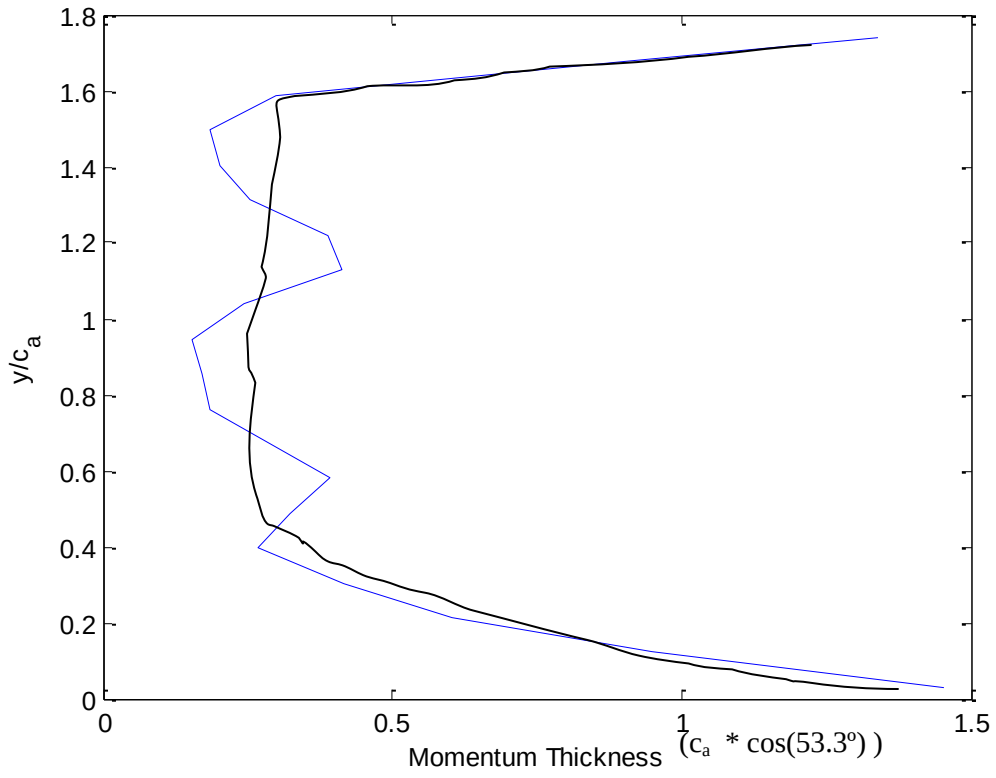

Figure 3.6 Pitchwise Integrated Momentum Thickness Across the Span of the TE2 Configuration (Baseline shown in black)

After testing configurations of vortex generators mounted only to one side of the blade, the results of using vortex generators on both the suction and pressure sides are of interest. This configuration involved combining the placement of configurations TE1 and TE2 into one configuration, referred to as TE3. **Figure 3.7** shows the effect on the shape of the wake resulting from the TE3 vortex generator configuration. As expected the TE3 configuration was able to stretch the wake in a fashion similar to the TE1 vortex generator placement. With this configuration, lobes of velocity deficit can be seen at spanwise locations of 0.9 and 1.4 axial chords from the floor of the test section. It is interesting to note that the lobes of velocity deficit that resulted from vortex generators placed on the pressure side of the blade (see

Figure 3.5) do not appear when combined with vortex generator placement on the suction side. Instead, it appears that the pressure side vortex generators serve to further stretch the wake when compared to configuration TE1 which utilizes generators only on the suction side.

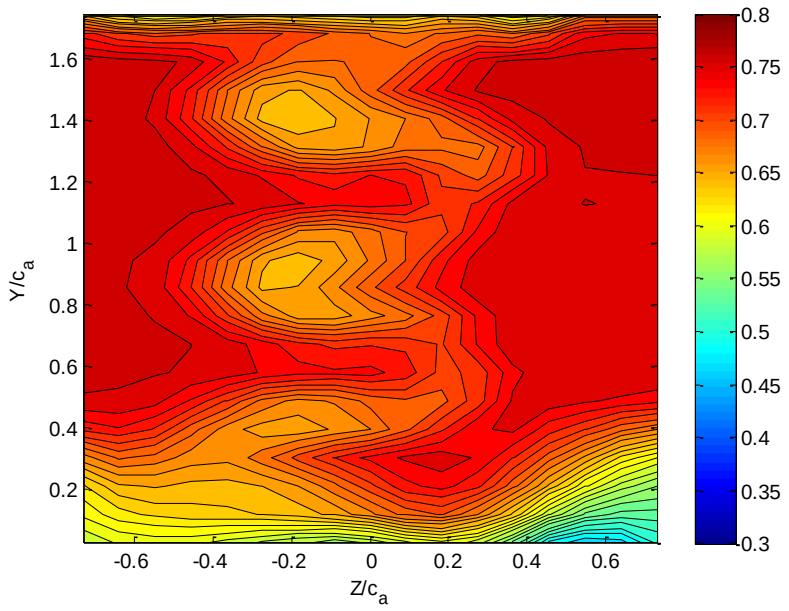

Figure 3.7 Normalized streamwise velocity measurements of Vortex Generator Configuration TE3

The momentum thickness variation produced by the TE3 configuration is nearly identical to the profiles produced by the previous vortex-generator TE configurations. These spanwise variations can be seen in **Figure 3.8**. As with the other configurations, the TE3 blade also shows a large region of high momentum thickness around the location of the tip leakage vortex which extends from the floor to a spanwise location of approximately 0.5 axial chords.

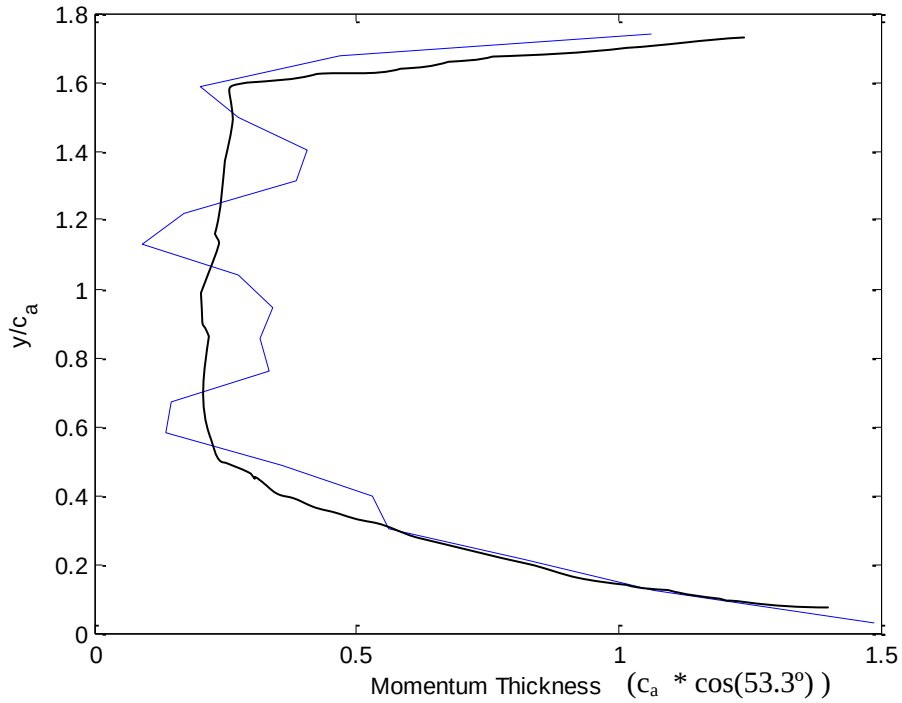

Figure 3.8 Pitchwise Integrated Momentum Thickness Across the Span of the TE3 Configuration (Baseline shown in black)

Configuration TE4 also involved placement of vortex generators on both the suction and pressure sides of the trailing edge. However, configuration TE4 utilized only semi-periodic placement on the suction side of the blade. The motivation behind this was to induce similar vorticity levels and wake modification as TE3 with a smaller wake deficit penalty resulting from the increased drag of more vortex generators. However, as

Figure 3.9 shows, configuration TE4 failed to fully stretch the wake across the entire span. Instead, this configuration only resulted in an increase in the wake width at the center span point, which resulted in only one lobe produced at a spanwise location of 0.9 axial chords above the test section floor. Although there do seem to be additional locations of increased velocity deficit at spanwise locations of 0.45 and 1.3 axial chords, these pockets are not stretched away from the wake center. Because of its inability to effectively stretch the wake across the entire span, the TE4 configuration was removed from consideration for further analysis.

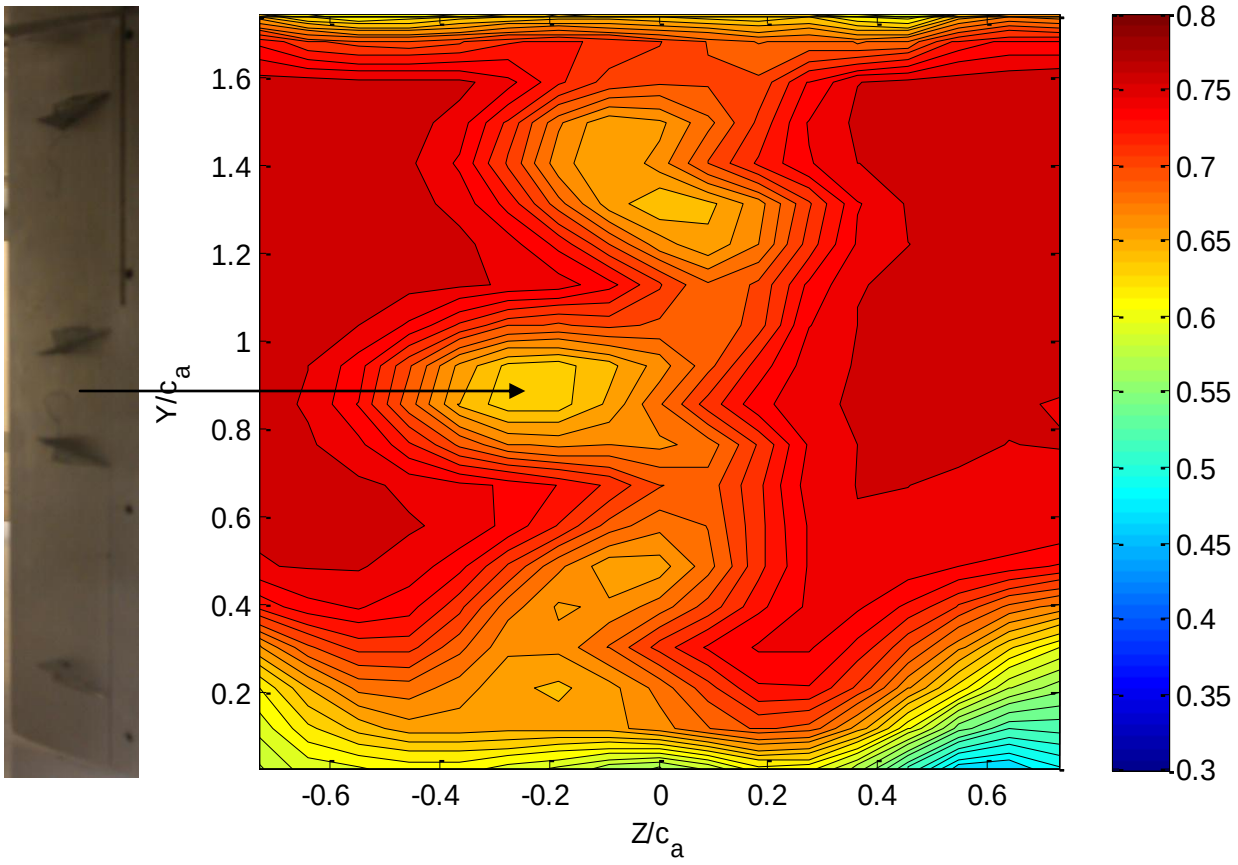

Figure 3.9 Normalized streamwise velocity measurements of Vortex Generator Configuration TE4

The TE4 configuration shows a similar, but unique spanwise variation in momentum thickness. As **Figure 3.10** shows, the TE4 configuration shows a single larger region of high momentum thickness which extends from 0.7 to just below 1.0 axial chords in the spanwise direction. This corresponds to the protruding lobe seen in the streamwise velocity contour for TE4 (

Figure 3.9).

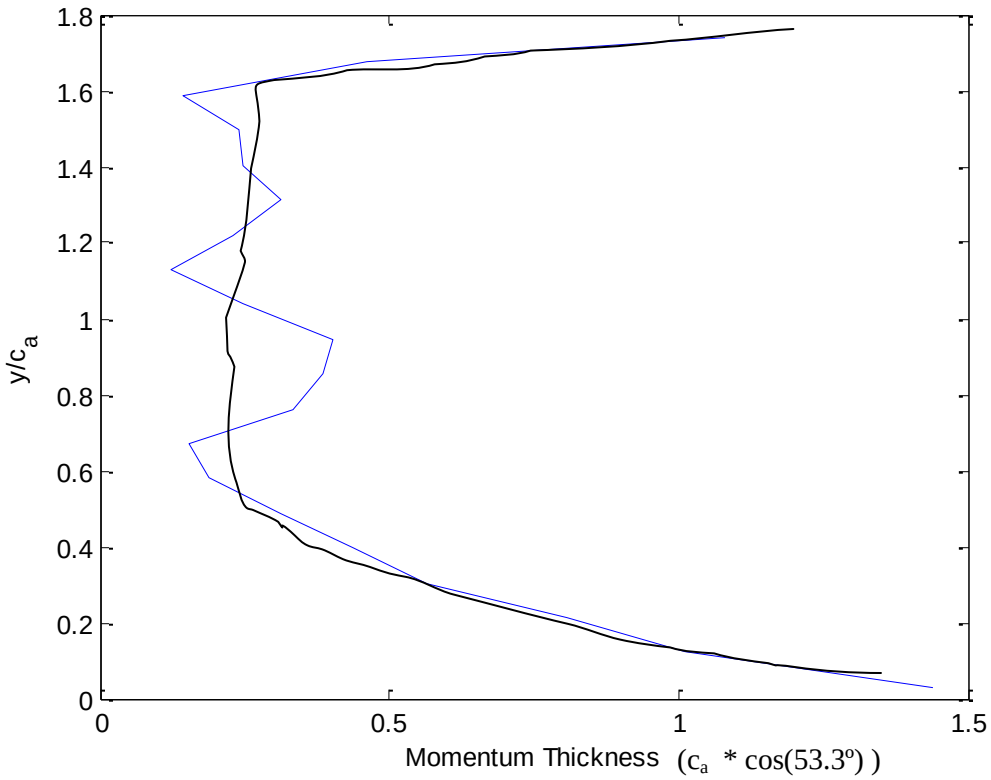

Figure 3.10 Pitchwise Integrated Momentum Thickness Across the Span of the TE4 Configuration (Baseline shown in black)

The final vortex generator configurations were developed based on the TE1 and TE2 setups, but used the small vortex generators. **Figure 3.11** shows configuration TE5 which mounted the small vortex generators to the suction side of the trailing edge, and **Figure 3.12** shows configuration TE6 which uses small vortex generators only on the pressure side of the blade. As might be expected, these small vortex generators do very little to affect the overall structure of the wake. The TE5 configuration (**Figure 3.11**) shows lobes of velocity deficit and stretching at the same locations as TE1 (**Figure 3.3**), but these lobes are noticeably smaller.

The results of configuration TE6 indicates that the placement of small vortex generators on the pressure side of the trailing edge has almost no effect on the wake structure, and only causes an increase in the wake deficit at the location of the generators. As **Figure 3.11** and **Figure 3.12** show, the suction side of the blade offers significantly more authority in modifying the structure of the wake behind the trailing edge.

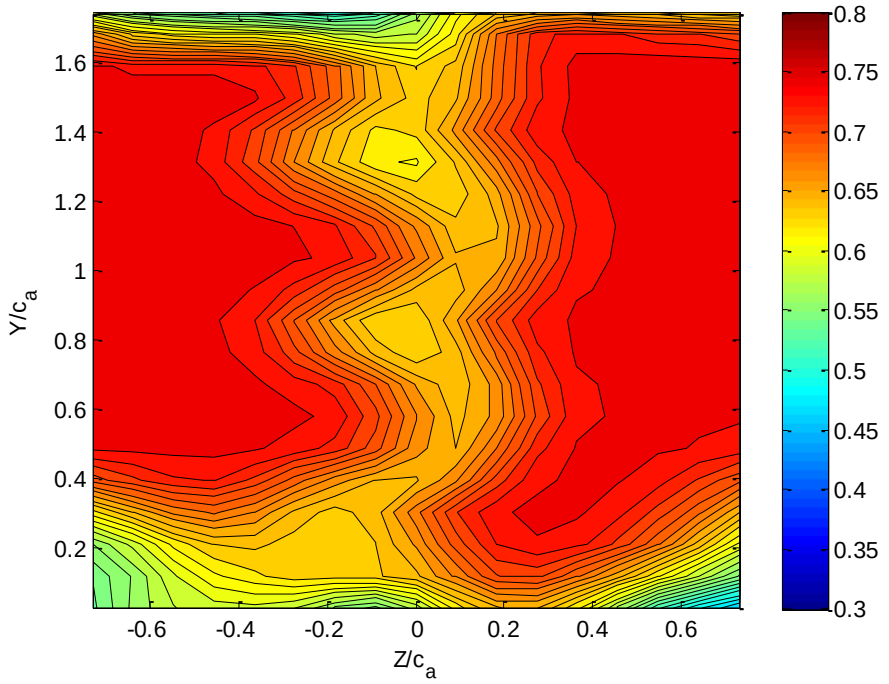

Figure 3.11 Normalized streamwise velocity measurements of Vortex Generator Configuration TE5

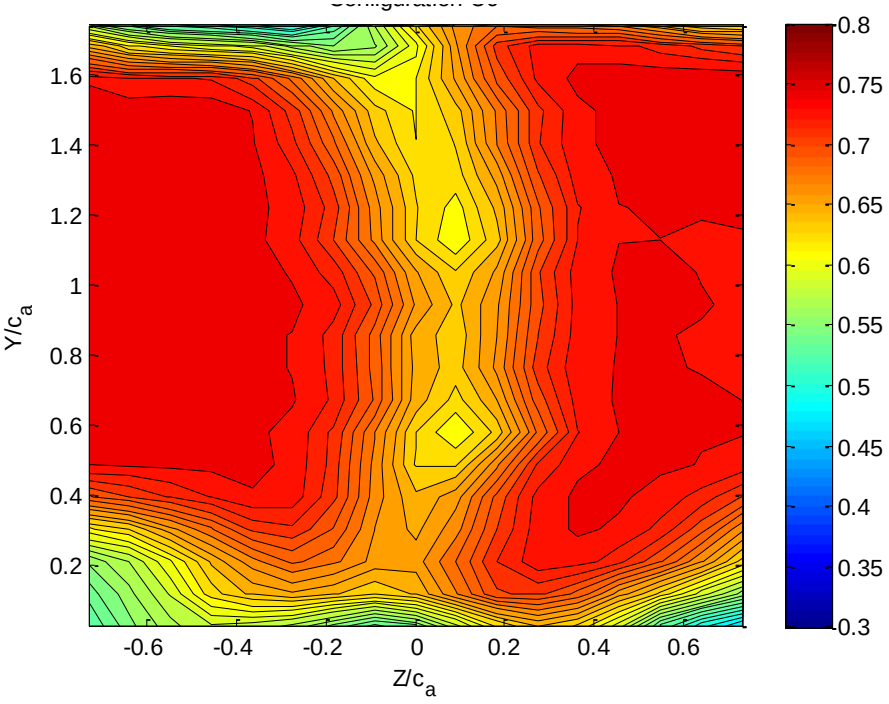

Figure 3.12 Normalized streamwise velocity measurements of Vortex Generator Configuration TE6

The final spanwise momentum thickness plots are presented in **Figure 3.13** and **Figure 3.14**. Although these trailing edge configurations do show similar spanwise variations, the levels of these changes are

much lower than those seen in the previous vortex generator trailing edge designs. This corresponds with the relatively minor velocity profile changes produced by these trailing edge configurations.

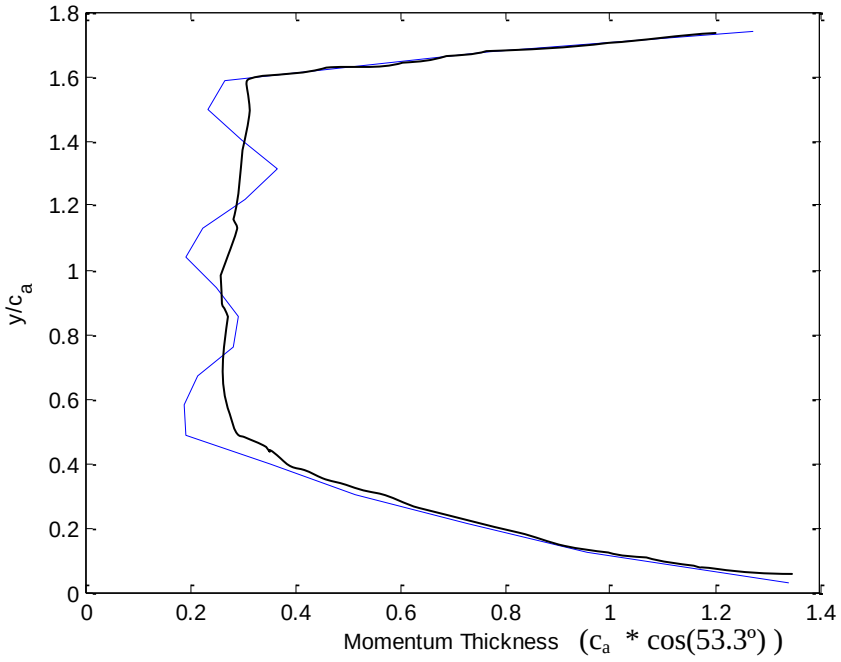

Figure 3.13 Pitchwise Integrated Momentum Thickness Across the Span of the TE5 Configuration (Baseline shown in black)

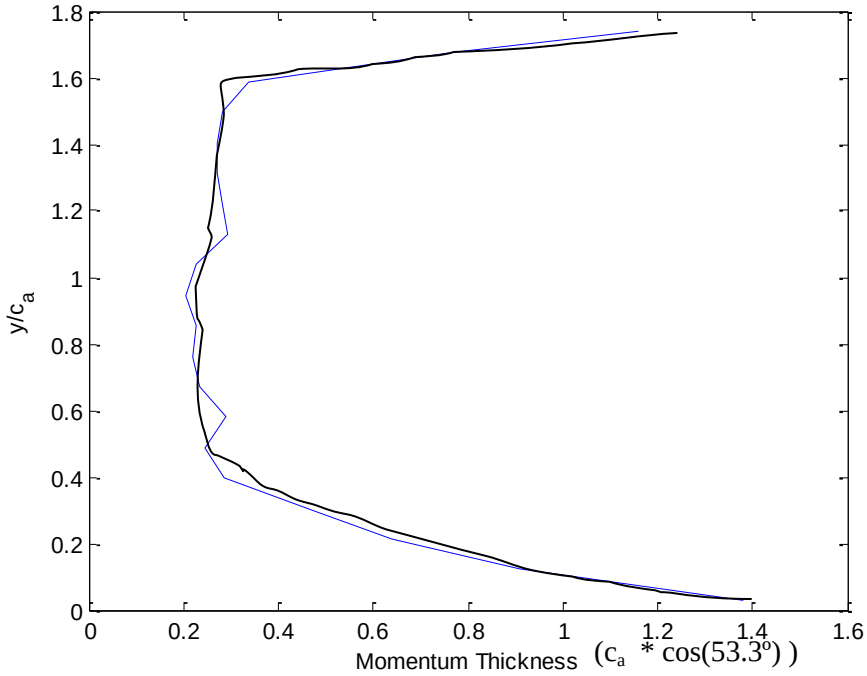

Figure 3.14 Pitchwise Integrated Momentum Thickness Across the Span of the TE6 Configuration (Baseline shown in black)

In order to obtain a single value of momentum thickness, the pitchwise variation of momentum thickness was averaged across one period of vorticity injection. As can be seen in **Table 3-1**, each vortex generator configuration does have a negative effect on the averaged momentum thickness, with the exception of TE-6 which shows a slightly reduced momentum thickness compared to the baseline.

Table 3-1. Averaged Momentum Thickness of the Wake Produced by Each TE configuration

Configuration	Momentum Thickness ($c_a/\cos(53.3º)$)	Change from Baseline (%)
Baseline	0.2499	--
TE1	0.2999	20
TE2	0.2640	5.6
TE3	0.2784	11.4
TE4	0.2631	5.28
TE5	0.2718	8.76
TE6	0.2425	-2.96

A qualitative and quantitative comparison of the wake profiles shown through the Pitot-static measurements suggests that configuration TE1 is the optimal configuration of vortex generators to allow for sufficient wake stretching with minimal penalties in velocity deficit. Additionally, TE-1 was chosen for further analysis because it showed the greatest ability to diffuse the wake with the least amount of additions required to the baseline trailing edge.

3.2.2 Detailed Analysis of Vortex Generator Configuration TE1

The TE1 configuration utilizes surface mounted vortex generators on the suction side of the trailing edge, as described in Section 3.2.1. The following sections detail the four-sensor hotwire measurements taken at four locations downstream of the trailing edge. The data presented in this section is normalized on the spanwise period of the vortex generators, λ_{TE1}. Data was extracted from the vortex generator period that encompasses the midspan section of the airfoil, which can be seen by the two lobes of velocity deficit in **Figure 3.3**. This corresponds to a spanwise range of $0.8 \leq z/c_a \leq 1.3$ for this analysis. The measurement grid used 0.5 inch spacing in the pitchwise direction (y), and created 20 points in the spanwise direction (z). For the TE1 configuration, λ_{TE1} is set to 3 inches.

3.2.2.1 TE1 Wake Velocity cross-section Measurements

The four-sensor hotwire data acquisition system is able to provide detailed information on each of the three velocity components in the wake behind the trailing edge of the blade. This can give the specifics of how the vortex generators are directly affecting all aspects of the flow behind the trailing edge of the blade. These quadwire measurements were taken in a fashion similar to the Pitot measurements described in Section 3.2, and each of the velocity cross-sections presented are normalized on the free stream inlet velocity, U_∞. Gradient errors as described in Section 2.2.2.3 are corrected for the TE-1 configuration by enforcing symmetry across the span of the blade.

The first and most interesting velocity measurement is the change in streamwise velocity as a result of the blade and vortex generator configuration. The streamwise velocity cross-section can be

used to identify the resulting momentum deficit from the trailing edge configuration. Figure 3.15 through Figure 3.18 show how the streamwise velocity distribution changes as the wake convects from 0.4 to 1.6 axial chords downstream of the trailing edge. The horizontal axes of these figures represent the pitchwise distance across the blade wake normalized on λ_{TE1}, and the vertical axis shows the spanwise location measured as a percentage of λ. The zero percentage point is located at the lower location of the vortex generators.

Figure 3.15 shows the streamwise velocity component at a distance of 0.4 axial chords downstream of the baseline trailing edge. The overall shape of the wake resulting from the TE1 configuration can be seen. The two lobes of maximum velocity deficit appear to be stretched in the pitchwise direction as a result of the vorticity induced by the generators. Between these two lobes of high velocity deficit a region of smaller velocity deficit is observed. This region of thin wake appears between 40% and 60% of λ_{TE1}. The velocity in this region is only $0.55U_\infty$ compared to the $0.45U_\infty$ found in the two lobes of maximum deficit.

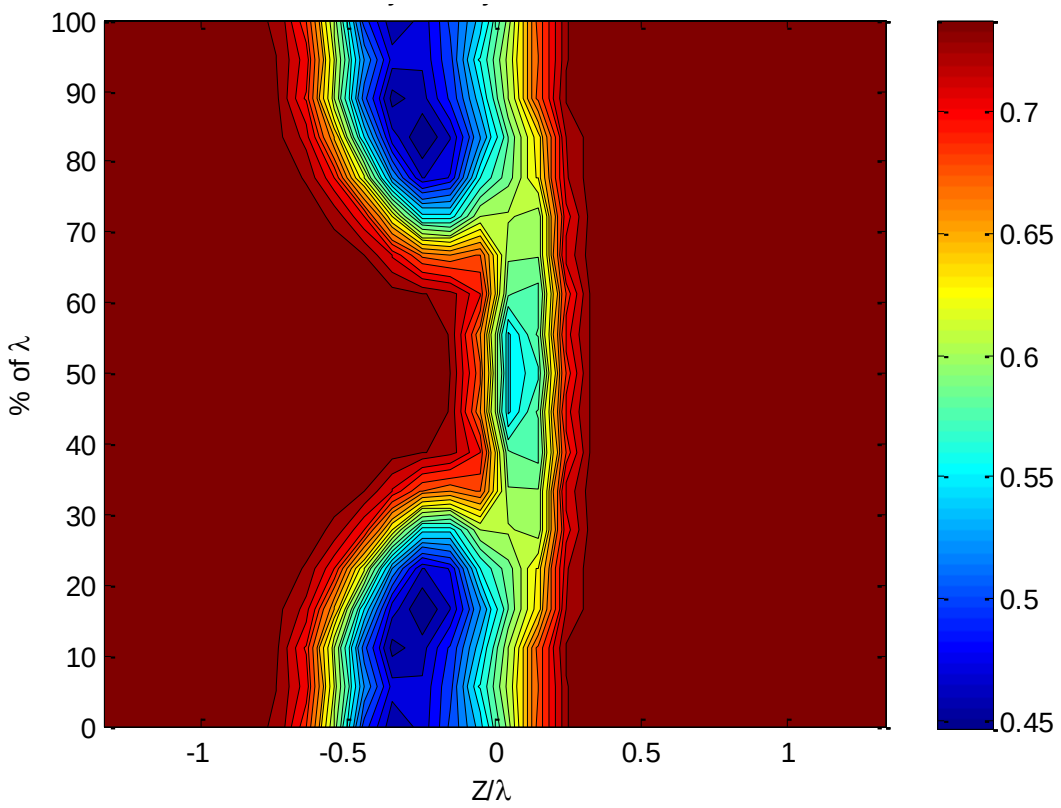

Figure 3.15 TE-1 Streamwise (U/U_∞) Velocity cross-section at 0.4 Axial Chords Downstream (symmetry enforced)

As it convects further downstream, **Figure 3.16** shows the wake development to 0.8 axial chords. The general structure of the wake seen at 0.4 axial chords downstream remains intact, but it can be seen that the thickness has increased. This trend continues as the wake propagates further downstream to distances of 1.17 and 1.6 axial chords as shown in **Figure 3.17** and **Figure 3.18**.

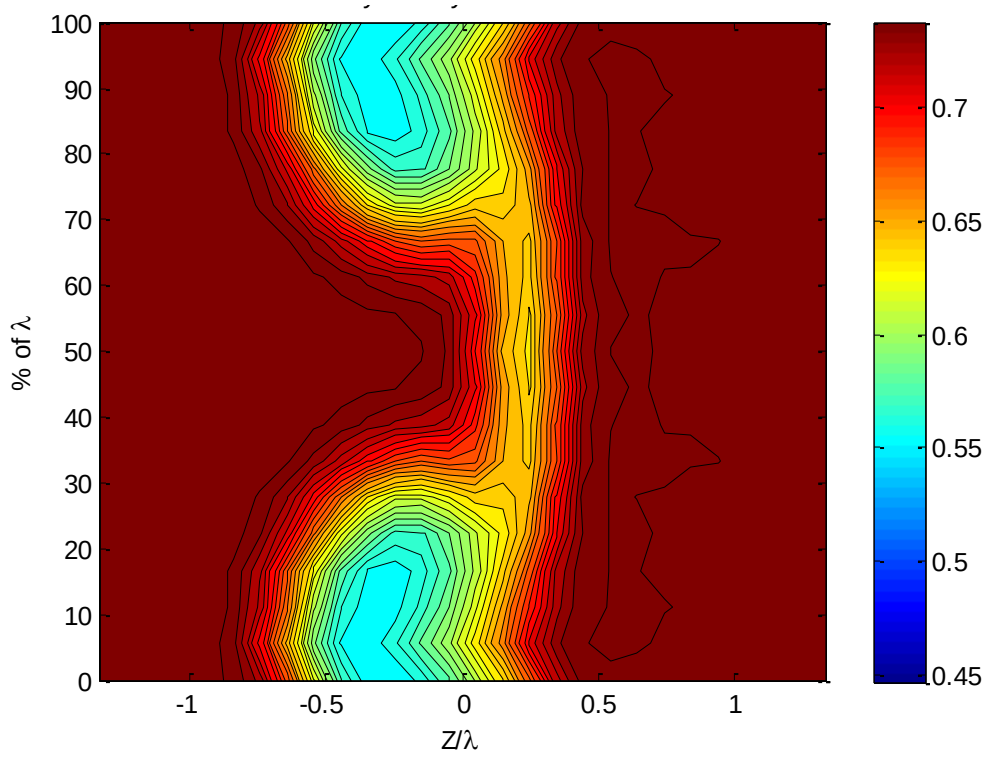

Figure 3.16 TE-1 Streamwise Velocity (U/U_∞) cross-section at 0.8 Axial Chords Downstream (Symmetry enforced)

At each of the four downstream locations measured for the TE1 configuration, the lobes of maximum velocity deficit maintain their position at just below 10 percent and just above 90 percent of λ_{TE1}. This indicates that the production of vorticity at these spanwise sites using this configuration does not cause significant spanwise drift in the wake. This goes to further assure proper application of the gradient error correction techniques presented in Section 2.2.2.3.

Comparing the streamwise velocities at each of the downstream shows that as the wake convects downstream, the mean velocity deficit becomes reduces and the wake breadth increases. At 0.4 axial chords downstream of the trailing edge (**Figure 3.15**) the lobe at 90 percent λ_{TE1} has a minimum streamwise velocity of 55% of the freestream potential core velocity outside of the wake. Once the wake reaches 1.6 axial chords downstream (**Figure 3.18**), the minimum velocity of this lobe increases to 82% of the freestream potential core velocity.

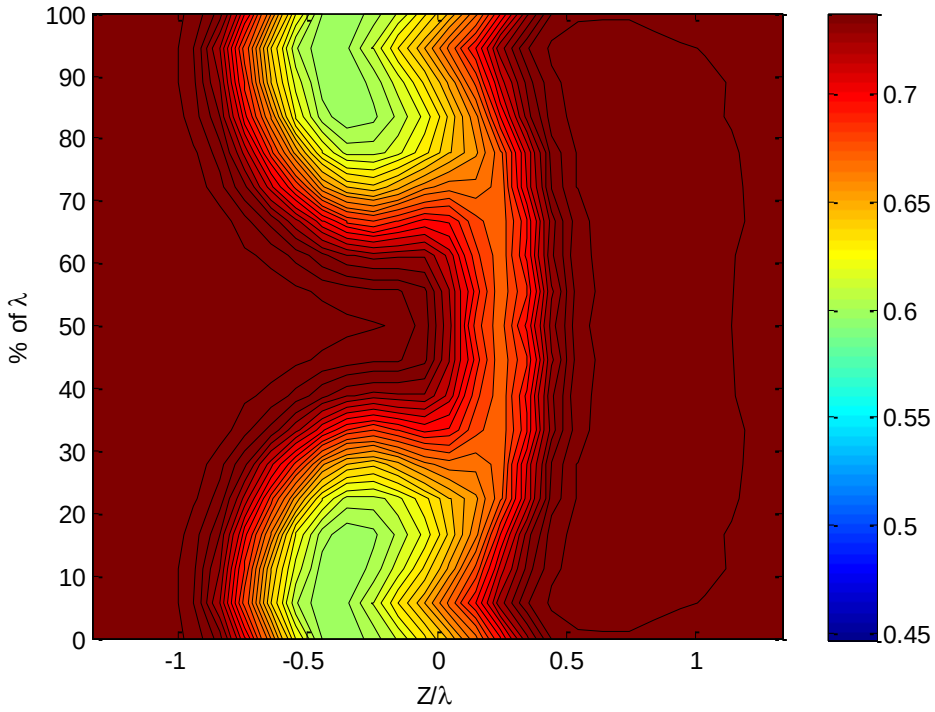

Figure 3.17 TE-1 Streamwise Velocity (U/U_∞) cross-section at 1.17 Axial Chords Downstream (Symmetry enforced)

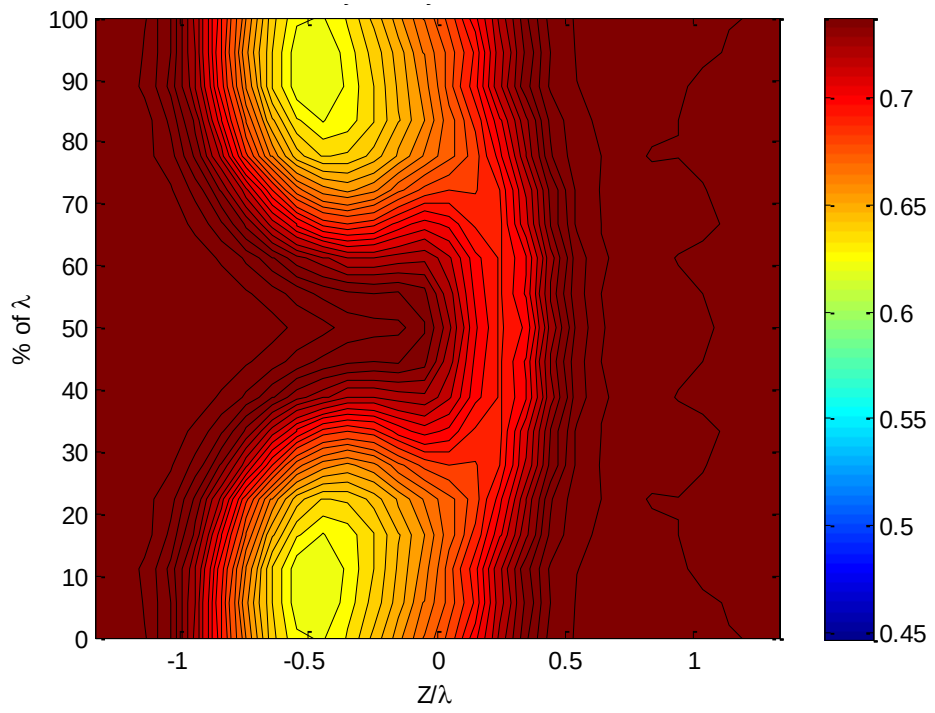

Figure 3.18 TE-1 Streamwise Velocity (U/U_∞) cross-section at 1.6 Axial Chords Downstream (Symmetry enforced)

The distribution of streamwise velocity gives significant insight into how the application of the surface mounted vortex generators dramatically affects the shape of the wake behind the trailing edge. It is interesting to note that, although there is an increased velocity deficit at the spanwise location of the vortex generators, the spanwise location midway between vortex generators (50% λ) actually has a smaller velocity deficit than the baseline when normalized on the velocity of the potential core. This further suggests that the introduction of vorticity can cause a smaller momentum deficit at certain locations across its spanwise period.

Wake aligned velocity components perpendicular to the streamwise direction show the three dimensional effects of both the blade and the TE1 vortex generator configuration. The following figures are presented in the flow-aligned coordinate system described in Section 2.1.3 of this report. These velocity cross-sections again show how each component of the flow propagates downstream of the blade trailing edge, and are presented in **Figure 3.19** through **Figure 3.22**. As these figures show, the vortex generators placed on the trailing edge add only a small amount of velocity in both the lateral and spanwise direction. At 0.4 axial chords downstream (**Figure 3.19**), the v- and w- wake flow aligned velocity components have a maximum absolute value of $0.079U_\infty$ and $0.11U_\infty$, respectively. As the wake propagates downstream these patterns of these velocity cross-sections remain constant, but the levels rapidly decrease. Once the flow reaches 1.6 axial chords downstream (**Figure 3.22**), the maximum v- and w- wake aligned velocities drop to $0.025U_\infty$ and $0.039U_\infty$, respectively. Because the v- and w- velocity components are decreasing as the wake convects downstream, this suggests that the vortices produced by the generator placement of TE1 diffuse as wake propagates behind the trailing edge.

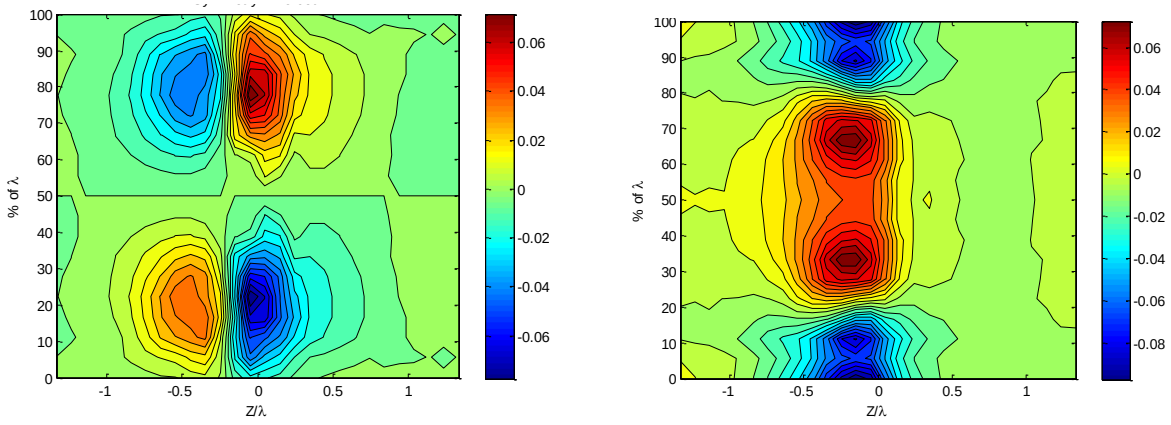

Figure 3.19 Spanwise (V/U_∞, left) and Lateral (W/U_∞, right) Velocity cross-sections at 0.4 Axial Chords Downstream (Symmetry enforced)

Starting with **Figure 3.19**, it can be seen that the TE1 trailing edge configuration produces spanwise alternating areas of v- velocity. Just above the site of vorticity production, located at 20% and 80% of λ_{TE1}, the v-velocity cross-section shows the primary flow direction is away from the chord line of the blade. However, at the 50% period location, there is negligible flow in the v-direction. The shape of the v-velocity cross-section across the spanwise period of vorticity injection for TE1 explains the widened edges of the streamwise velocity cross-section seen in **Figure 3.15**. The w- velocity cross-section seen in **Figure 3.19** suggests that the TE1 configuration results in a positive flow direction

(towards 100% λ) at the centerspan location, and velocities away from the centerspan location at the sites of injection. This also suggests that the w-velocity is influenced most heavily just above the location of the vortex generators. This may indicate why **Figure 3.15** seems to show that the center of the streamwise velocity wake profile appears to be stretched towards the 0 and 100 percent λ locations. The w-velocity cross-section at 0.4 axial chords downstream (**Figure 3.19**) shows two lobes of high velocity just outside of the centerspan location. As the wake convects downstream these lobes appear to merge together (indicating that the vortex cores also merge together), until they have combined into a single lobe of positive w-velocity at 1.6 axial chords downstream of the trailing edge, as seen in **Figure 3.22**.

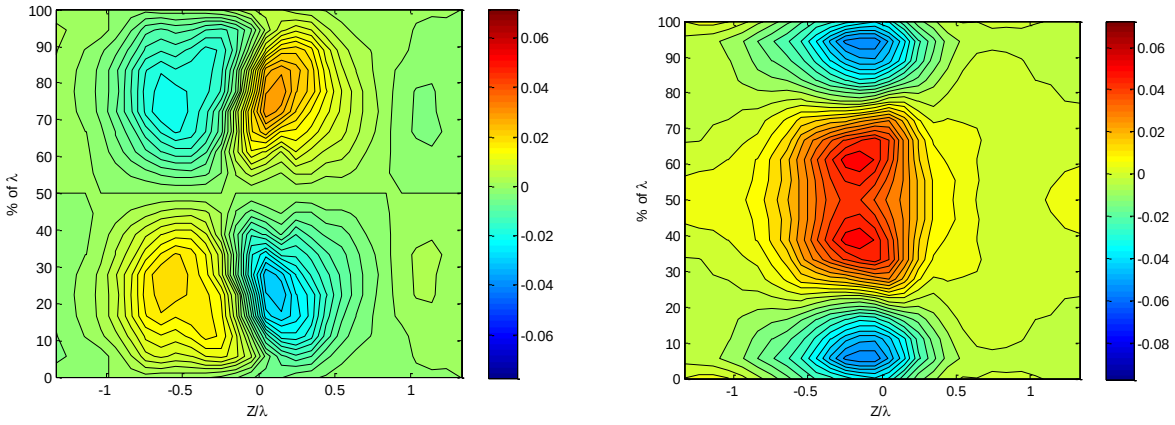

Figure 3.20 Spanwise (V/U_∞, left) and Lateral (W/U_∞, right) Velocity cross-sections at 0.8 Axial Chords Downstream

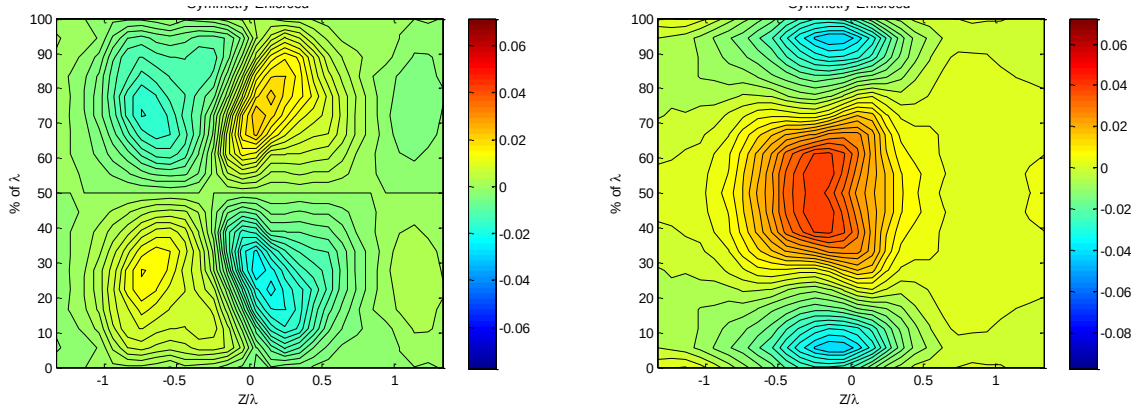

Figure 3.21 Spanwise (left) and Lateral (right) Velocity cross-sections at 1.17 Axial Chords Downstream

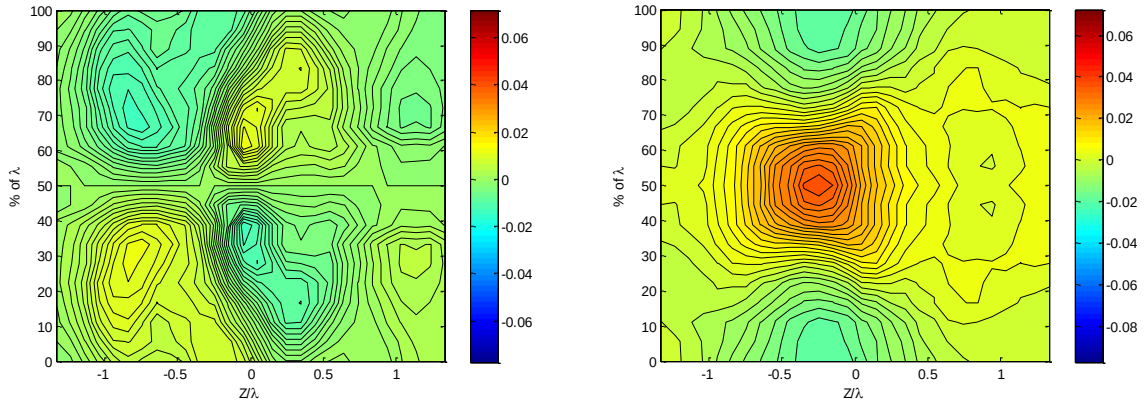

Figure 3.22 Spanwise (left) and Lateral (right) Velocity cross-sections at 1.6 Axial Chords Downstream

3.2.2.2 TE-1 Streamwise Vorticity Measurements and Analysis

In order to ensure consistency across vorticity comparisons for all the trailing edges considered, the values presented for vorticity are normalized on the axial chord, c_a, of the baseline blade and U_∞, the inlet freestream velocity. The streamwise vorticity variation resulting from the TE-1 configuration is presented in **Figure 3.23** through **Figure 3.26**. These figures indicate that the vorticity levels produced by the TE-1 configuration begin to rapidly decrease as the downstream distance is increased. It takes approximately 1.6 axial chords for the mean streamwise vorticity to lose half of its intensity. Examining **Figure 3.23** closely shows that 0.4 axial chords downstream of the trailing edge there are alternating regions of positive and negative streamwise vorticity. The maximum value of vorticity produced by the TE1 configuration at 0.4 axial chords downstream is 2.02 c_a/U_∞, and occurs at 33% of the injection period in the negative direction and 67% of the injection period in the positive direction. This region of high vorticity is paired with a region of opposing vorticity that is slightly weaker at 1.9 c_a/U_∞. These two regions of vorticity can be seen to be mirror image of each other across the 50% λ line. As the wake convects downstream, the vortices maintain the same general structure but lose intensity. Additionally, the vortices appear to grow larger until 1.17 axial chords downstream (**Figure 3.25**), after which the vortices no longer appear to enlarge. **Figure 3.26** shows that as the wake reaches 1.6 axial chords downstream of the trailing edge, the maximum vorticity magnitude drops to 0.61 c_a/U_∞. Thus, the maximum vortex intensity drops to 30% of the original measured intensity after propagating only 1.2 axial chords downstream.

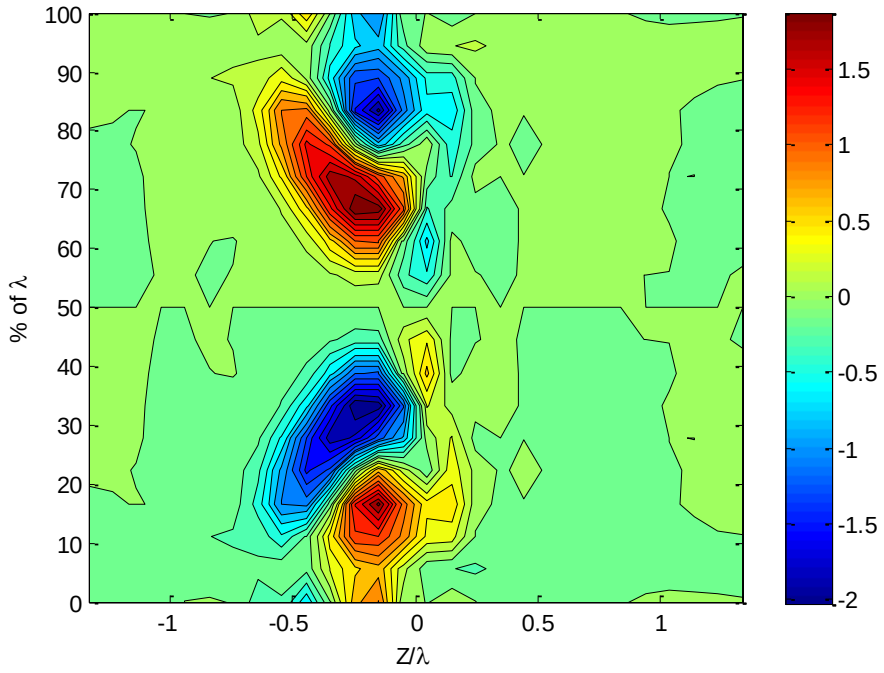

Figure 3.23 Streamwise Vorticity Contour of TE-1 at 0.4 Axial Chords Downstream (symmetry enforced)

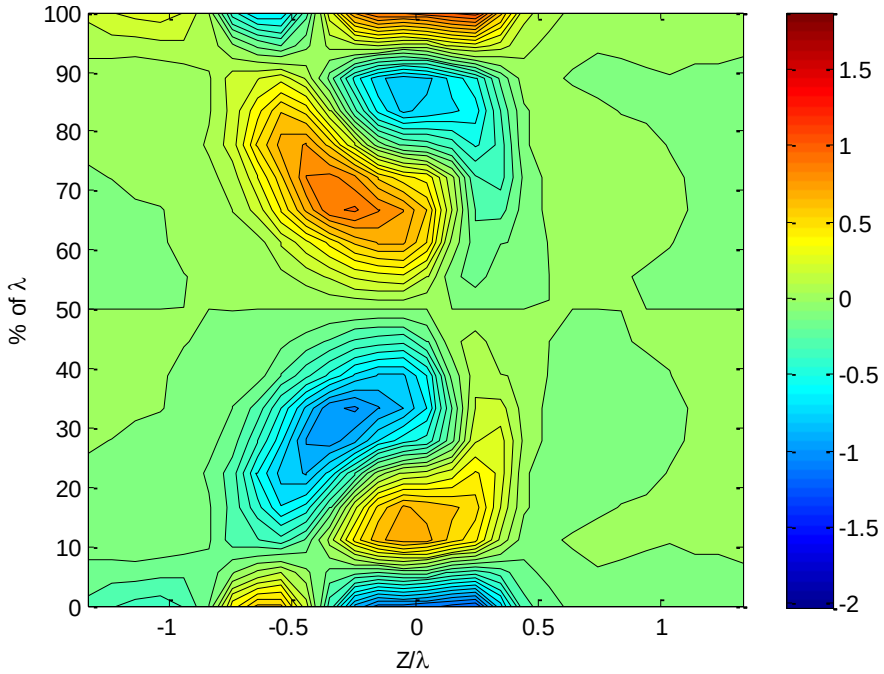

Figure 3.24 Streamwise Vorticity Contour of TE-1 at 0.8 Axial Chords Downstream (symmetry enforced)

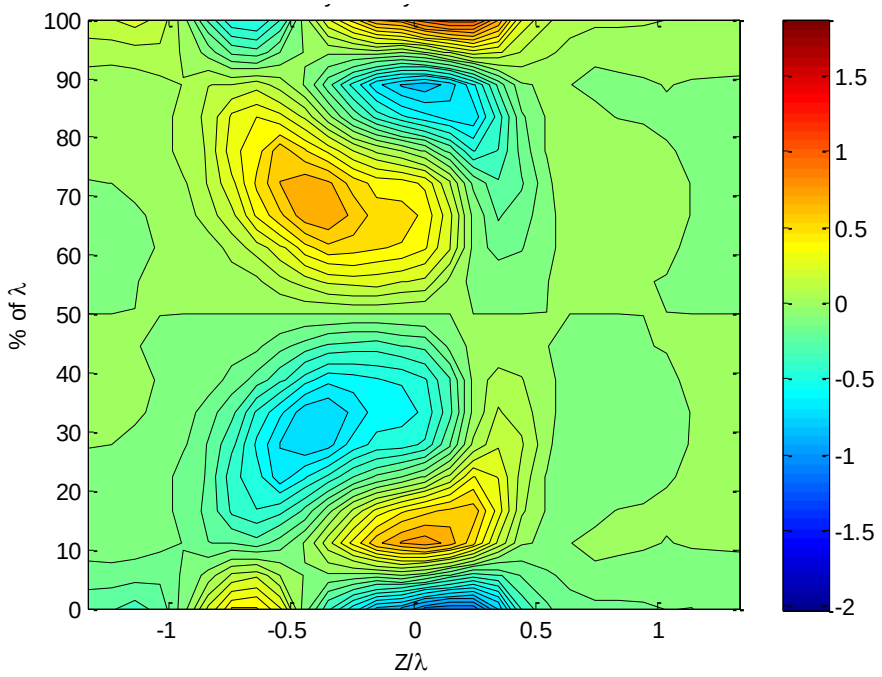

Figure 3.25 Streamwise Vorticity Contour of TE-1 at 1.2 Axial Chords Downstream (symmetry enforced)

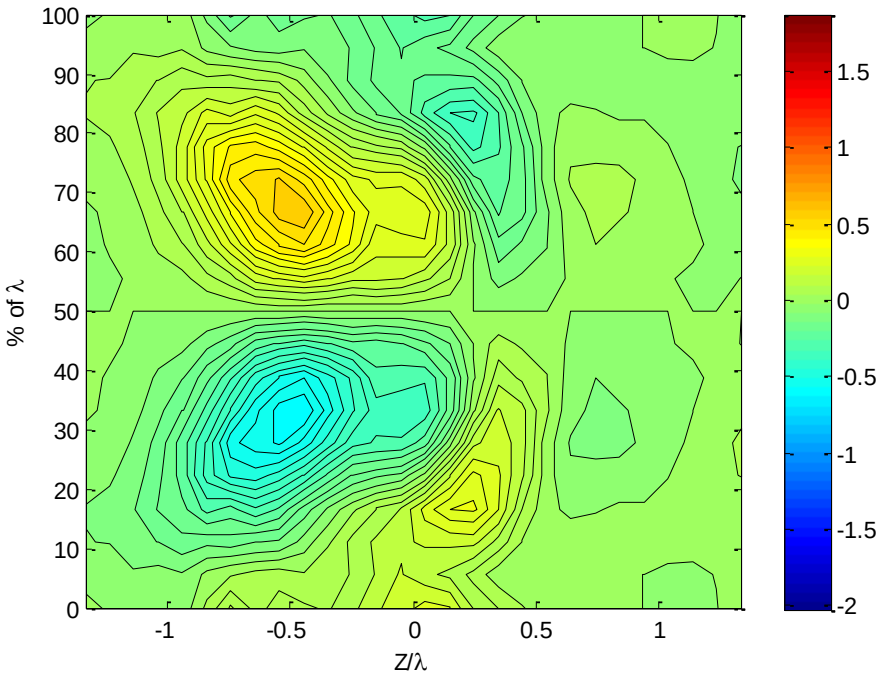

Figure 3.26 Streamwise Vorticity Contour of TE-1 at 1.6 Axial Chords Downstream (symmetry enforced)

3.2.2.3 TE-1 Mean Turbulence Kinetic Energy Analysis

The existence of turbulence downstream of the trailing edge of the blades is a key contributor to the development of unsteady surface pressure on the hypothetical downstream stator, which ultimately

results in the production of broadband noise. Thus, the analysis of the turbulence produced by vorticity generation is useful in estimating the impact that each configuration has on noise production. The following section presents the spanwise cross section of the mean turbulence kinetic energy, TKE. The TKE is calculated as half the sum of the streamwise, spanwise, and pitchwise Reynolds' stresses, which are normalized on the inlet freestream velocity, so

$$\boldsymbol{TKE = \frac{\overline{u}^2 + \overline{v}^2 + \overline{w}^2}{2}.} \qquad \textbf{(3-3)}$$

As with the velocity and vorticity plots, the TKE coordinate system is normalized on the spanwise period, λ, of the vortex generator placement. Because the variations are not symmetric, no gradient error corrections have been applied to the following TKE data. Additionally, some plots indicate that the measurement grid was not perfectly aligned with the actual spanwise period of vorticity as a result of wake shifting. This can be seen in **Figure 3.27**, where the y axis does not encompass 0 to 100 % λ.

Starting from **Figure 3.27**, it can be seen that the turbulence structure has a highest value at the location where the vortex generators are placed along the span of the trailing edge. The TKE is a minimum at the midpoint between the vortex generators, which corresponds to the spanwise location where the blade essentially models a clean trailing edge. The highest value of TKE is measured just below the 100 percent λ_{TE1} location reaches $0.0135U_\infty^2$, and the minimum TKE in the wake occurs just above the 50 percent λ_{TE1} and measures $0.0071U_\infty^2$ at 0.4 axial chords downstream of the trailing edge. In a previous study conducted in the same facility by Geiger 2005, the baseline blade was shown to produce a minimum TKE value at midspan of $0.008\ U_\infty^2$

Figure 3.27 through **Figure 3.30** show the rapid decline in observed TKE levels, as the wake propagates downstream. As this occurs, the turbulence can also be seen dispersing further into the freestream, which essentially widens the area subjected to turbulence downstream of the trailing edge. At the furthest measured location of 1.6 axial chords downstream of the trailing edge, the peak TKE is measured as $0.0031U_\infty^2$, while the minimum wake TKE level drops to $0.0015U_\infty^2$. While the wake turbulence levels decrease, the locations of peak TKE begin to travel towards the centerspan location, as the turbulence becomes more uniform throughout the wake.

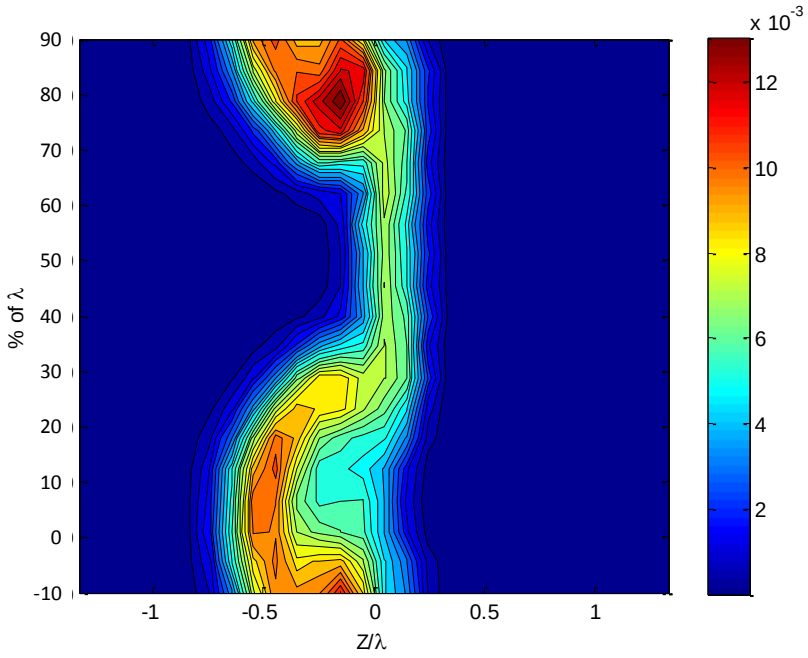

Figure 3.27 Mean Turbulence Kinetic Energy Profile of TE-1 at 0.4 Axial Chords Downstream

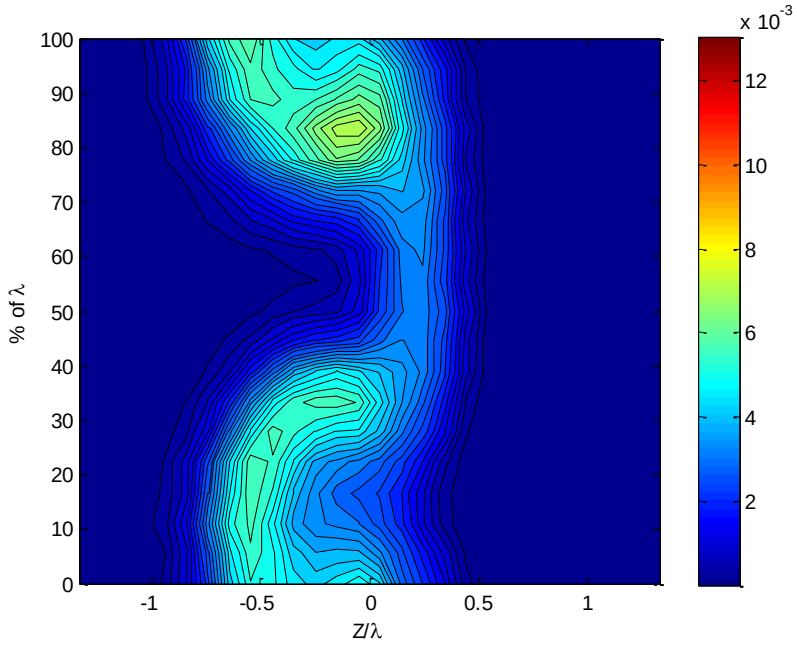

Figure 3.28 Mean Turbulence Kinetic Energy Profile of TE-1 at 0.8 Axial Chords Downstream

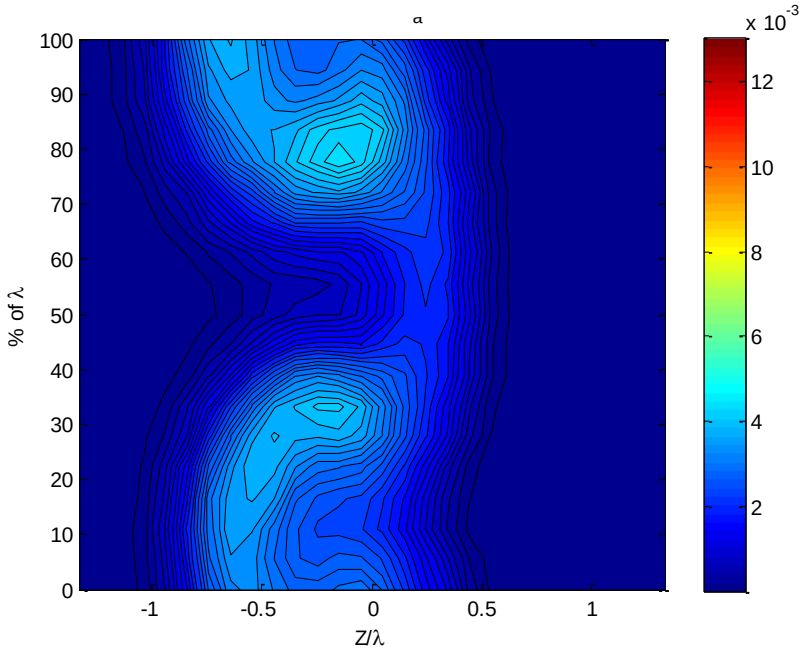

Figure 3.29 Mean Turbulence Kinetic Energy Profile of TE-1 at 1.2 Axial Chords Downstream

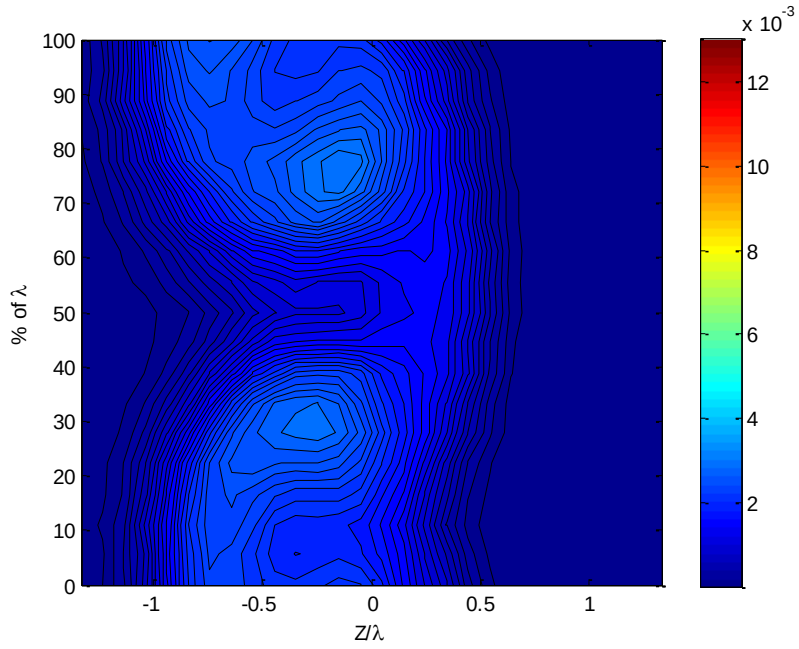

Figure 3.30 Mean Turbulence Kinetic Energy Profile of TE-1 at 1.6 Axial Chords Downstream

3.2.2.4 TE-1 Wake Width Characteristics

The amount by which the TE-1 configuration is able to effectively widen the wake can be measured through the spanwise average velocity profile. This average profile is obtained by taking the average of each pitchwise velocity profile at each of the measured spanwise location. This effectively

collapses the curve into one average pitchwise velocity profile which represents the average spanwise characteristics of the trailing edge configuration. With this spanwise average profile, the half wake width of the blade wake can be calculated. This value is the pitchwise width of the wake at the point where the velocity deficit is 50% of the maximum velocity deficit recorded.

The spanwise average velocity profile for TE-1 is presented in **Figure 3.31**. The vertical axis shows the velocity deficit normalized on edge velocity, and the horizontal axis represents the pitchwise width of the profile. As identified in the figure, the half wake width is $0.33c_a$ for the baseline trailing edge and $0.59c_a$ for the TE-1 configuration. **Figure 3.31** shows that the TE-1 configuration produces a far wider wake than the baseline configuration.

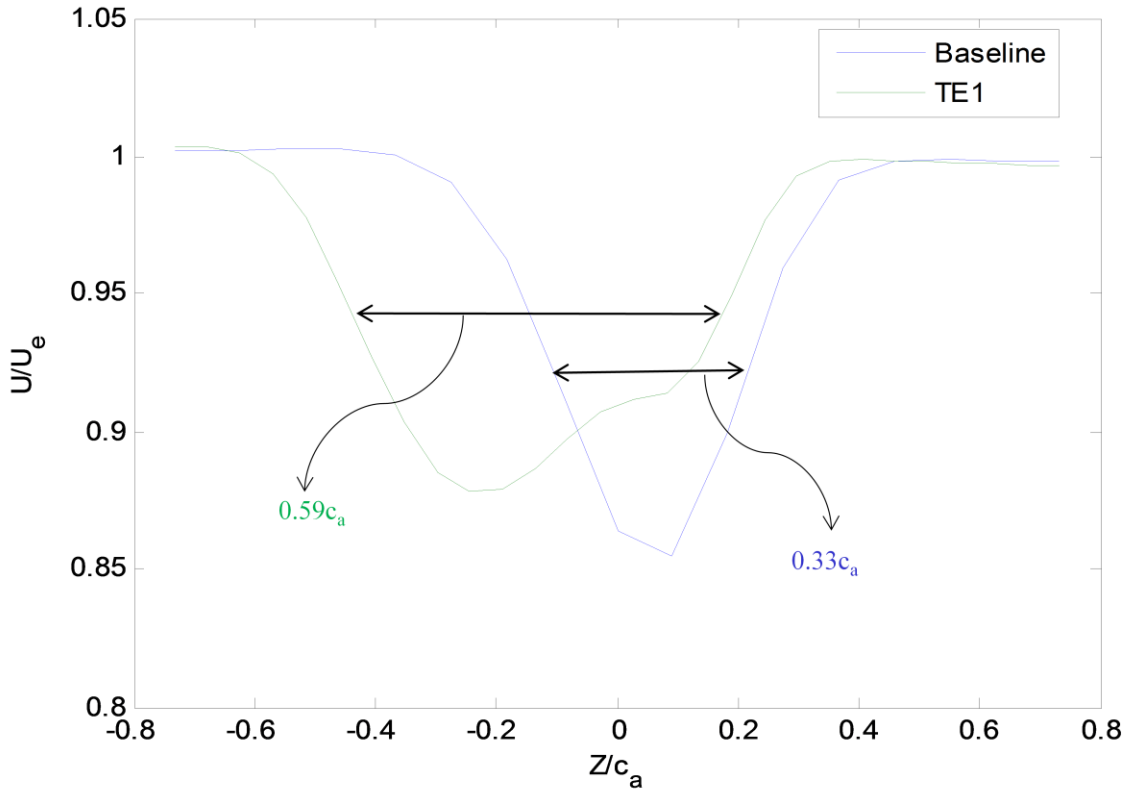

Figure 3.31 Spanwise Average Velocity Profile Comparison for TE-1 and the Baseline Trailing Edge at 1.6 Axial Chords Downstream

3.3 Advanced Wake Mixing Technology

The TE-7 and TE-8 configurations presented in the following sections are proprietary trailing edge configurations designed to improve wake mixing. Due to the proprietary nature of these trailing edges, the specifics of these configurations as well as the full spanwise profiles are not included in this report.

Like the previous vortex generator configurations, the TE-7 and TE-8 designs also have a spanwise period of vorticity injection, λ_{TE7} and λ_{TE8}, upon which the graphs have been normalized. The data for TE-7 was measured by Dr. Aurelien Borgoltz of the Aerospace and Ocean Engineering Department at Virginia Tech. This data was analyzed and processed by the current author in order to be consistent with the remaining data measured.

3.3.1 Blade Loading Comparisons

The surface pressure distribution (blade loading) was measured using surface pressure ports located across the chord line of the baseline blade, and on the removable trailing edge section for each configuration tested. The blade loading measurements reveals significant information regarding the flow caused by the blade configuration, and enables calculation of circulation and thus lift produced by each trailing edge.

The blade loading for each trailing edge configuration is presented in terms of the surface pressure coefficient, C_P, and is plotted normalized on the axial distance (x/c_a) from the leading edge of the blade. This surface static pressure coefficient is calculated using the equation

$$C_p = \frac{P_s - P_\infty}{P_{0\infty} - P_\infty}, \quad \textbf{(3-4)}$$

where the ∞ subscript indicates inlet freestream measurements, P_s is the local static pressure, and P_0 is the total pressure measurement. The results for the baseline blade as well as TE-7 and TE-8 are presented in **Figure 3.32**. This figure shows variations on the leading edge of the blade which are typical for measurements taken with trip strips located near the leading edge of the blade. Additionally, these results show that each of the trailing edge configurations does not significantly affect the blade loading upstream of the removable trailing edge which is located starting at 0.8 axial chords downstream. It can be seen, however, that these two trailing edge configurations do appear to alter the blade loading downstream of the trailing edge attachment point, indicating some subtle differences in the design of these configurations. It should be noted that the low point of TE-7 that occurs at approximately x/c_a = 0.85 is a resulted of a clogged pressure port and not a characteristic of the blade loading.

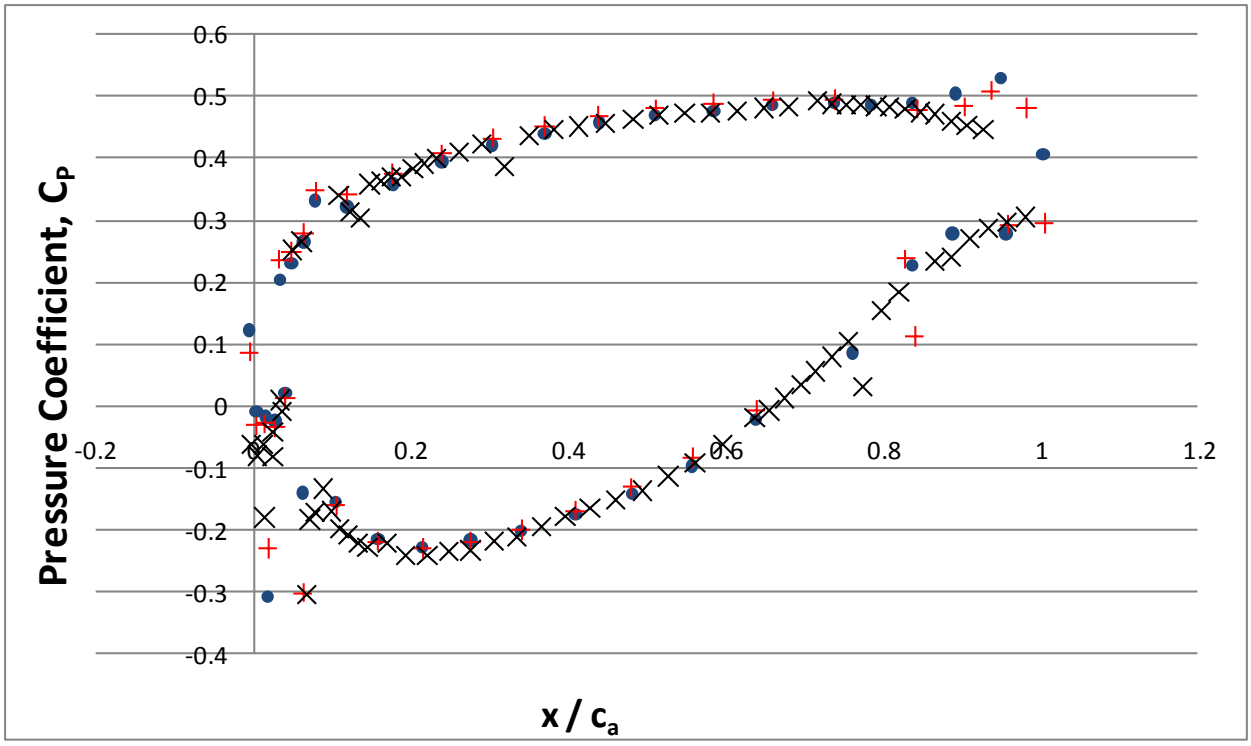

Figure 3.32 Surface Blade Loading Comparisons for the Baseline (×), TE-7 (+), and TE-8 (●) configurations

3.3.2 Detailed Analysis of Vortex Generator Configuration TE-7

The following sections detail the four-sensor hotwire measurements taken at eight locations downstream of the trailing edge. The data presented in this section is normalized on the spanwise period of the vortex generation, λ_{TE7}. Data was extracted from the vortex generator period that encompasses the midspan section of the airfoil. These quadwire measurements were taken in a fashion similar to the quadwire measurements described in Section 3.2.2, and each of the velocity cross-sections presented are normalized on the free stream inlet velocity, U_∞. Gradient errors as described in Section 2.2.2.3 are corrected for the TE-7 configuration. Measurements in this section were performed by Dr. Aurelien Borgoltz.

3.3.2.1 TE-7 Wake Velocity cross-section Measurements

The first and most interesting velocity measurement is the change in streamwise velocity as a result of the blade and vortex generator configuration. **Figure 3.33** through **Figure 3.40** show how the streamwise velocity distribution changes as the wake convects from 0.1 to 1.88 axial chords downstream of the trailing edge. The horizontal axes of these figures represent the pitchwise distance across the blade wake normalized on λ_{TE7}, and the vertical axis shows the spanwise location measured as a percentage of λ. It should be noted that the z-axis in the following plots are reversed as a result of differences in measurement techniques.

Figure 3.33 shows the streamwise velocity component at a distance of 0.1 axial chords downstream of the baseline trailing edge. The overall shape of the wake resulting from the TE7

configuration can be seen. The two lobes of maximum velocity deficit appear to be further towards the pressure side of the blade (positive Z/λ) when compared to the centerspan region. Between these two lobes of high velocity deficit a region of smaller velocity deficit is observed. This region of thinner wake with a smaller velocity deficit appears between 40% and 60% of λ_{TE7}. The velocity in this region is only $0.56U_\infty$ compared to the $0.15U_\infty$found in the two lobes of maximum deficit.

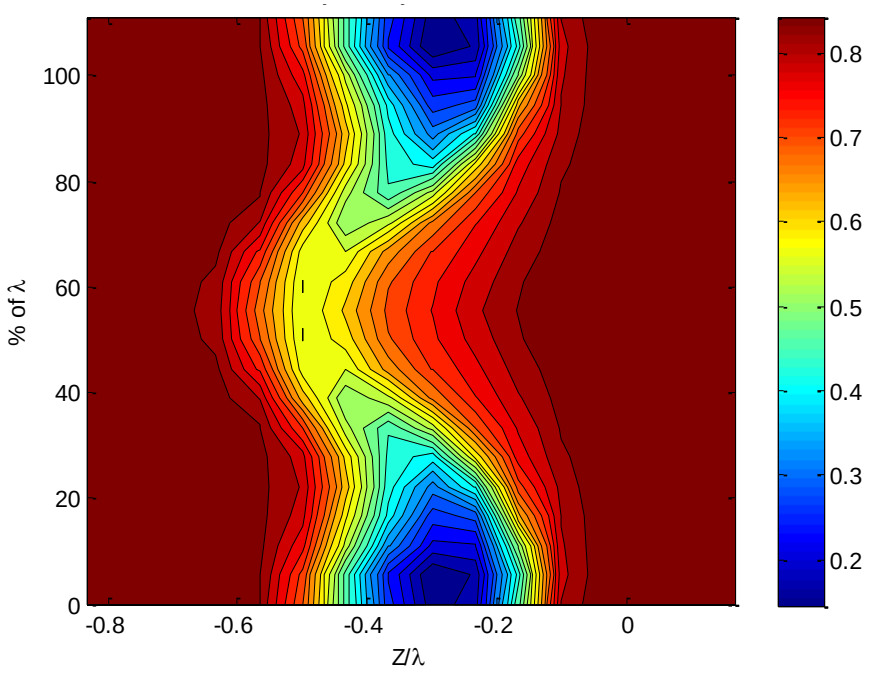

Figure 3.33 TE-7 Streamwise Velocity (U/U_∞) cross-section at 0.1 Axial Chords Downstream (symmetry enforced)

As the wake convects further downstream, **Figure 3.34** shows the wake development to 0.2 axial chords. The general structure of the wake seen at 0.1 axial chords downstream remains intact, but it can be seen that the thickness has begun to slightly increase. This trend continues as the wake propagates further downstream as shown in the remaining figures.

Once the wake reaches a downstream distance of 0.4 axial chords (**Figure 3.35**), the streamwise velocity deficits observed are significantly reduced, indicating the flow is mixing with the freestream. By 0.4 axial chords downstream, the two lobes of minimum velocity seen at 0% and 100% of λ increase to $0.41U_\infty$, and the centerspan region increases to $0.62U_\infty$. This brings the wake velocity deficits comparable to those seen in the TE-1 configuration of Section 3.2.2.1. At each of the eight downstream locations measured for the TE7 configuration, the lobes of maximum velocity deficit maintain their position at just above 0 percent and just above 100 percent of λ_{TE7}.

Comparing the streamwise velocities at each of the downstream locations shows that as the wake convects downstream, the mean velocity deficit becomes smaller. At 0.4 axial chords downstream of the trailing edge (**Figure 3.35**) the lobe at 100 percent λ_{TE7} has a minimum streamwise velocity of 52% of the freestream velocity outside of the wake. Once the wake reaches 1.6 axial chords downstream (**Figure 3.39**), the minimum velocity of this lobe increases to 86% of the potential core velocity. Finally, as the wake propagates to the farthest downstream position measured (**Figure 3.40**) the minimum velocity measured in this lobe reaches 88% of the potential core velocity, while the centerspan location reaches 90% of the potential core velocity.

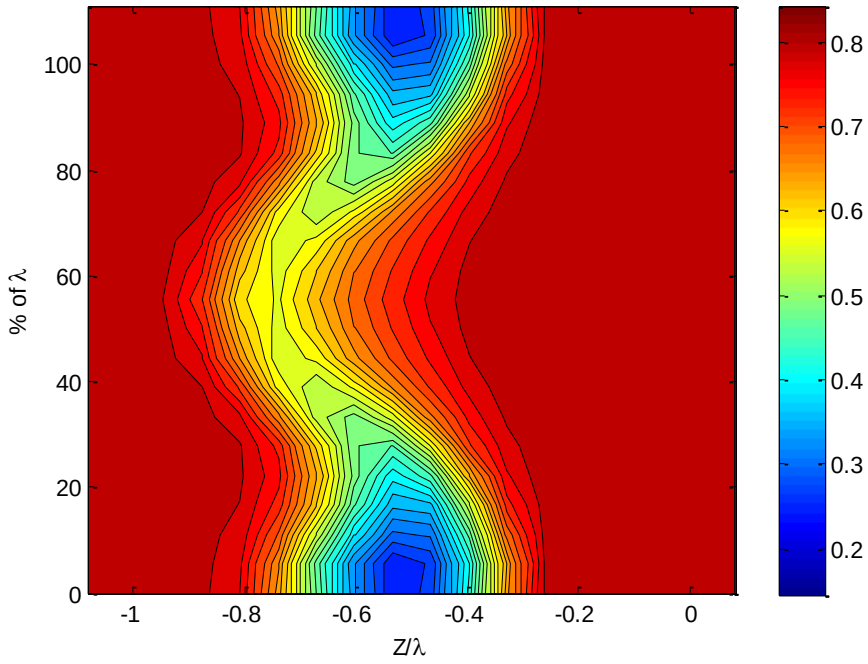

Figure 3.34 TE-7 Streamwise Velocity (U/U_∞) cross-section at 0.2 Axial Chords Downstream (symmetry enforced)

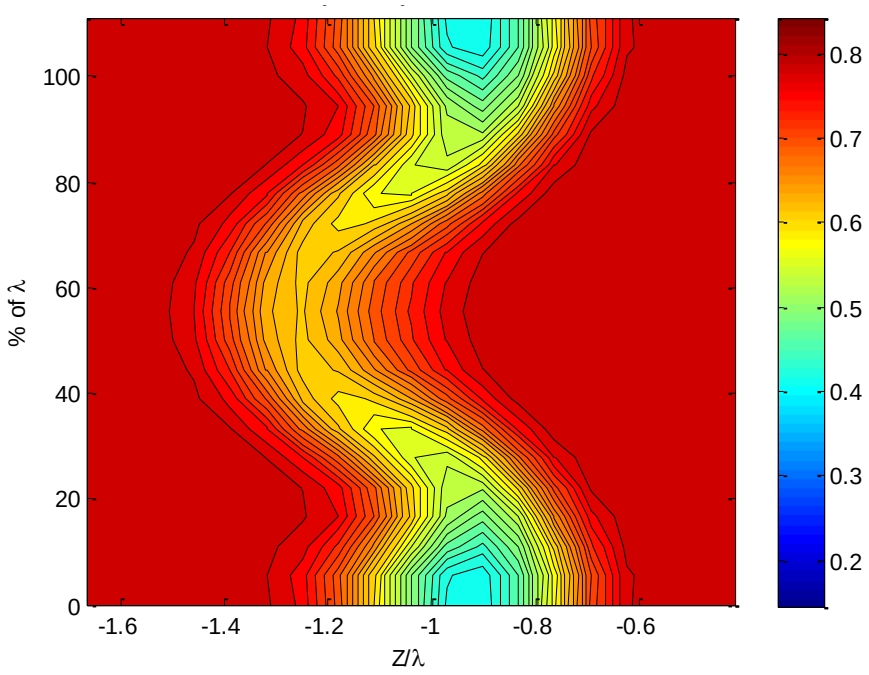

Figure 3.35 TE-7 Streamwise Velocity (U/U_∞) cross-section at 0.4 Axial Chords Downstream (symmetry enforced)

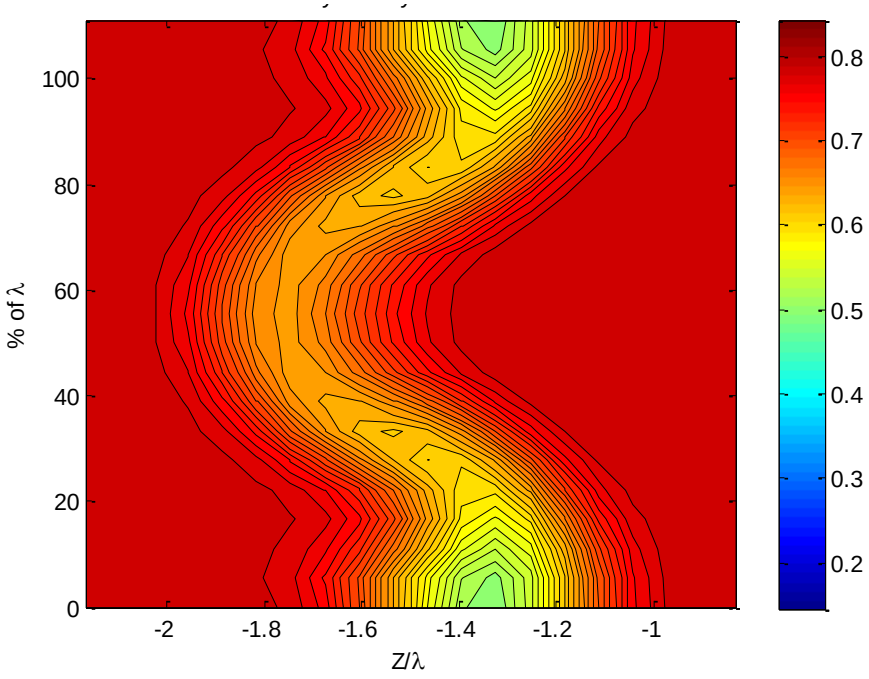

Figure 3.36 TE-7 Streamwise Velocity (U/U_∞) cross-section at 0.6 Axial Chords Downstream (symmetry enforced)

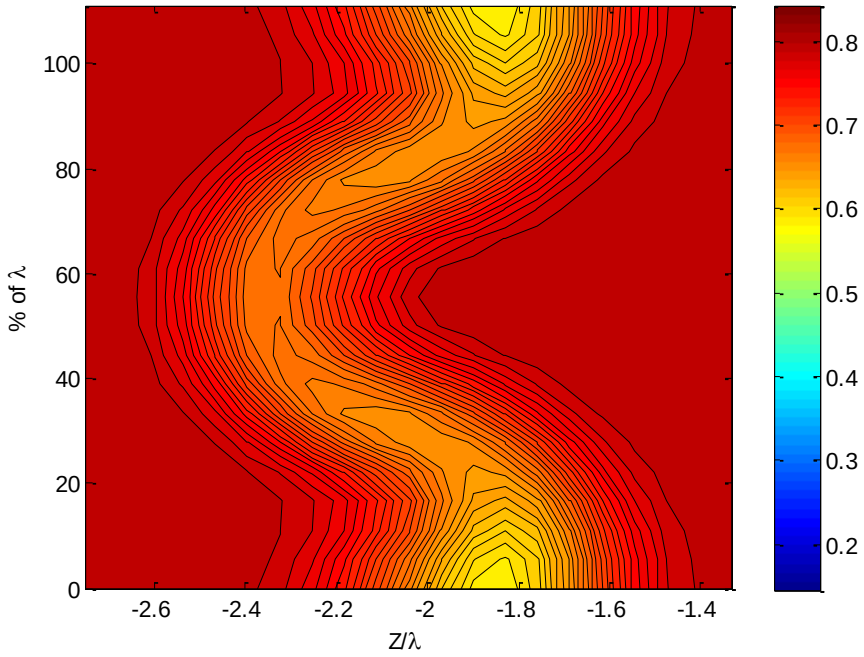

Figure 3.37 TE-7 Streamwise Velocity (U/U_∞) cross-section at 0.84 Axial Chords Downstream (symmetry enforced)

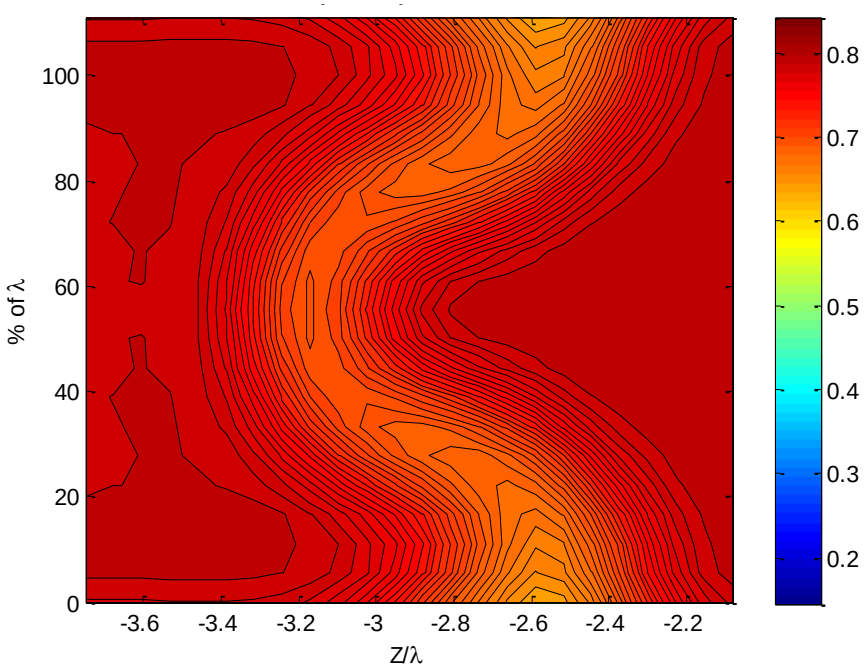

Figure 3.38 TE-7 Streamwise Velocity (U/U_∞) cross-section at 1.18 Axial Chords Downstream (symmetry enforced)

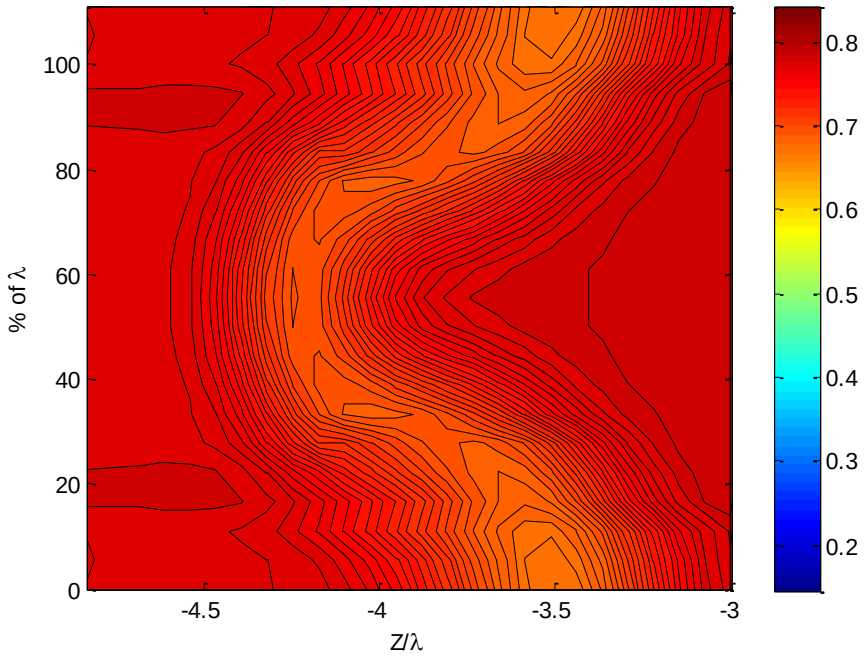

Figure 3.39 TE-7 Streamwise Velocity (U/U_∞) cross-section at 1.6 Axial Chords Downstream (symmetry enforced)

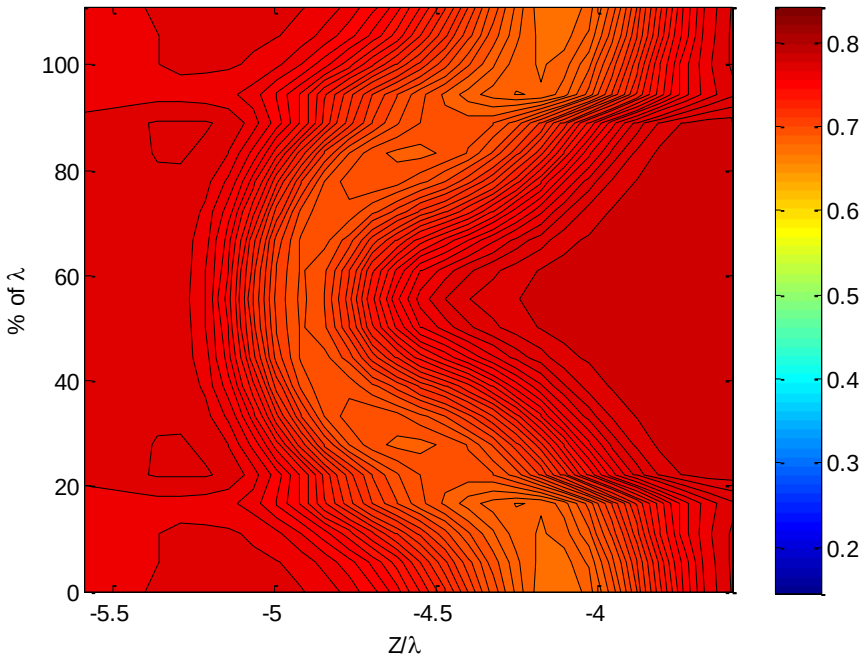

Figure 3.40 TE-7 Streamwise Velocity cross-section at 1.88 Axial Chords Downstream (symmetry enforced)

The streamwise velocity plots give significant insight into how this vortex generation technology dramatically affects the shape of the wake behind the trailing edge. It is interesting to note that,

although there is an increased velocity deficit at the 0% and 100% λ spanwise locations, the 50% λ location actually has a smaller velocity deficit than the baseline when normalized on the velocity of the potential core. The baseline blade shows a normalized velocity, U/U_{edge}, of 0.85, while the TE-7 configuration produces U/U_{edge} = 0.90, indicating a nearly 6% increase in the velocity deficit compared to the baseline at 0.4 axial chords downstream. Because this improvement at the centerspan location was also apparent with the TE-1 configuration, this suggests that the introduction of vorticity can actually cause a smaller momentum deficit at certain locations across its spanwise period regardless of the technique used to do so. At the two furthest downstream locations, small discontinuities become apparent in the streamwise velocity contours. These discontinuities are a byproduct of minor measurement errors and are insignificant to the flow.

Wake aligned velocity components perpendicular to the streamwise direction show the three dimensional effects of both the blade and the TE7 vortex generator configuration. The following figures are presented in the flow-aligned coordinate system described in Section 2.1.3 of this report. These velocity cross-sections again show how each component of the flow propagates downstream of the blade trailing edge, and are presented in **Figure 3.41** through **Figure 3.48**. As these figures show, the TE-7 trailing edge configuration adds only a small amount of velocity in both the pitchwise and spanwise direction. At 0.1 axial chords downstream (**Figure 3.41**), the v- and w- wake flow aligned velocity components have a maximum absolute value of $0.098U_{\infty}$ and $0.112U_{\infty}$, respectively. Once the flow reaches 0.4 axial chords downstream (**Figure 3.43**), the maximum v- and w- wake aligned velocities drop to $0.043U_{\infty}$ and $0.078U_{\infty}$, respectively. In contrast, at this same downstream location (**Figure 3.19**), the v- and w- velocity components of TE-7 are about 54% and 71% of the intensity of the TE-1 configuration, respectively.

As the wake propagates to the furthest downstream locations, the v- and w- velocity components rapidly diminish while the overall structures remain constant. Throughout all the plots, the v-velocity components (in the spanwise direction), suggest that there is an opposing shear across the spanwise period. At approximately 80% λ_{TE7}, the suction side of the trailing edge is producing a negative spanwise velocity, while the pressure side produces an opposing positive spanwise velocity. The mirror image about the 50% λ_{TE7} location is apparent at 30% λ_{TE7}. As the wake widens downstream, the regions of spanwise velocity begin to spread while the intensity drops. At 1.6 axial chords downstream the v-velocity has reduced to $.027U_{\infty}$ (**Figure 3.47**), and remains nearly constant as the wake convects to the farthest downstream location of 1.6 axial chords seen in **Figure 3.48**.

The structure of the w-velocity component helps explain the overall shape of the streamwise velocity plots seen in **Figure 3.33**. At the 0% and 100% λ locations there is a velocity component in the positive direction, coupled with a w-velocity in the negative direction at the 50% λ location. The positive w-velocity components at the top and bottom of the serration period are effectively pulling the wake towards the suction side of the blade at these locations. While this occurs, the region of negative velocity is causing the wake to shift towards the pressure side of the blade, which explains the corrugated nature of the streamwise wake contours seen in **Figure 3.33** through **Figure 3.40**. From its initial peak value of $0.11U_{\infty\ at}$ 0.1axial chords downstream (**Figure 3.41**), the w-velocity component begins to diminish to a value of $0.064\ U_{\infty}$ at 0.84 axial chords downstream (**Figure 3.45**). This decline in

intensity then slowly drops to its final value of .062 U_∞ at the furthest measured downstream location of 1.88 axial chords (**Figure 3.48**).

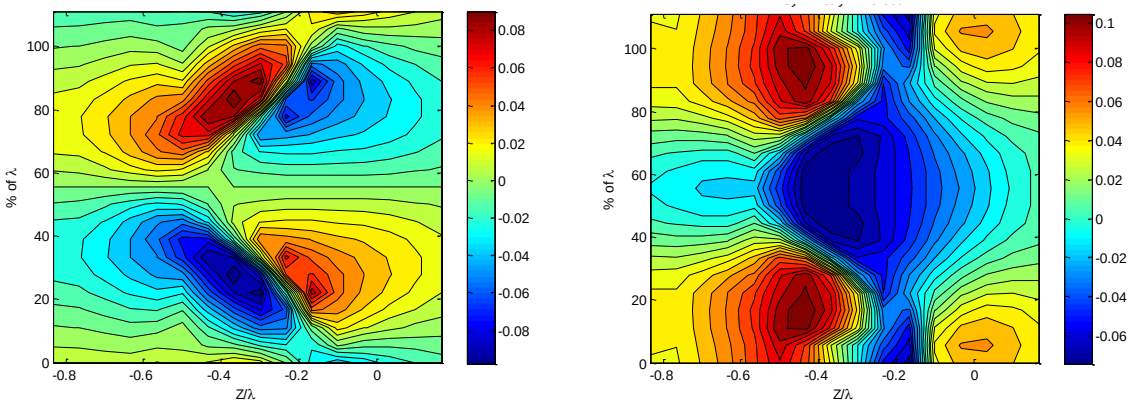

Figure 3.41 Spanwise (V/U_∞, left) and Lateral (W/U_∞, right) Velocity cross-sections (m/s) for TE-7 at $0.1c_a$ Downstream (symmetry enforced)

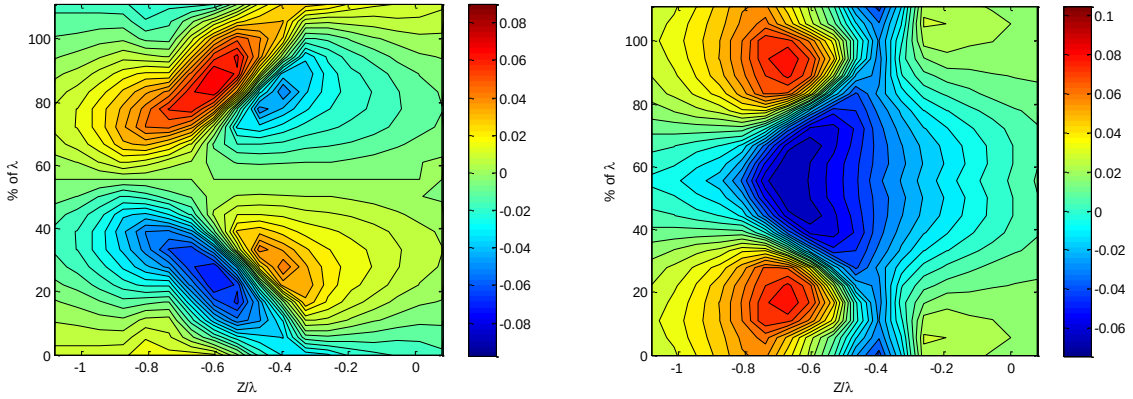

Figure 3.42 Spanwise (left) and Lateral (right) Velocity cross-sections (m/s) for TE-7 at $0.2c_a$ Downstream (symmetry enforced)

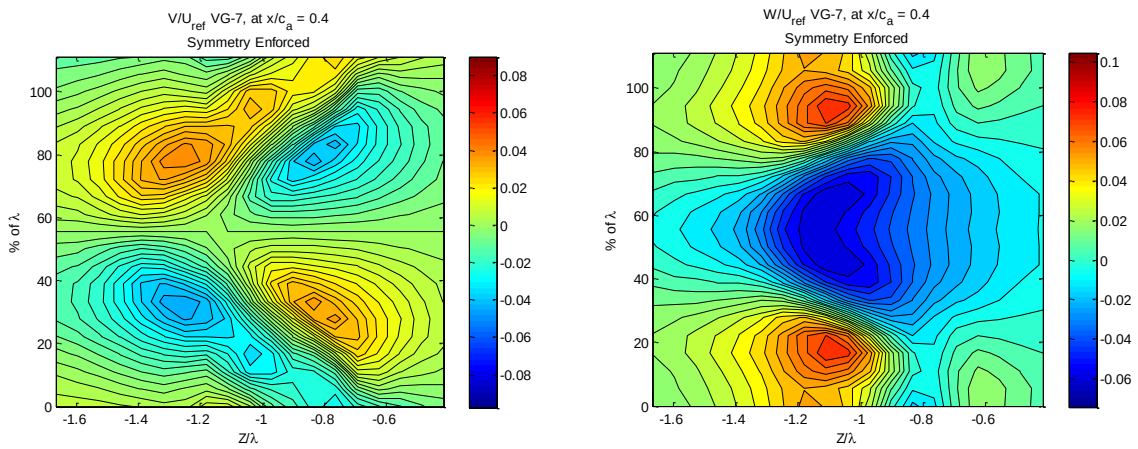

Figure 3.43 Spanwise (left) and Lateral (right) Velocity cross-sections (m/s) for TE-7 at $0.4c_a$ Downstream (symmetry enforced)

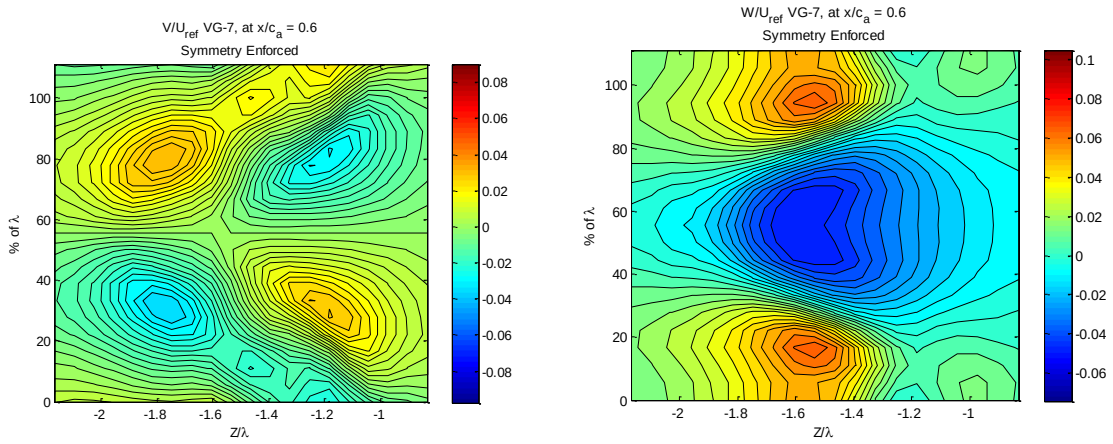

Figure 3.44 Spanwise (left) and Lateral (right) Velocity cross-sections (m/s) for TE-7 at $0.6c_a$ Downstream (symmetry enforced)

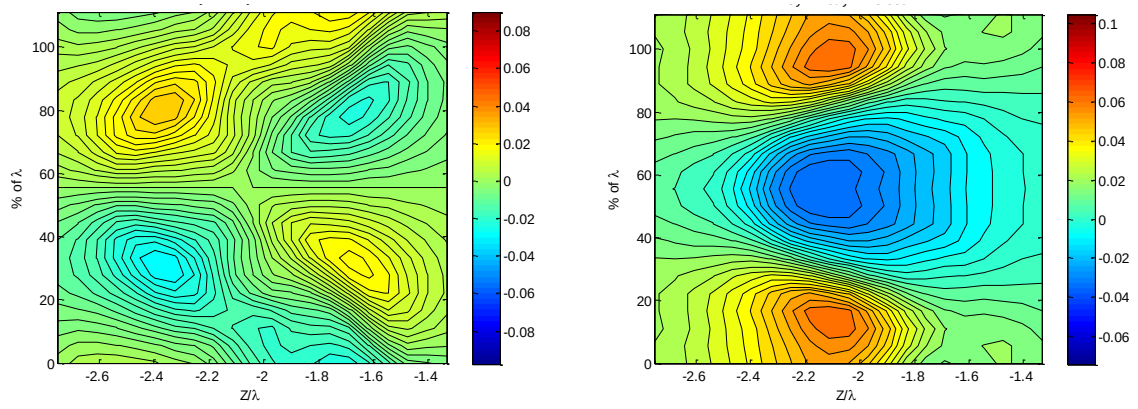

Figure 3.45 Spanwise (left) and Lateral (right) Velocity cross-sections (m/s) for TE-7 at $0.84c_a$ Downstream (symmetry enforced)

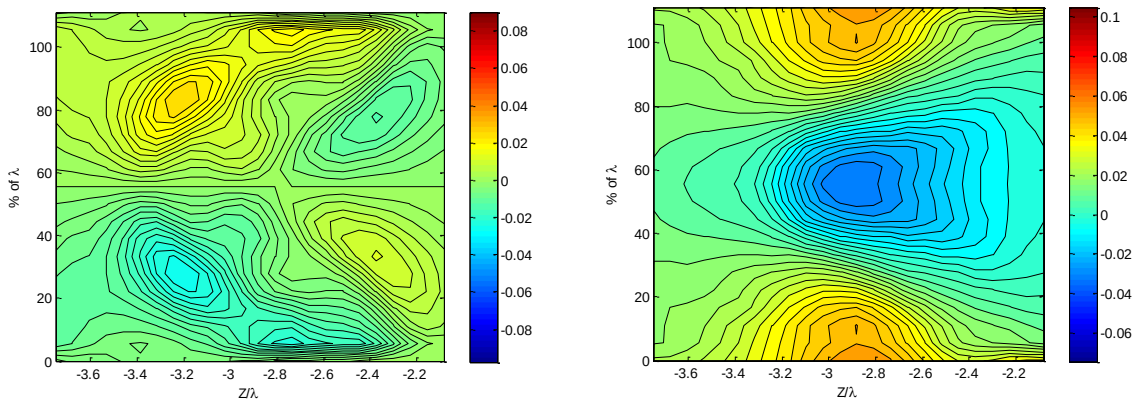

Figure 3.46 Spanwise (left) and Lateral (right) Velocity cross-sections (m/s) for TE-7 at 1.18c_a Downstream (symmetry enforced)

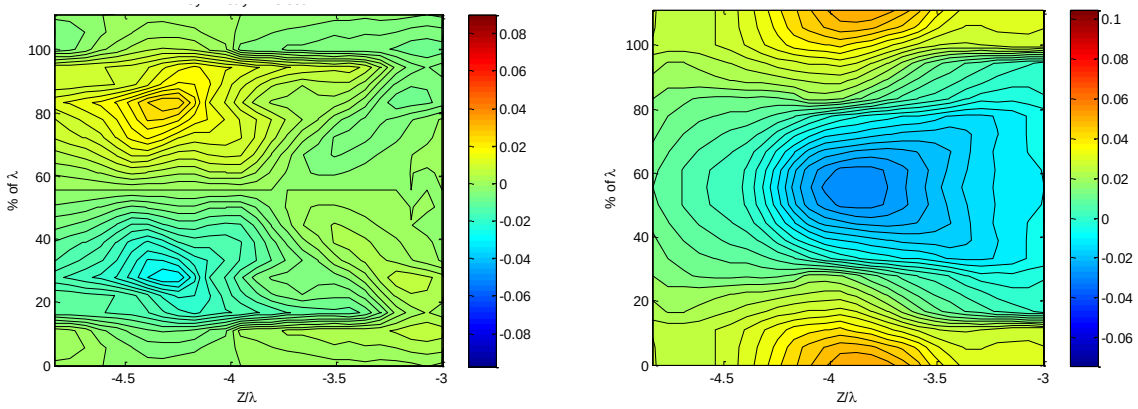

Figure 3.47 Spanwise (left) and Lateral (right) Velocity cross-sections (m/s) for TE-7 at 1.6c_a Downstream (symmetry enforced)

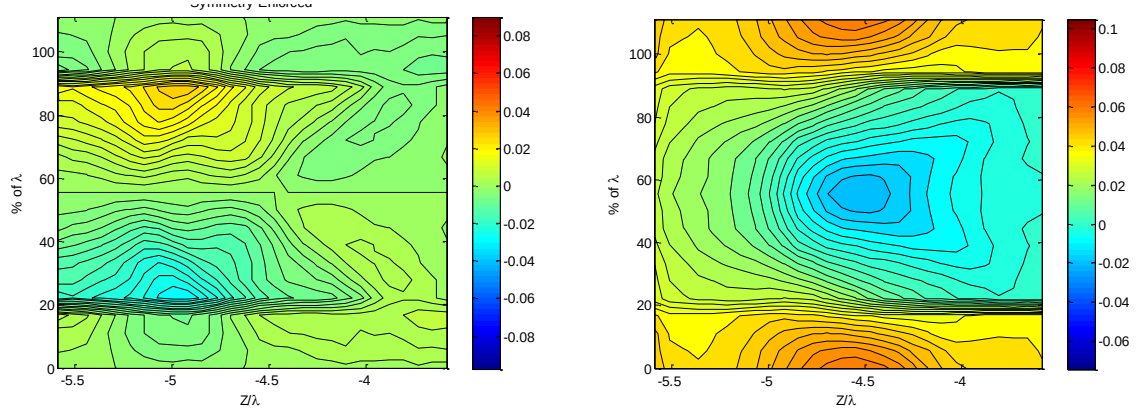

Figure 3.48 Spanwise (left) and Lateral (right) Velocity cross-sections (m/s) for TE-7 at 1.88c_a Downstream (symmetry enforced)

3.3.2.2 TE-7 Streamwise Vorticity Measurements and Analysis

The streamwise vorticity plots resulting from the TE-7 configuration are presented in **Figure 3.49** through **Figure 3.56**. These figures indicate that the vorticity levels produced by the TE-7 configuration begin to rapidly decrease as the downstream distance is increased. Starting from the initial point of 0.1 axial chords downstream, the wake travels less than 0.3 axial chords bfore the peak streamwise vorticity is reduced by half. Examining **Figure 3.49** closely shows that 0.1 axial chords downstream of the trailing edge there are alternating regions of positive and negative streamwise vorticity. The maximum value of vorticity produced by the TE7 configuration at 0.1 axial chords downstream is 6.52 c_a/U_∞, and occurs at 22% of the injection period in the negative direction and 88% of the injection period in the positive direction. This region of high vorticity is paired with a region of opposing vorticity that is significantly weaker at 2.19 c_a/U_∞. These two regions of vorticity can be seen to be mirror image of each other across the 50% λ line.

As the wake convects downstream, the vortices maintain the same general structure but lose intensity. Additionally, the vortices appear to grow larger until 0.84 axial chords downstream (**Figure 3.53**), after which the vortices no longer appear to enlarge but the intensity diminishes. **Figure 3.56** shows that as the wake reaches 1.88 axial chords downstream of the trailing edge, the maximum vorticity drops to 1.23 c_a/U_∞, or 19% of the original measured intensity after propagating 1.78 axial chords downstream. From the 0.4 axial chord location (**Figure 3.51**) the intensity of the maximum streamwise vorticity drops to 35% of the original intensity after convecting 1.2 axial chords downstream (**Figure 3.55**).

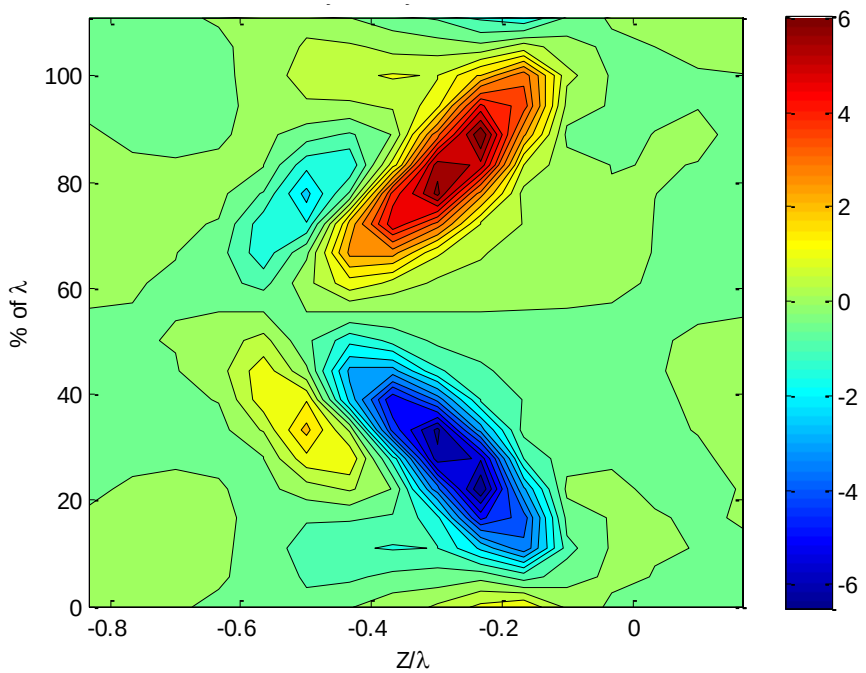

Figure 3.49 Streamwise Vorticity Contour of TE-7 at 0.1 Axial Chords Downstream (symmetry enforced, normalized on c_a and U_∞)

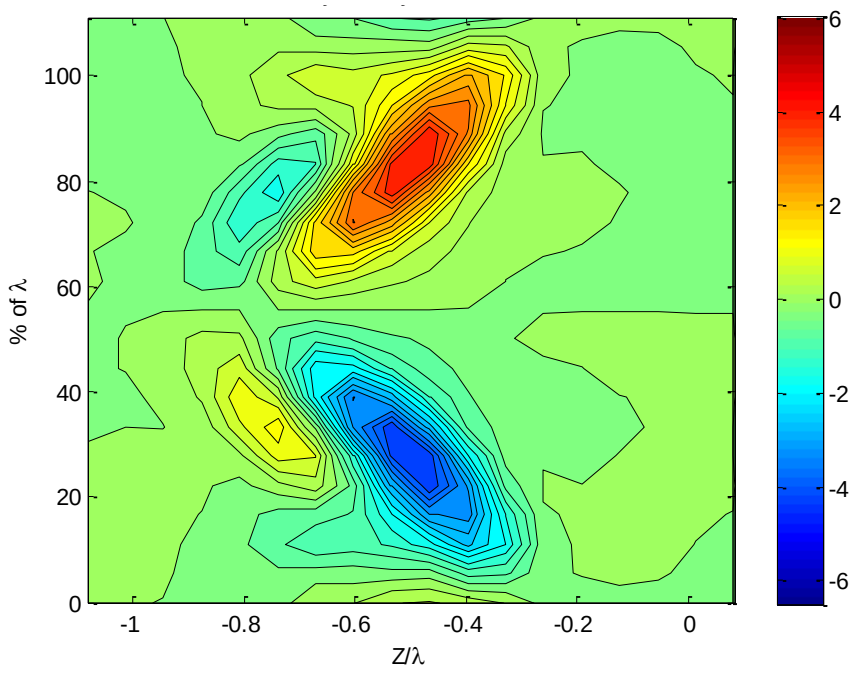

Figure 3.50 Streamwise Vorticity Contour of TE-7 at 0.2 Axial Chords Downstream (symmetry enforced)

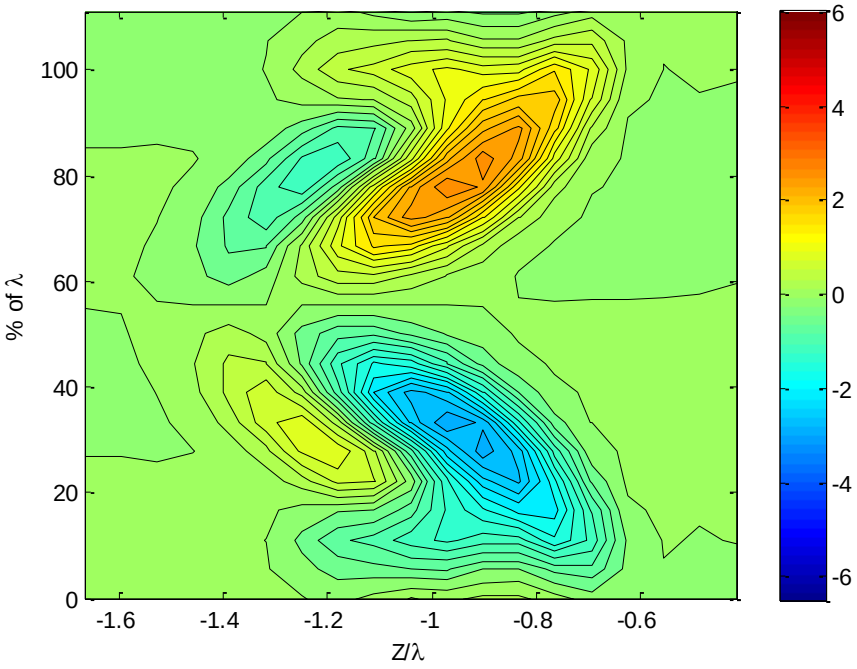

Figure 3.51 Streamwise Vorticity Contour of TE-7 at 0.4 Axial Chords Downstream (symmetry enforced)

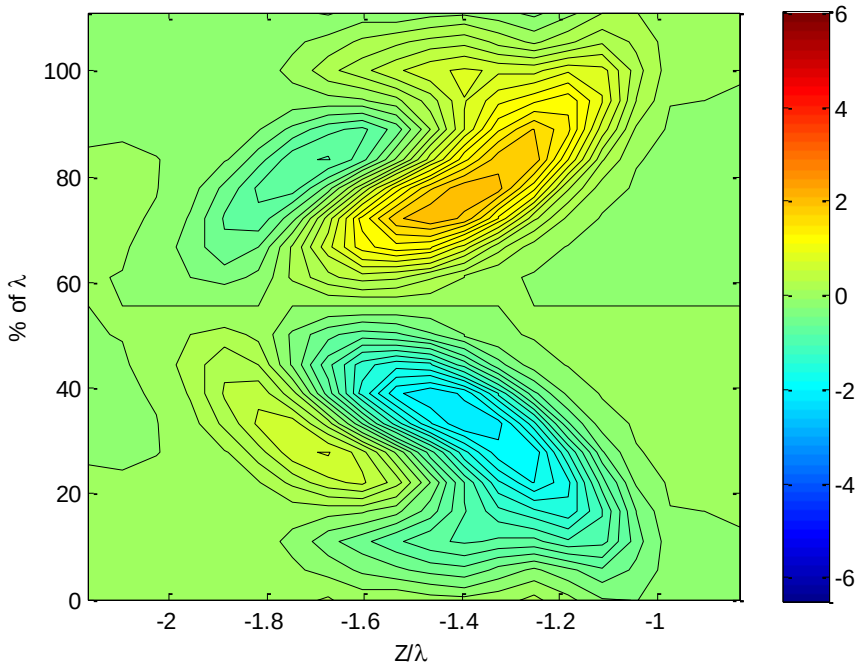

Figure 3.52 Streamwise Vorticity Contour of TE-7 at 0.6 Axial Chords Downstream (symmetry enforced)

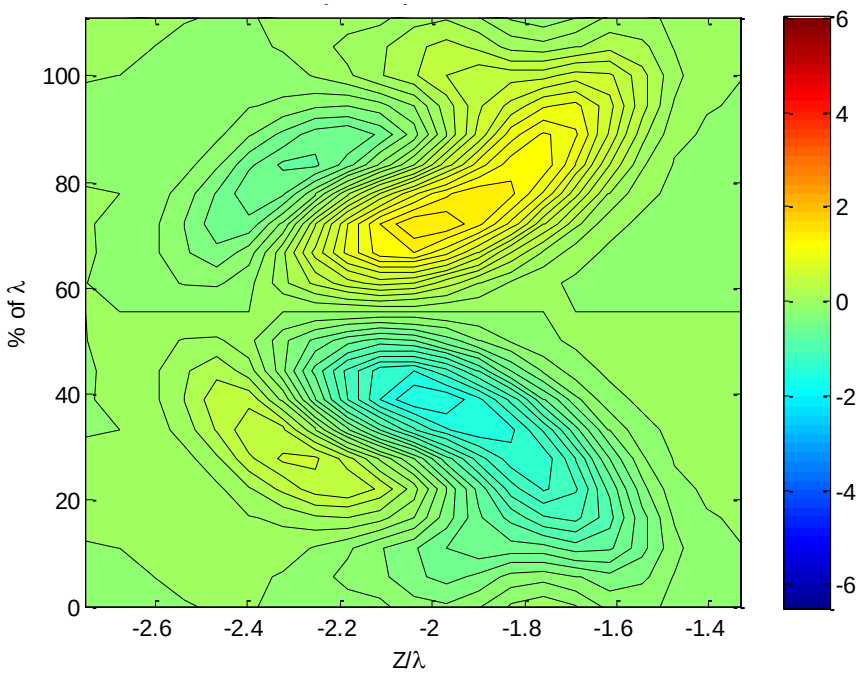

Figure 3.53 Streamwise Vorticity Contour of TE-7 at 0.84 Axial Chords Downstream (symmetry enforced)

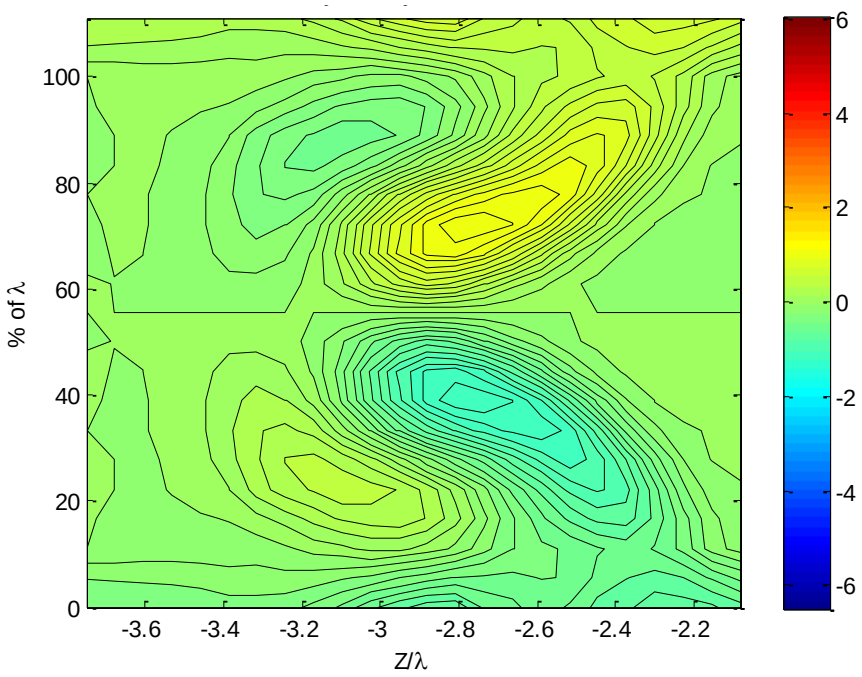

Figure 3.54 Streamwise Vorticity Contour of TE-7 at 1.18 Axial Chords Downstream (symmetry enforced)

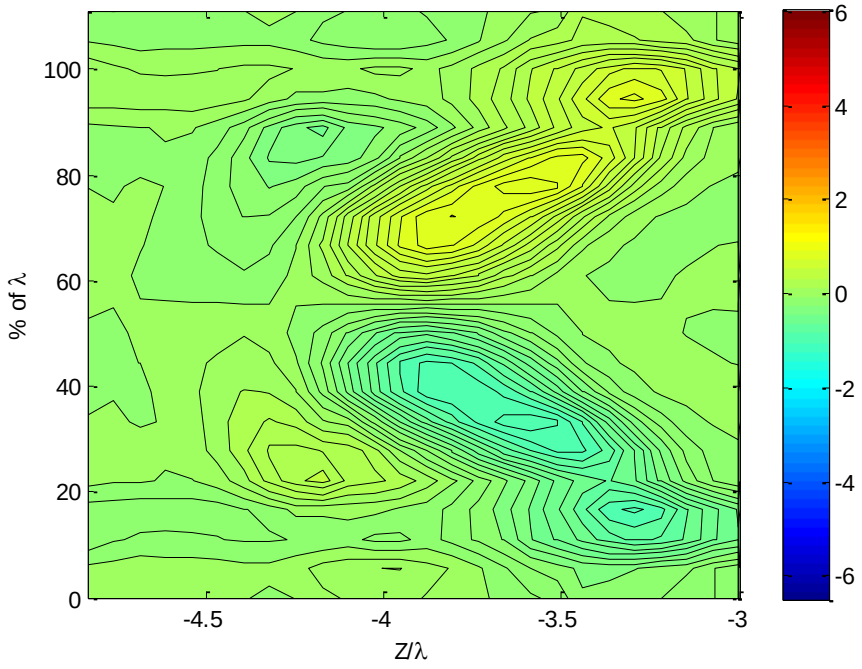

Figure 3.55 Streamwise Vorticity Contour of TE-7 at 1.6 Axial Chords Downstream (symmetry enforced)

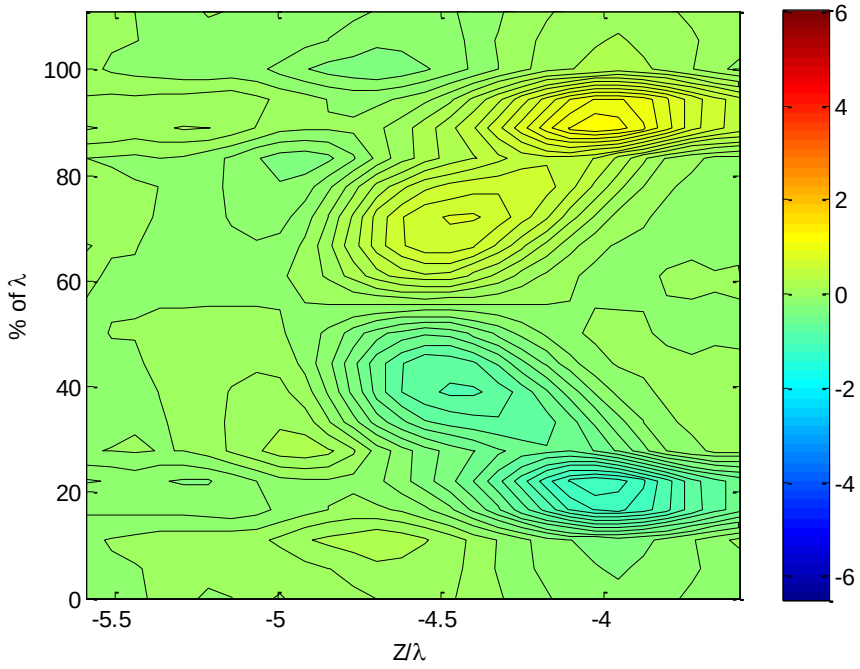

Figure 3.56 Streamwise Vorticity Contour of TE-7 at 1.88 Axial Chords Downstream (symmetry enforced)

3.3.2.3 TE-7 Mean Turbulence Kinetic Energy Analysis

The following section presents the spanwise cross section of the mean turbulence kinetic energy, TKE, for the TE7 configuration. As with the velocity and vorticity plots, the TKE coordinate system is normalized on the spanwise period, λ, of the vortex generator placement. No gradient error corrections have been applied to the following TKE data.

Starting from **Figure 3.57**, it can be seen that the wake turbulence has a highest value at the 0% and 100% λ location. The TKE is at a minimum at the 50 percent span location. The highest value of TKE is measured just above the 100 percent λ_{TE7} location reaches $0.0289U_\infty^2$ at 0.1 axial chords downstream. The minimum TKE value occurs just above the 50 percent λ_{TE7} location and measures $0.0088U_\infty^2$ at 0.1 axial chords downstream of the trailing edge.

As the wake propagates downstream, **Figure 3.58** through **Figure 3.64** show the rapid decline in observed TKE levels. As this occurs, the turbulence can also be seen dispersing further into the freestream, which essentially widens the area subjected to turbulence downstream of the trailing edge. At the furthest measured location of 1.88 axial chords downstream of the trailing edge, the peak TKE is measured as $0.0037U_\infty^2$, while the minimum wake TKE level drops to $0.0016U_\infty^2$. While the wake turbulence levels decrease, the locations of peak TKE do not appear to show significant spanwise drift as the turbulence becomes more uniform throughout the wake.

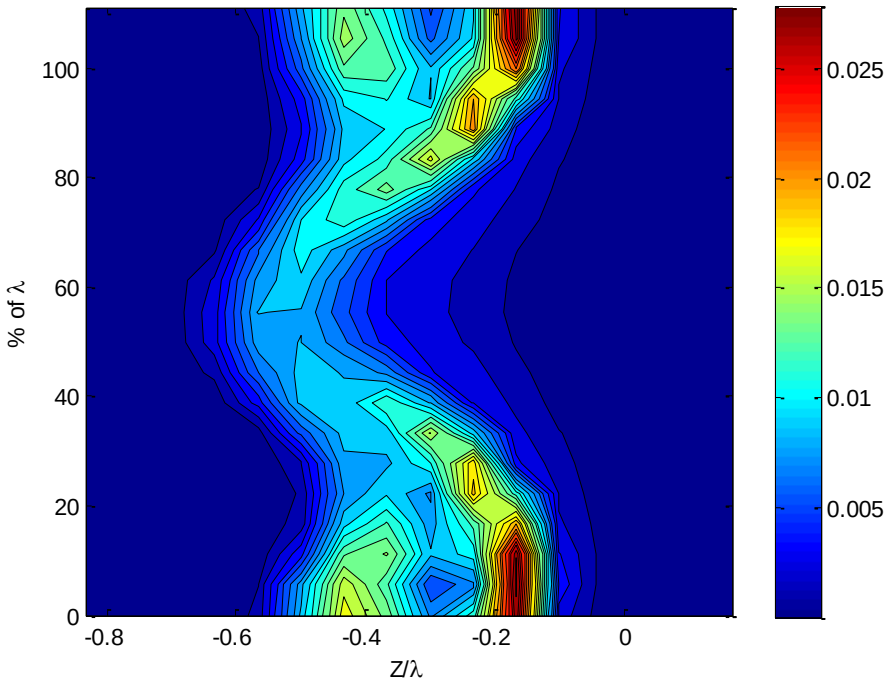

Figure 3.57 Mean Turbulence Kinetic Energy Profile of TE-7 at 0.1 Axial Chords Downstream

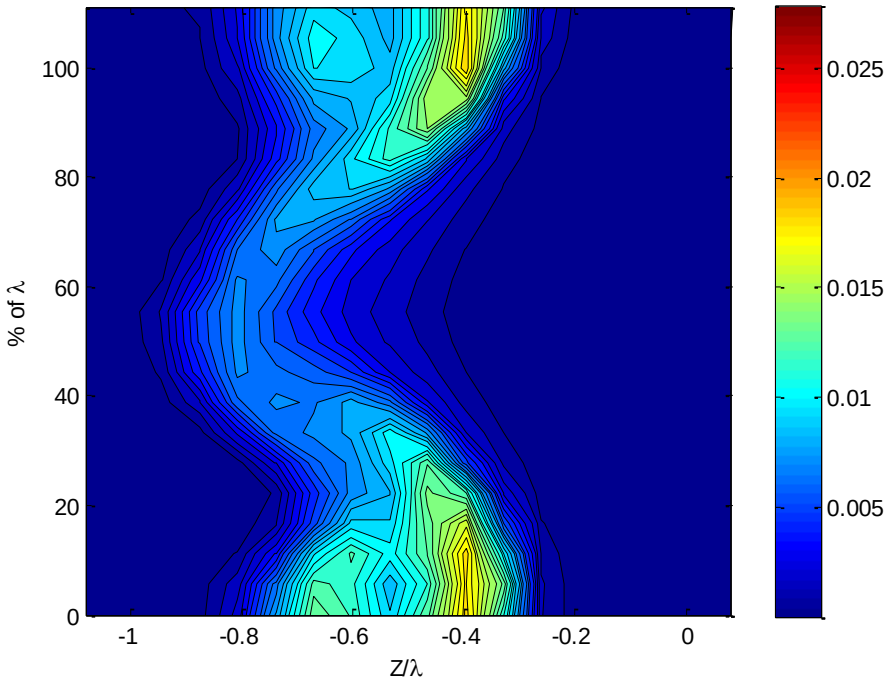

Figure 3.58 Mean Turbulence Kinetic Energy Profile of TE-7 at 0.2 Axial Chords Downstream

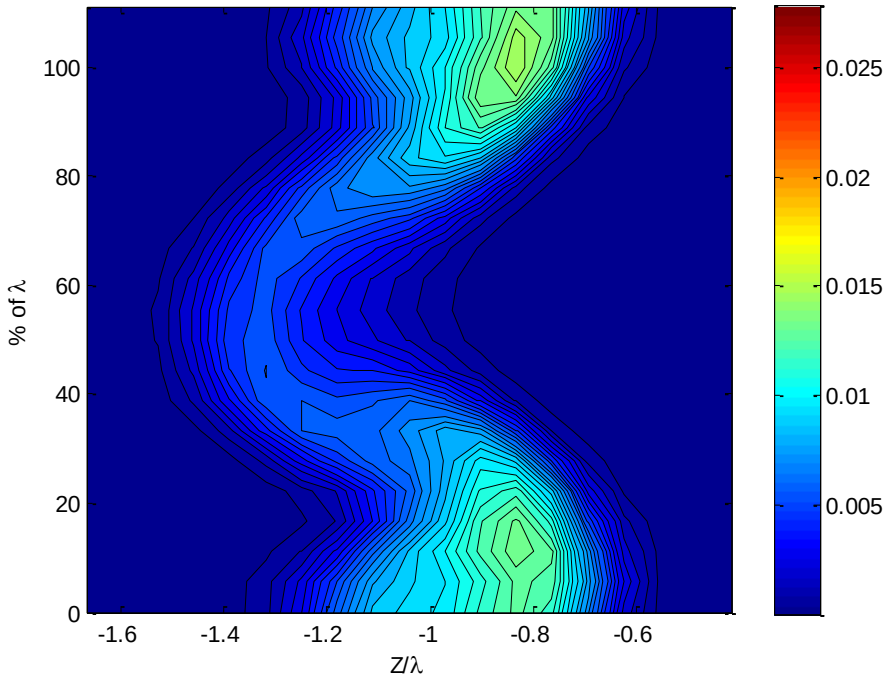

Figure 3.59 Mean Turbulence Kinetic Energy Profile of TE-7 at 0.4 Axial Chords Downstream

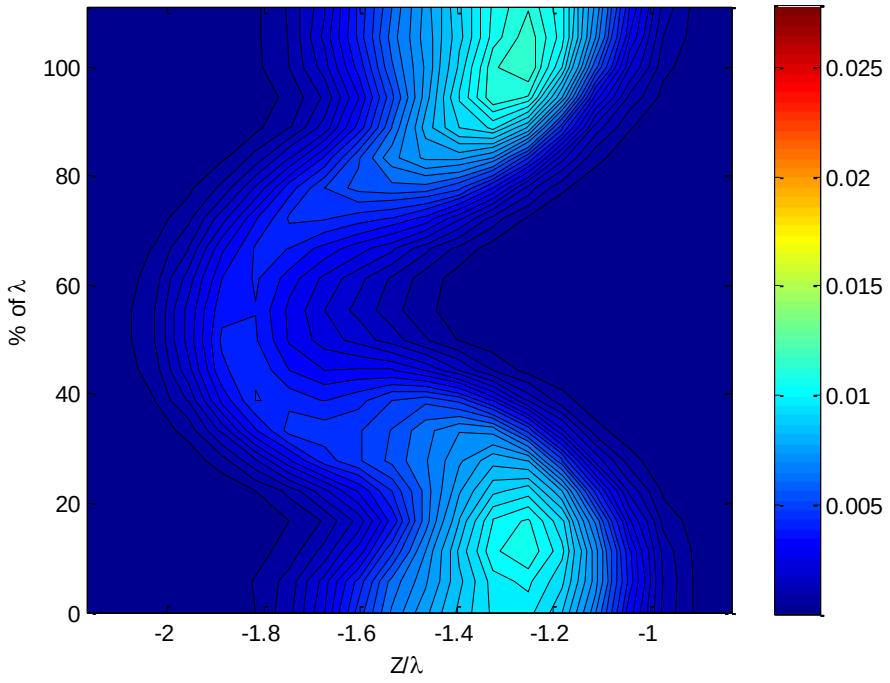

Figure 3.60 Mean Turbulence Kinetic Energy Profile of TE-7 at 0.6 Axial Chords Downstream

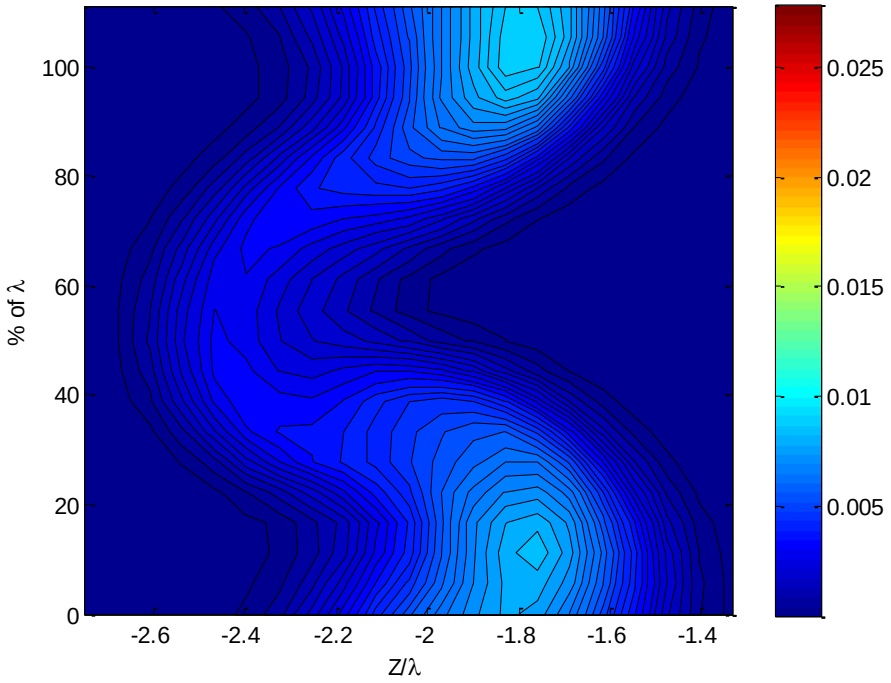

Figure 3.61 Mean Turbulence Kinetic Energy Profile, TE-7 at 0.84 Axial Chords Downstream

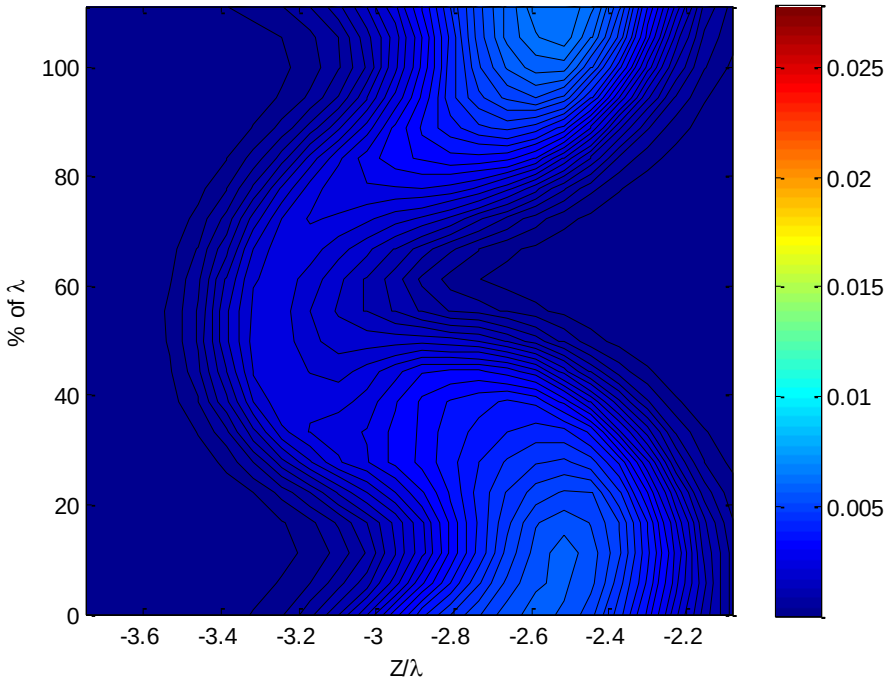

Figure 3.62 Mean Turbulence Kinetic Energy Profile, TE-7 at 1.18 Axial Chords Downstream

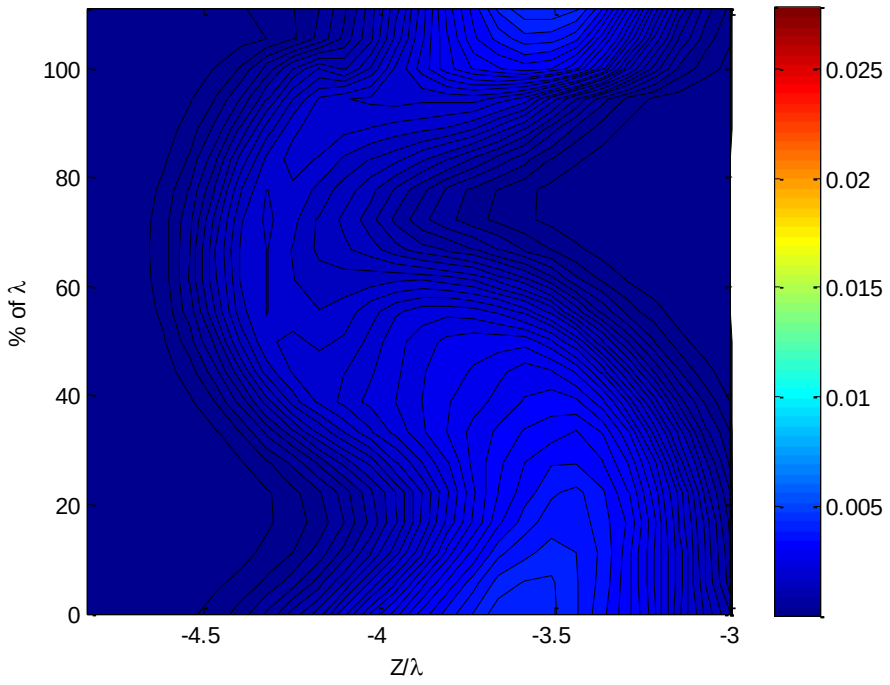

Figure 3.63 Mean Turbulence Kinetic Energy Profile of TE-7 at 1.6 Axial Chords Downstream

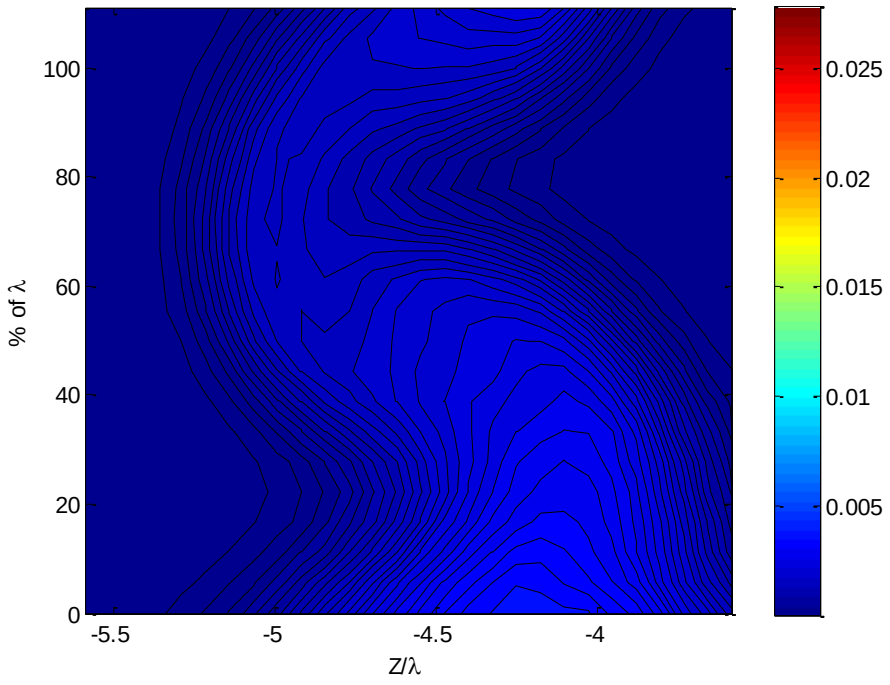

Figure 3.64 Mean Turbulence Kinetic Energy Profile, TE-7 at 1.88 Axial Chords Downstream

3.3.3 Detailed Analysis of Vortex Generator Configuration TE-8

The following sections detail the four-sensor hotwire measurements taken at eight locations downstream of the trailing edge. The data presented in this section is normalized on the spanwise period of the vortex generation, λ_{TE8}. Data was extracted from the vortex generator period that encompasses the midspan section of the airfoil. These quadwire measurements were taken in a fashion similar to the quadwire measurements described in Section 3.2.2, and each of the velocity cross-sections presented are normalized on the free stream inlet velocity, U_∞. Gradient errors as described in Section 2.2.2.3 are corrected for the TE-8 configuration.

3.3.3.1 TE-8 Wake Velocity cross-section Measurements

The first and most interesting velocity measurement is the change in streamwise velocity as a result of the trailing edge configuration. **Figure 3.65** through **Figure 3.72** show how the streamwise velocity distribution changes as the wake convects from 0.1 to 1.88 axial chords downstream of the trailing edge. The horizontal axes of these figures represent the pitchwise distance across the blade wake normalized on λ_{TE8}, and the vertical axis shows the spanwise location measured as a percentage of λ.

Figure 3.65 shows the streamwise velocity component at a distance of 0.1 axial chords downstream of the baseline trailing edge. The overall shape of the wake resulting from the TE-8 configuration can be seen. The two lobes of maximum velocity deficit appear to be further towards the pressure side of the blade (positive Z/λ) when compared to the centerspan region. As with the TE-7 configuration (**Figure 3.33**), these two lobes of high velocity deficit sandwich a region of smaller velocity deficit located around the centerspan of λ_{TE8}. This region of thinner wake with a smaller velocity deficit appears between 40% and 80% of λ_{TE8}. The centerline velocity in this region is $0.46U_{ref}$ compared to the $0.12U_\infty$ found in the two lobes of maximum deficit at the 0% and 100% λ_{TE8} locations. The wake profile of the TE-8 configuration appears to be corrugated in a manner similar to that of the TE-7 configuration across all downstream locations. This suggests that the vorticity produced by the TE-8 configuration is able to produce wake stretching to a similar degree as TE-7.

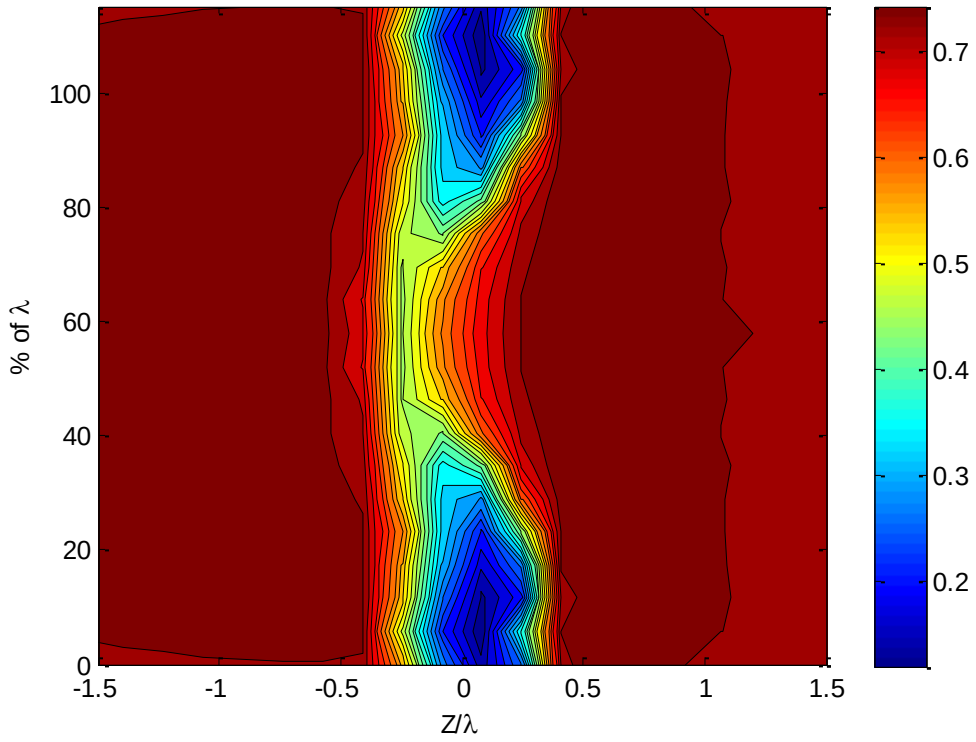

Figure 3.65 TE-8 Streamwise Velocity (U/U_∞) cross-section at 0.1 Axial Chords Downstream (symmetry enforced)

As the wake convects further downstream, **Figure 3.66** shows the wake development to 0.2 axial chords. The general structure of the wake seen at 0.1 axial chords downstream remains intact, but it can be seen that the thickness has begun to slightly increase. This trend continues as the wake propagates further downstream as shown in the remaining figures.

Once the wake reaches a downstream distance of 0.4 axial chords (**Figure 3.67**), the streamwise velocity deficits observed are significantly reduced, indicating the flow is mixing with the freestream. By 0.4 axial chords downstream, the two lobes of maximum velocity deficit seen at 0% and 100% of λ increase to $0.39U_\infty$, and the centerspan region increases to $0.59U_\infty$. Thus, these observed maximum and minimum centerline velocities for TE-8 are slightly lower than those observed for the TE-7 configuration at this downstream location (**Figure 3.35**).

At each of the eight downstream locations measured for the TE-8 configuration, the lobes of maximum velocity deficit maintain their position at just above 0 percent and just above 100 percent of λ_{TE8}, indicating a function similar to the TE-7 configuration. This method of producing streamwise vorticity does not appear to cause significant spanwise drift in the wake.

Comparing the streamwise velocities at each location downstream shows that as the wake convects, the mean velocity deficit becomes smaller. At 0.4 axial chords downstream of the trailing edge (**Figure 3.67**) the lobe at 100 percent λ_{TE8} has a minimum streamwise velocity of 53.4% of the potential flow velocity outside of the wake. Once the wake reaches 1.6 axial chords downstream (**Figure**

3.71), the minimum velocity of this lobe increases to 86% of the potential core velocity. Finally, as the wake propagates to the farthest downstream position measured (**Figure 3.40**) the minimum velocity measured in this lobe reaches 86.1% of the potential core velocity, while the centerspan location reaches 90.5% of the potential core velocity.

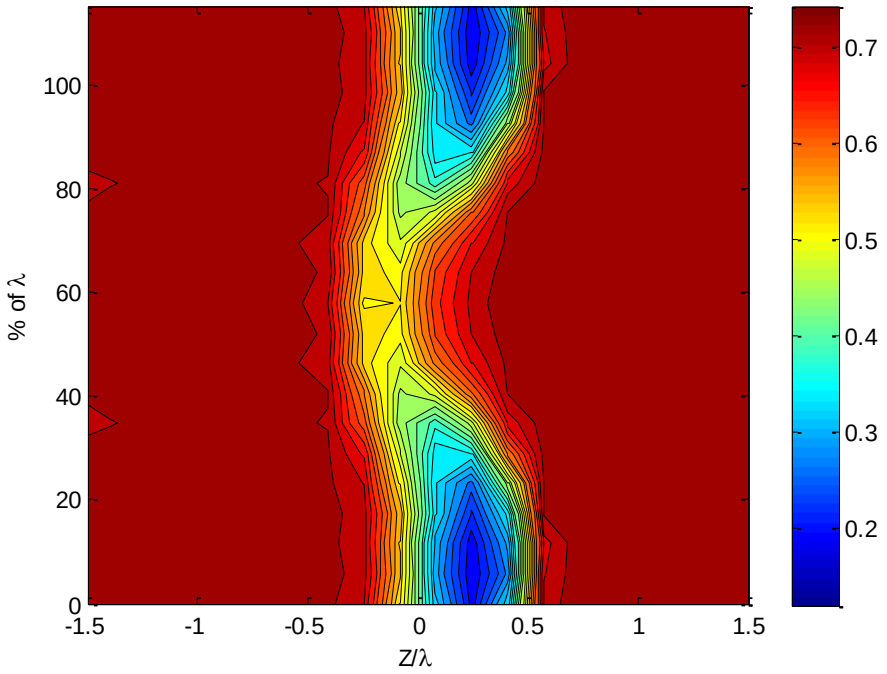

Figure 3.66 TE-8 Streamwise Velocity (U/U_∞) cross-section at 0.2 Axial Chords Downstream (symmetry enforced)

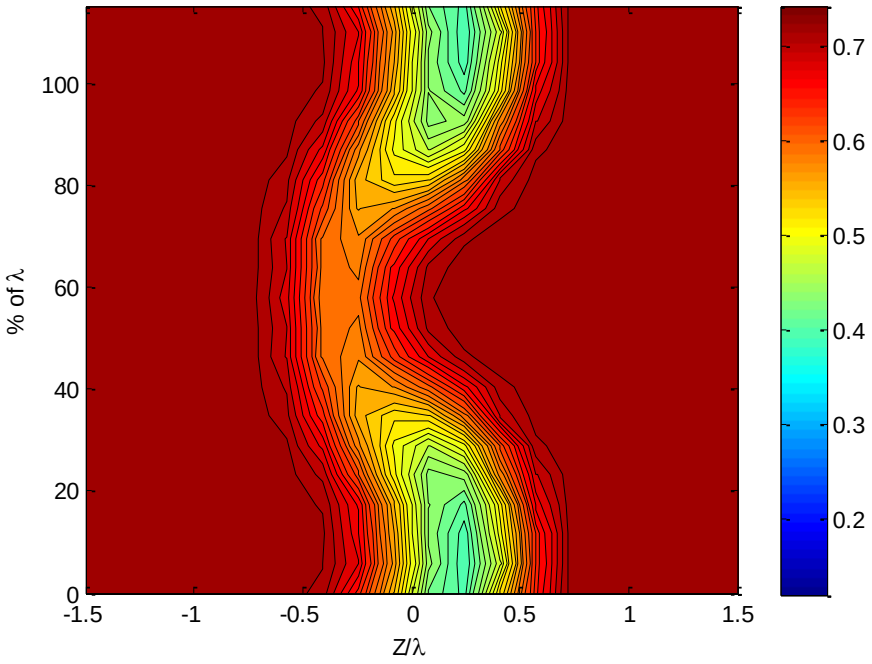

Figure 3.67 TE-8 Streamwise Velocity (U/U_∞) cross-section at 0.4 Axial Chords Downstream (symmetry enforced)

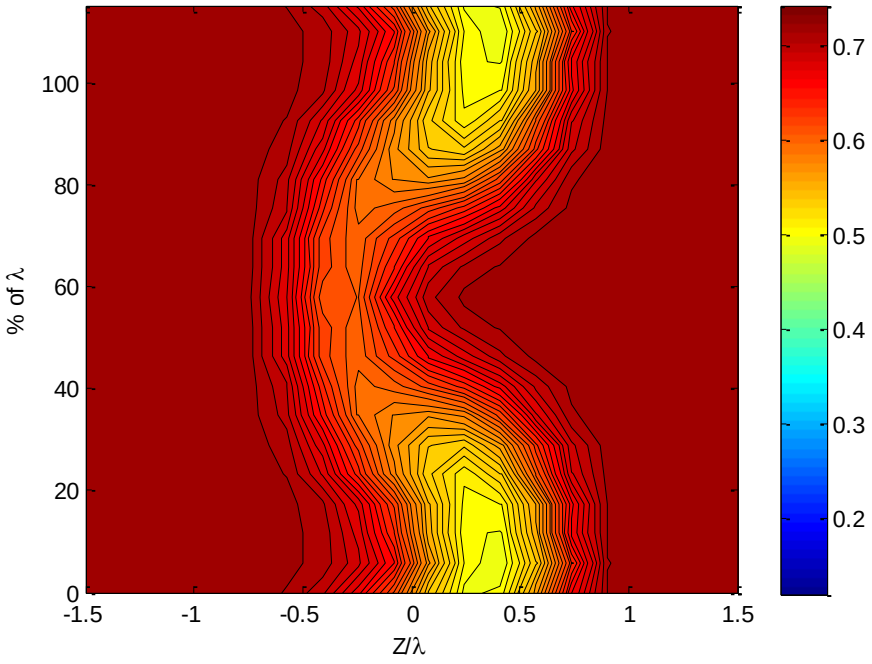

Figure 3.68 TE-8 Streamwise Velocity (U/U_∞) cross-section at 0.6 Axial Chords Downstream (symmetry enforced)

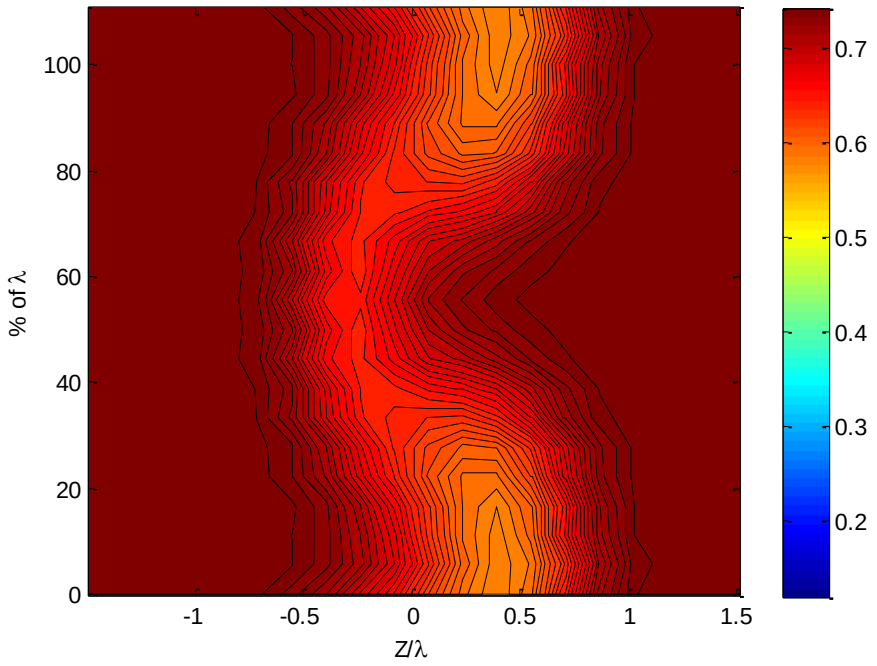

Figure 3.69 TE-8 Streamwise Velocity (U/U_∞) cross-section at 0.84 Axial Chords Downstream (symmetry enforced)

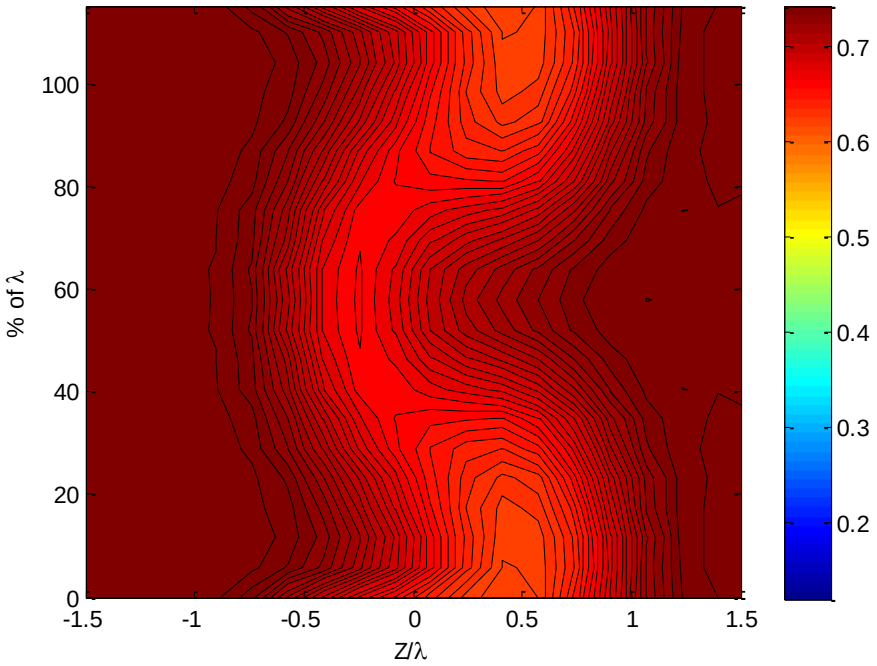

Figure 3.70 TE-8 Streamwise Velocity (U/U_∞) cross-section at 1.18 Axial Chords Downstream (symmetry enforced)

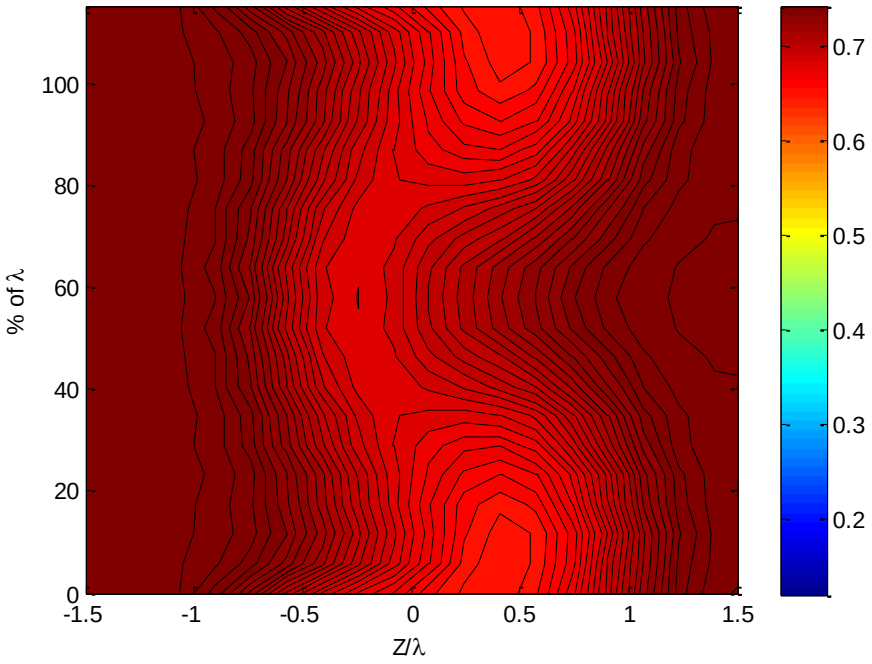

Figure 3.71 TE-8 Streamwise Velocity (U/U_∞) cross-section at 1.6 Axial Chords Downstream (symmetry enforced)

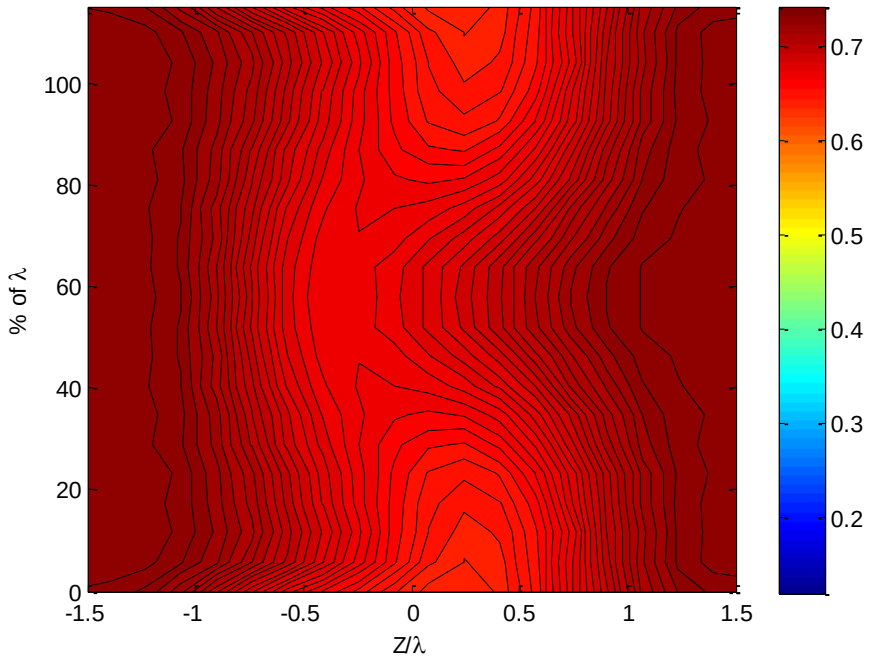

Figure 3.72 TE-8 Streamwise Velocity (U/U_∞) cross-section at 1.88 Axial Chords Downstream (symmetry enforced)

Wake aligned velocity components perpendicular to the streamwise direction show the three dimensional effects produced by the TE-8 configuration. The following figures are presented in the flow-

aligned coordinate system described in Section 2.1.3 of this report. These velocity cross-sections again show how each component of the flow propagates downstream of the blade trailing edge, and are presented in **Figure 3.73** through **Figure 3.80**. As these figures show, this trailing edge design does produce a small amount of velocity perpendicular to the streamwise direction. At 0.1 axial chords downstream (**Figure 3.73Figure 3.41**), the v- and w- wake flow aligned velocity components have a maximum absolute value of $0.082U_\infty$ and $0.106U_\infty$, respectively. The TE-7 velocities at this downstream location had values of .098 U_∞ in the v-direction and 0.112 U_∞ in the w-direction (**Figure 3.41**). This indicates that the TE-8 configuration is slightly less effective at producing velocities in the perpendicular to streamwise directions.

Once the flow reaches 0.4 axial chords downstream (**Figure 3.75**), the maximum v- and w- wake aligned velocities drop to $0.025U_\infty$ and $0.078U_\infty$, respectively. In contrast, at this same downstream location the v- and w- velocity components of TE-7 (**Figure 3.43**) measure 0.043 U_∞ and 0.078 U_∞, respectively. It is interesting to note that the v-velocity component of the TE-8 configuration drops of significantly compared to TE-7, but the w-velocity component remains comparable at this downstream location.

As the wake propagates to the furthest downstream locations, the v- and w- velocity components rapidly diminish while the overall structures remain constant. Throughout all the plots, the v-velocity components (in the spanwise direction), suggest that there is a similar opposing shear across the period of vorticity as with TE-7. At approximately 88% λ_{TE8}, the pressure side of the trailing edge is producing a strong positive spanwise velocity, while the suction side produces an opposing, but slightly weaker, negative spanwise velocity. The mirror images of these structures are apparent at 29% λ_{TE8}. As the wake widens downstream, the regions of high spanwise velocity begin to spread while the magnitude drops. At 1.6 axial chords downstream the v-velocity has reduced to $.0062U_\infty$ (**Figure 3.78**), and remains nearly constant as the wake convects to the farthest downstream location of 1.88 axial chords seen in **Figure 3.80**. When compared with the TE-7 trailing edge configuration, the TE-8 profile reaches this asymptote of v-velocity intensity sooner downstream of the trailing edge.

The structure of the w-velocity component helps explain the overall shape of the streamwise velocity plots seen in **Figure 3.70**. These profiles are nearly identical to those seen in the TE-7 configuration, and highlight similarities between these two configurations. At the 0% and 100% λ locations there is a velocity component in the positive direction, coupled with a w-velocity in the negative direction at the 50% λ location. The positive w-velocity components at the top and bottom of the serration period are effectively pulling the wake towards the suction side of the blade at these locations. While this occurs, the region of negative velocity is causing the wake to shift towards the pressure side of the blade, which explains the corrugated nature of the streamwise wake contours seen in **Figure 3.65** through **Figure 3.72**. From its initial peak value of $0.11U_\infty$ at 0.1 axial chords downstream (**Figure 3.73**), the w-velocity component begins to diminish to a value of 0.036 U_∞ at 0.84 axial chords downstream (**Figure 3.77**). This value is significantly lower than the w-velocity component of 0.064 U_∞ measured for the TE-7 configuration at this downstream location. The decline in intensity then continues to its final value of .007 U_∞ at the furthest measured downstream location of 1.88 axial chords (**Figure 3.80**).

It should be noted that the final w-velocity value of the TE-7 configuration at 1.88 axial chords is as high as .062 U_∞. This suggests that the TE-8 configuration mixes with the freestream significantly faster than the TE-7 configuration. The final v- and w- velocity values of 0.0062 U_∞ in the v-direction and 0.007 U_∞ in the w- direction suggest that, although these velocities start at a value similar to those seen in TE-7, the mixing occurs dramatically faster and these velocity components are negligible by 1.88 axial chords downstream for TE-8.

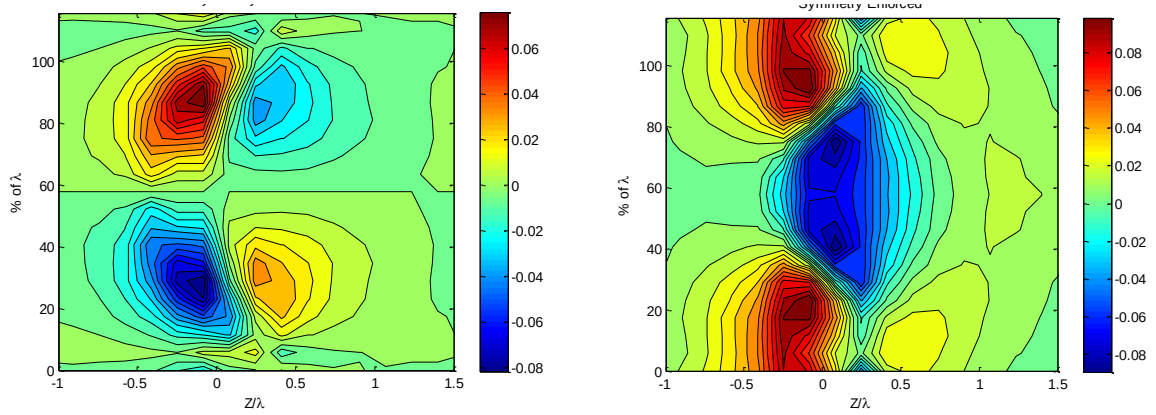

Figure 3.73 Spanwise (V/U_∞, left) and Lateral (W/U_∞, right) Velocity cross-sections for TE-8 at $0.1c_a$ Downstream (symmetry enforced)

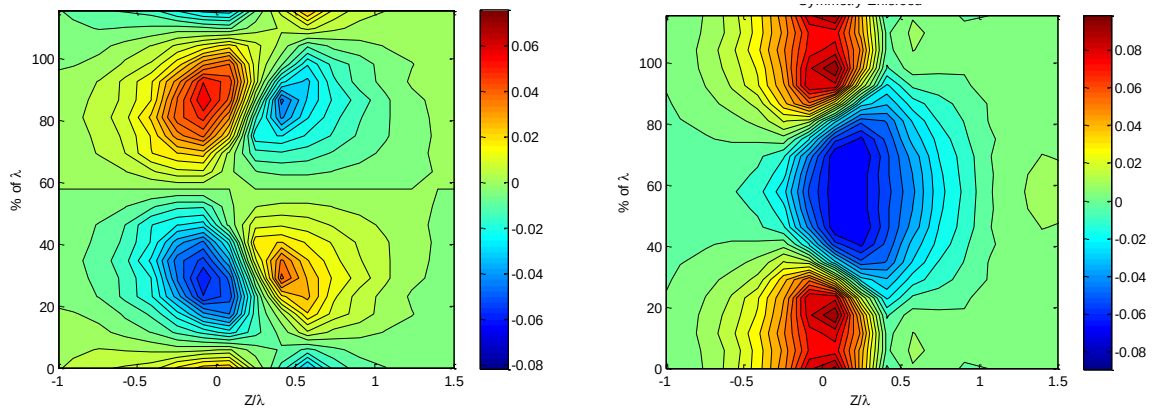

Figure 3.74 Spanwise (left) and Lateral (right) Velocity cross-sections for TE-8 at $0.2c_a$ Downstream (symmetry enforced)

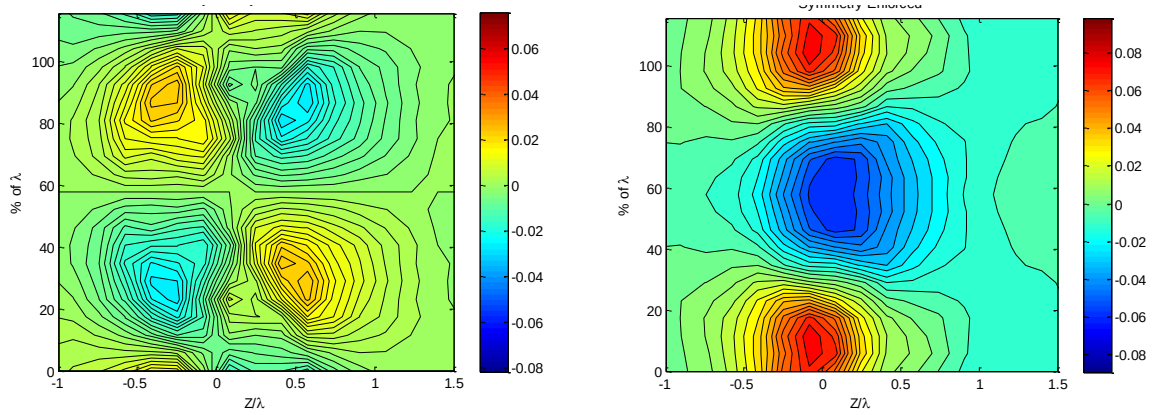

Figure 3.75 Spanwise (left) and Lateral (right) Velocity cross-sections for TE-8 at 0.4c_a Downstream (symmetry enforced)

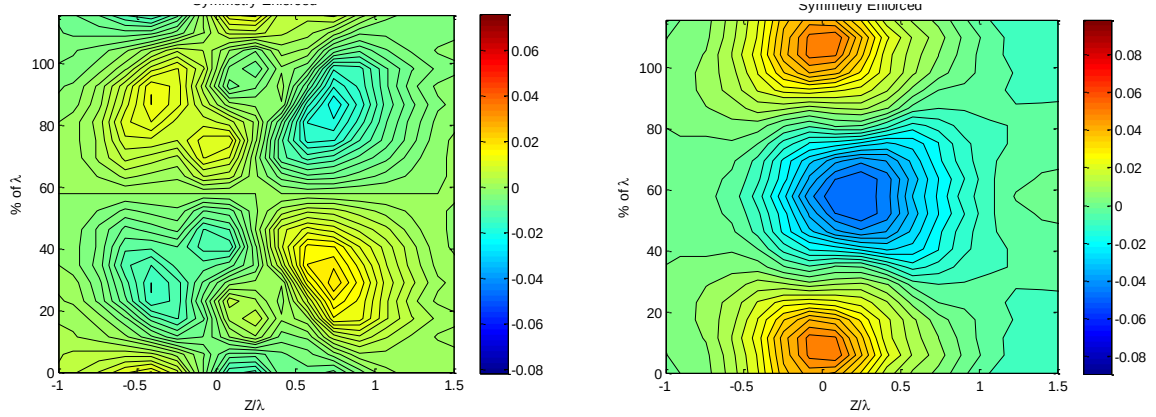

Figure 3.76 Spanwise (left) and Lateral (right) Velocity cross-sections for TE-8 at 0.6c_a Downstream (symmetry enforced)

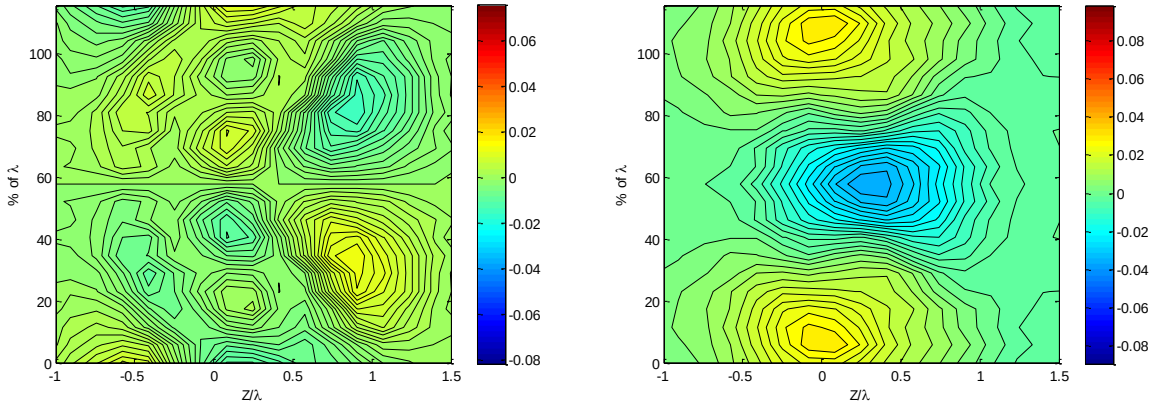

Figure 3.77 Spanwise (left) and Lateral (right) Velocity cross-sections for TE-8 at 0.84c_a Downstream (symmetry enforced)

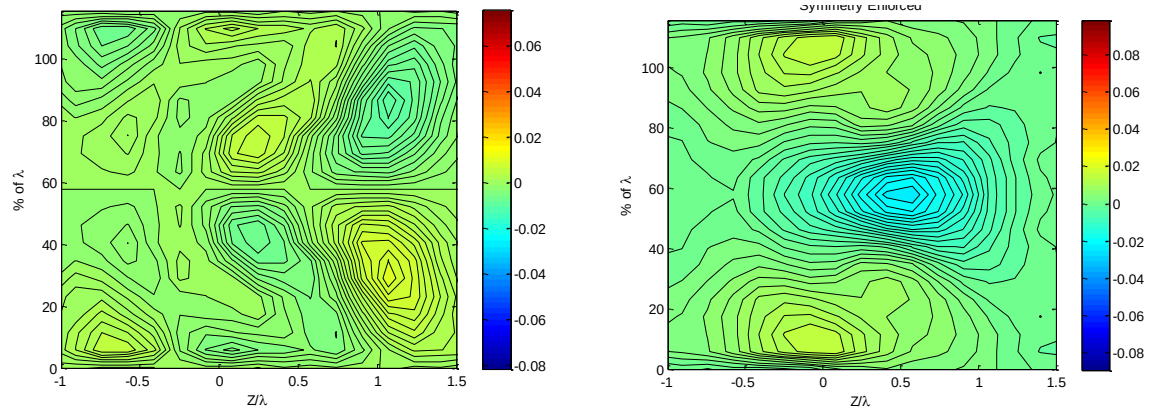

Figure 3.78 Spanwise (left) and Lateral (right) Velocity cross-sections for TE-8 at 1.18c_a Downstream (symmetry enforced)

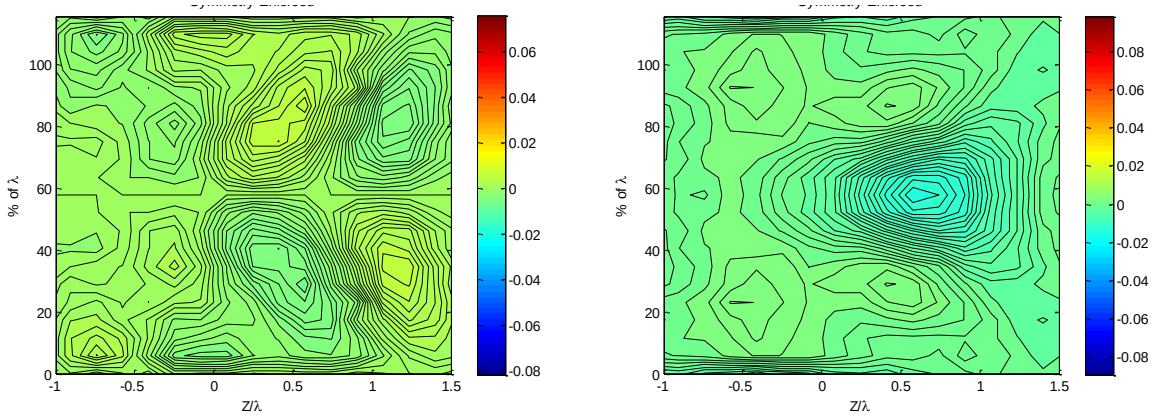

Figure 3.79 Spanwise (left) and Lateral (right) Velocity cross-sections for TE-8 at 1.6c_a Downstream (symmetry enforced)

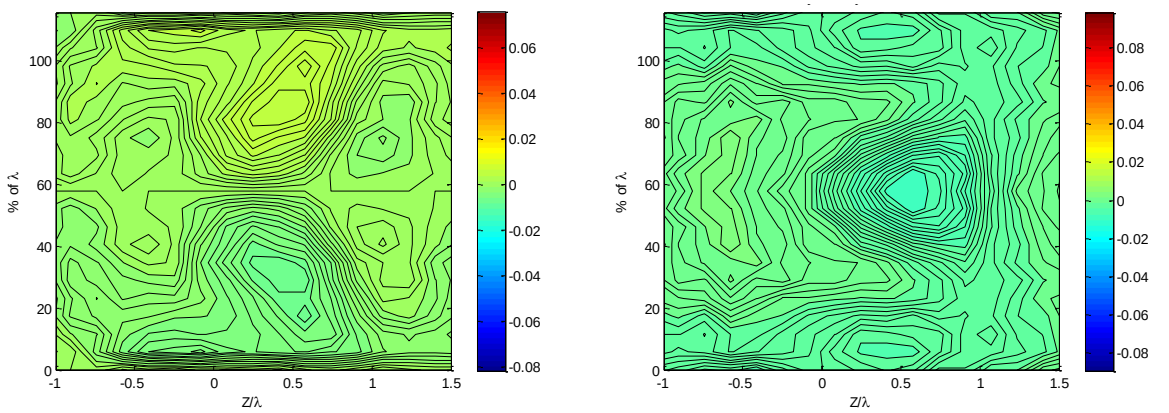

Figure 3.80 Spanwise (left) and Lateral (right) Velocity cross-sections for TE-8 at 1.88c_a Downstream (symmetry enforced)

3.3.3.2 TE-8 Streamwise Vorticity Measurements and Analysis

The streamwise vorticity resulting from the TE-8 configuration are presented in **Figure 3.81** through **Figure 3.88**. As with the previous configurations, the vorticity levels produced by the TE-8 configuration begin to rapidly diffuse downstream. Examining **Figure 3.81** closely shows that 0.1 axial chords downstream of the trailing edge there are alternating regions of positive and negative streamwise vorticity. The maximum value of vorticity produced by the TE-8 configuration at 0.1 axial chords downstream is 8.96 c_a/U_∞, and occurs at 35% of the span in the negative direction and 81% of the injection period in the positive direction. This region of high vorticity is paired with a region of opposing vorticity that is significantly weaker at -1.3 c_a/U_∞. These two regions of vorticity can be seen to be mirror image of each other across the 50% λ line. The vorticity levels produced by the TE-8 configuration are the highest seen for any of the three configurations analyzed, and is 37% stronger than the streamwise vorticity measured for the TE-7 configuration. Despite this increased initial intensity, the vorticity also shows a similar rapid decline when compared to TE-7. Just as with TE-7, the wake of TE-8 travels less than 0.3 axial chords downstream from the initial measurement point (0.1 c_a) to lose half of the initial peak vorticity.

As the wake convects downstream, the vortices maintain the same general structure but diffuse. Additionally, the vortices appear to grow larger until 0.84 axial chords downstream (**Figure 3.85**), after which the vortices no longer appear to enlarge but the intensity diminishes. **Figure 3.88** shows that as the wake reaches 1.88 axial chords downstream of the trailing edge, the maximum intensity drops to 0.495 c_a/U_∞. Thus, the maximum vortex intensity drops to 5.5% of the original measured intensity after propagating 1.78 axial chords downstream. This further confirms that the vorticity produced by the TE-8 configuration, despite starting with higher intensity, drops to a significantly lower value at the farthest downstream location when compared to both TE-1 and TE-7. From the 0.4 axial chord location (**Figure 3.83**) the maximum streamwise vorticity drops to 18.7% of the original magnitude after convecting an additional 1.2 axial chords downstream (**Figure 3.87**). In contrast, over this same downstream travel, the maximum streamwise vorticity level of TE-7 dropped to only 35% (Section 3.3.2.2), and the level of TE-1 dropped to only 30% (Section 3.2.2.2).

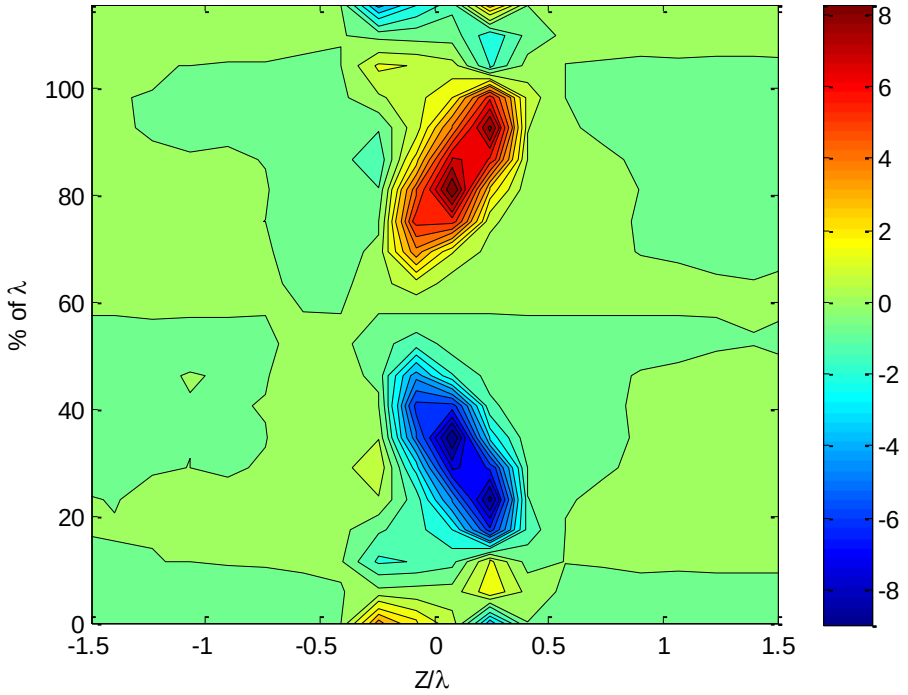

Figure 3.81 Streamwise Vorticity Contour of TE-8 at 0.1 Axial Chords Downstream (symmetry enforced)

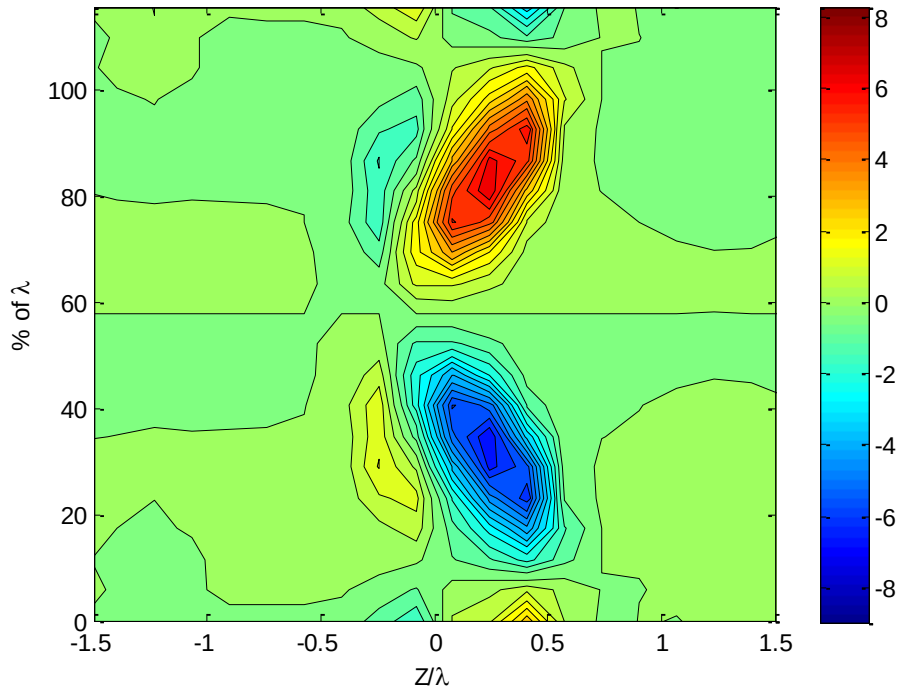

Figure 3.82 Streamwise Vorticity Contour of TE-8 at 0.2 Axial Chords Downstream (symmetry enforced)

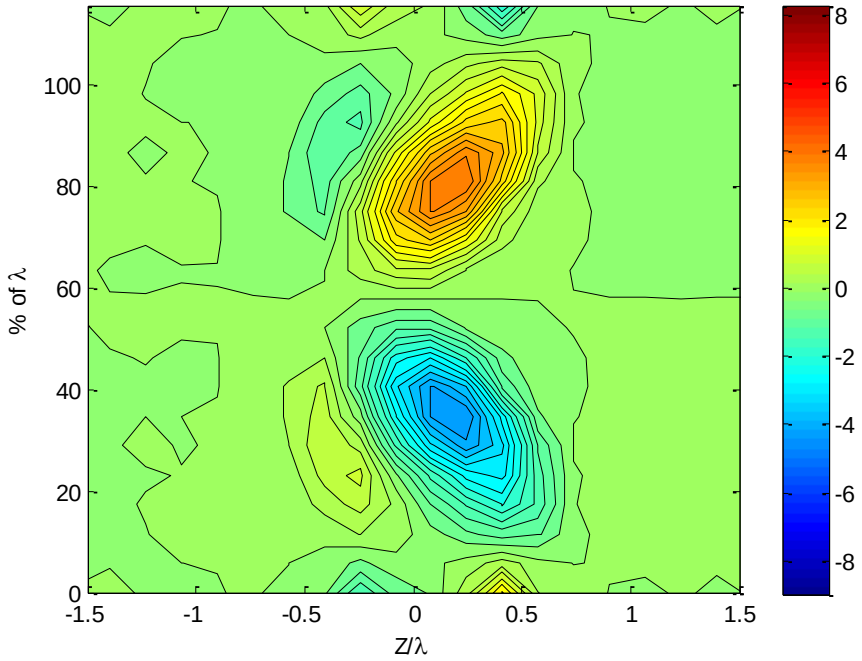

Figure 3.83 Streamwise Vorticity Contour of TE-8 at 0.4 Axial Chords Downstream (symmetry enforced)

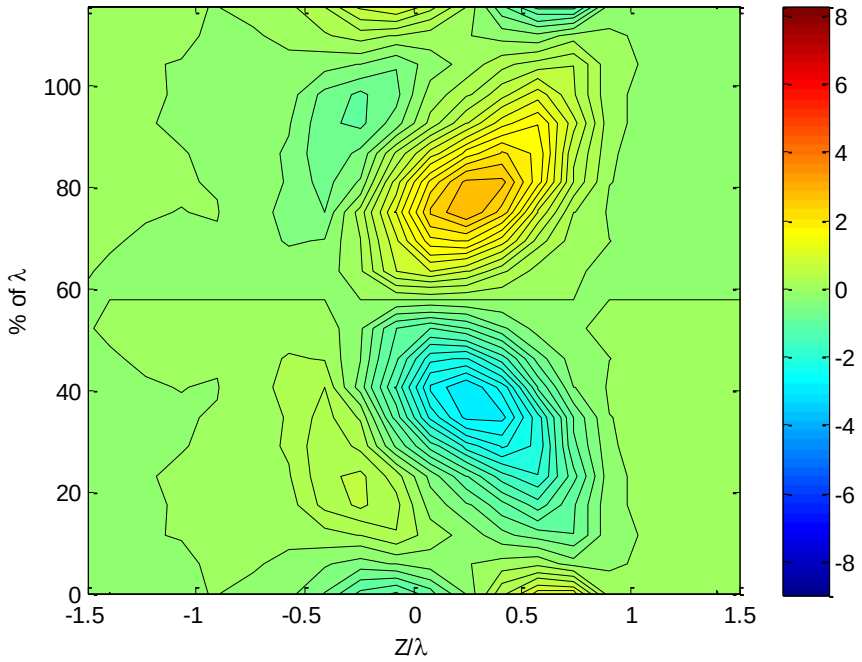

Figure 3.84 Streamwise Vorticity Contour of TE-8 at 0.6 Axial Chords Downstream (symmetry enforced)

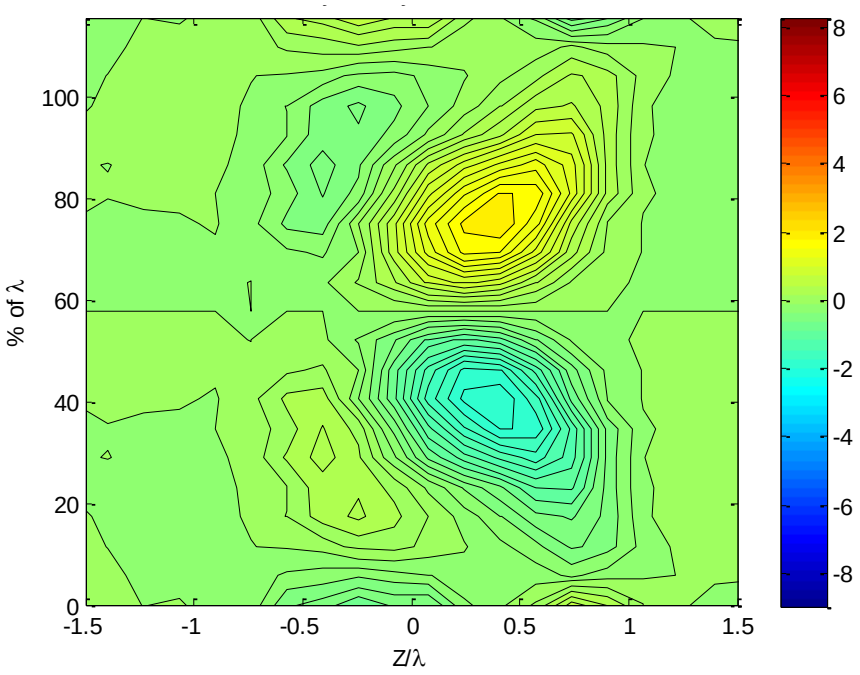

Figure 3.85 Streamwise Vorticity Contour of TE-8 at 0.84 Axial Chords Downstream (symmetry enforced)

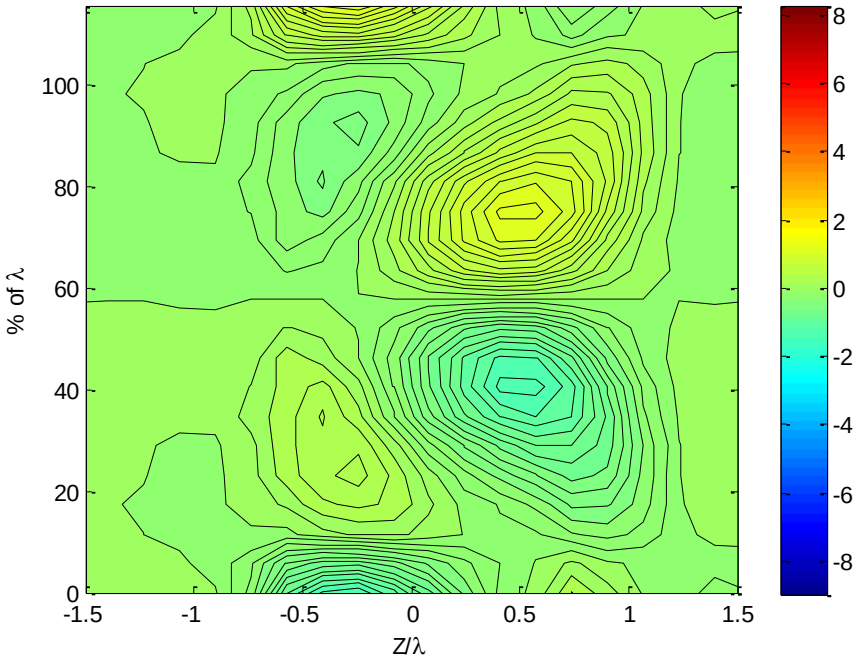

Figure 3.86 Streamwise Vorticity Contour of TE-8 at 1.18 Axial Chords Downstream (symmetry enforced)

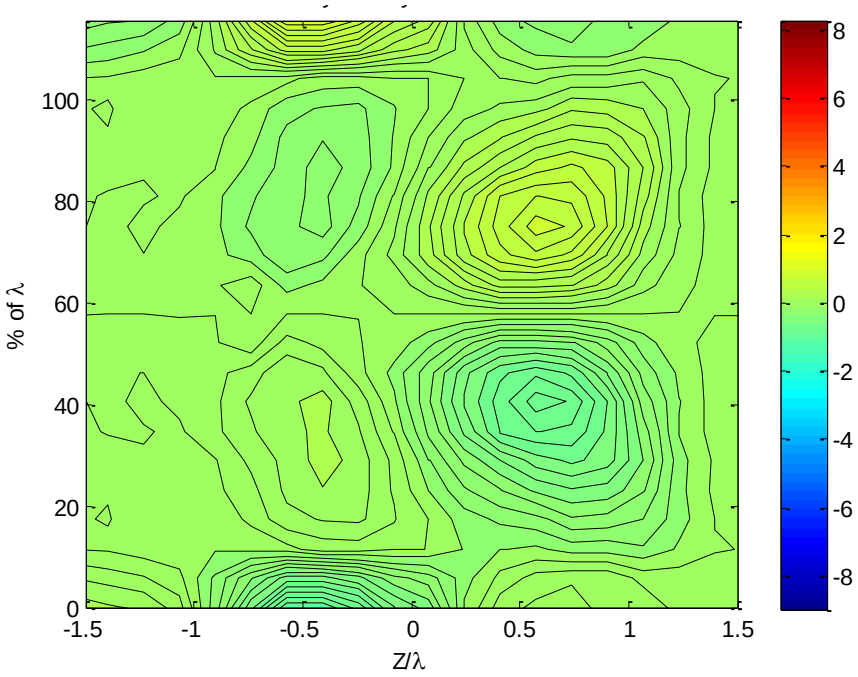

Figure 3.87 Streamwise Vorticity Contour of TE-8 at 1.6 Axial Chords Downstream (symmetry enforced)

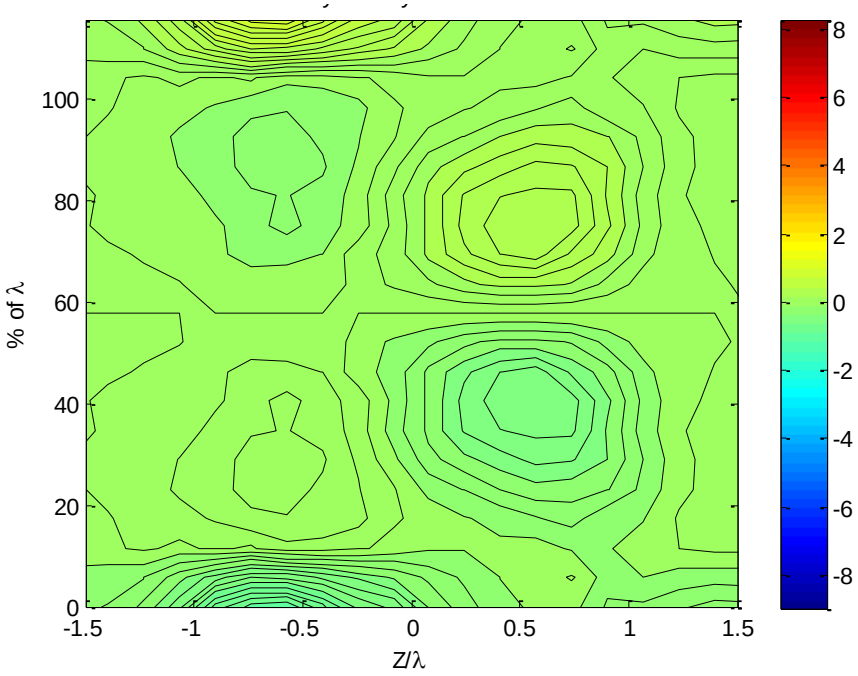

Figure 3.88 Streamwise Vorticity Contour of TE-8 at 1.88 Axial Chords Downstream (symmetry enforced)

3.3.3.3 TE-8 Mean Turbulence Kinetic Energy Analysis

The following section presents the spanwise cross section of the mean turbulence kinetic energy, TKE, for the TE8 configuration. As with the velocity and vorticity plots, the TKE coordinate

system is normalized on the spanwise period, λ, of the vortex generator placement. No gradient error corrections have been applied to the following TKE data.

Starting from **Figure 3.89**, it can be seen that the TKE has a highest value at the 0% and 100% λ location. The TKE is at a minimum at the 50 percent vorticity injection point. The highest value of TKE is measured just below the 100 percent λ_{TE8} location reaches $0.020U_\infty^2$ at 0.1 axial chords downstream. This is slightly lower than the $0.0287U_\infty^2$ measured for the TE-7 configuration (**Figure 3.57**). The TE-8 configuration has a unique aspect when compared to the other two configurations in that these regions of high TKE extend a significant way along the suction side of the wake. The high TKE regions appear to be less concentrated for this configuration. As with the previous configurations, there is a region of lower TKE at the50 percent λ_{TE7} location which measures $0.01U_\infty^{2.}$ However, this configuration is unique in that the minimum TKE value occurs in a small region located just above the 0 percent λ_{TE8} location and just below the 100 percent λ_{TE8} location. The value in these minimum regions measure $0.0043U_\infty^2$ at 0.1 axial chords downstream of the trailing edge.

As the wake propagates downstream, **Figure 3.89** through **Figure 3.96** show the decline in observed TKE levels. As this occurs, the turbulence can also be seen dispersing further into the freestream, which essentially widens the area subjected to turbulence downstream of the trailing edge. At the furthest measured location of 1.88 axial chords downstream of the trailing edge (**Figure 3.96**), the peak TKE is measured as $0.0018U_\infty^2$, while the minimum wake TKE level drops to $0.0015U_\infty^2$. In contrast, the peak TKE values measured for the TE-7 configuration is $0.0037\ U_\infty^2$, and the minimum is measured to be $0.0016\ U_\infty^2$. This suggests that the overall peak TKE levels of TE-8 are lower than those observed in TE-7.

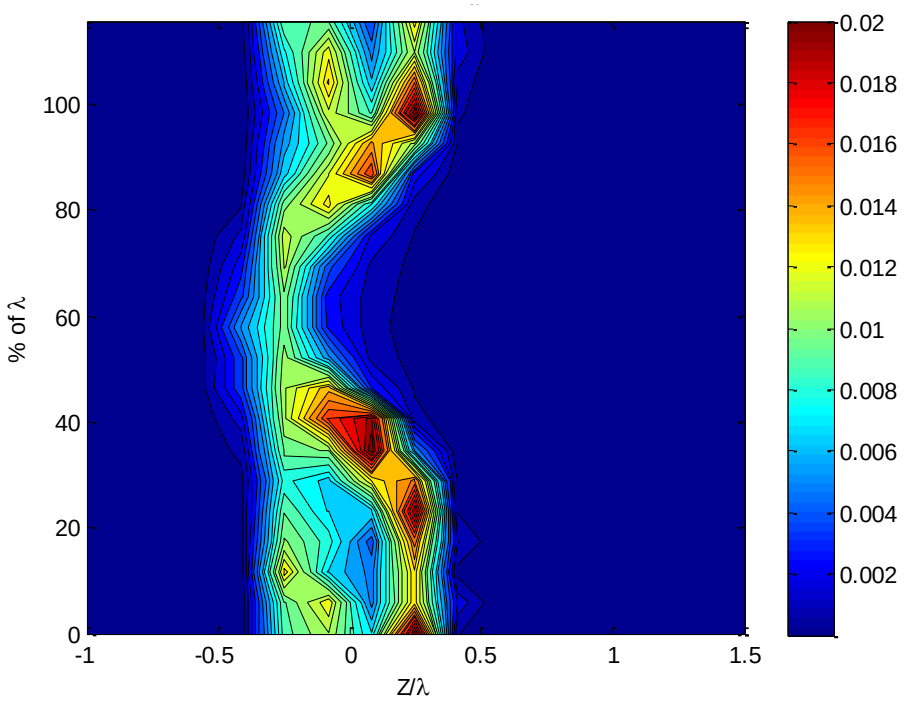

Figure 3.89 Mean Turbulence Kinetic Energy Profile of TE-8 at 0.1 Axial Chords Downstream

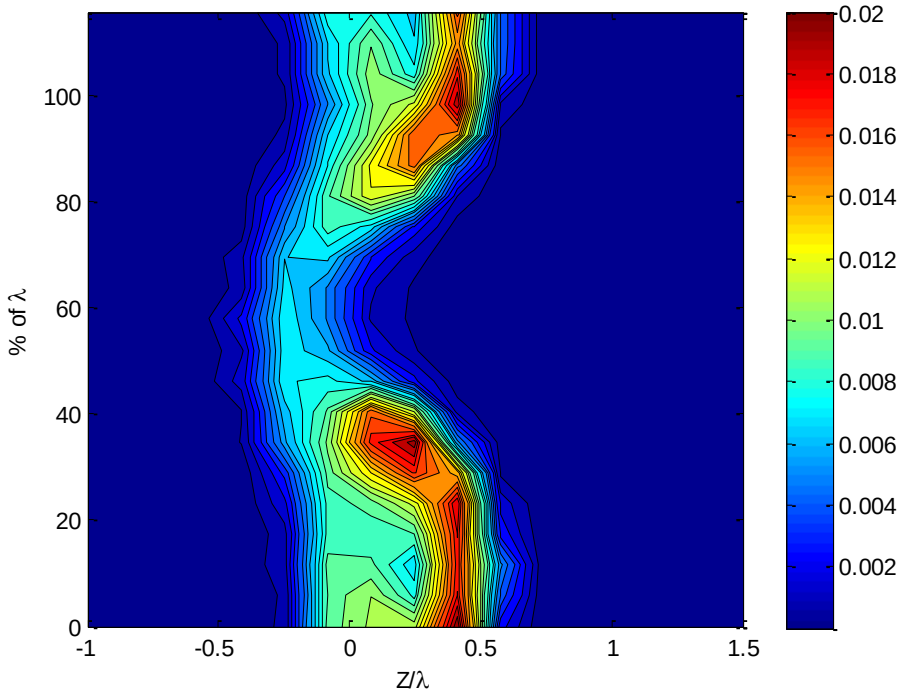

Figure 3.90 Mean Turbulence Kinetic Energy Profile of TE-8 at 0.2 Axial Chords Downstream

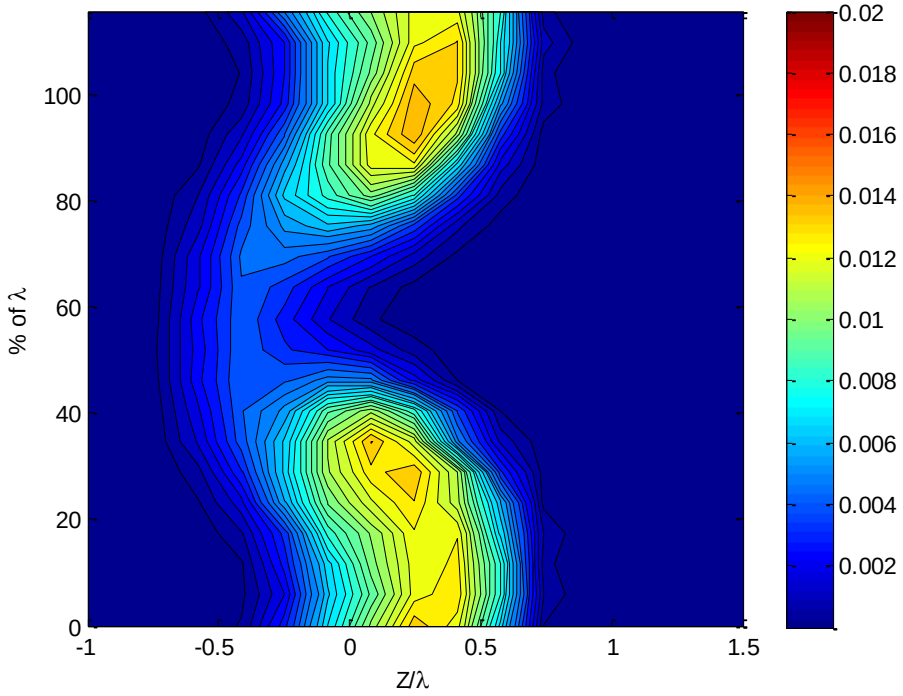

Figure 3.91 Mean Turbulence Kinetic Energy Profile of TE-8 at 0.4 Axial Chords Downstream

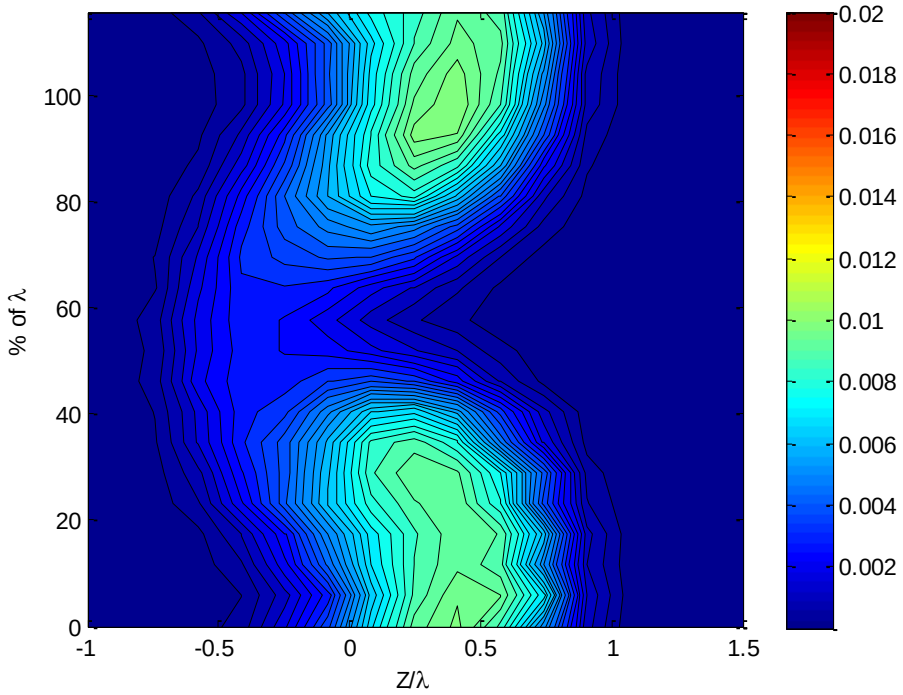

Figure 3.92 Mean Turbulence Kinetic Energy Profile of TE-8 at 0.6 Axial Chords Downstream

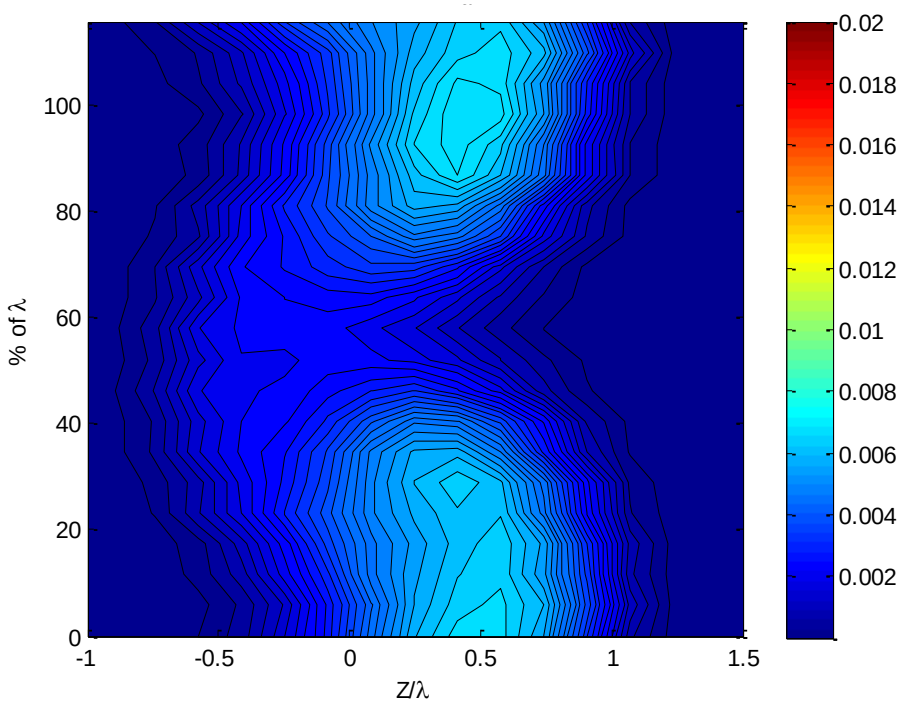

Figure 3.93 Mean Turbulence Kinetic Energy Profile of TE-8 at 0.84 Axial Chords Downstream

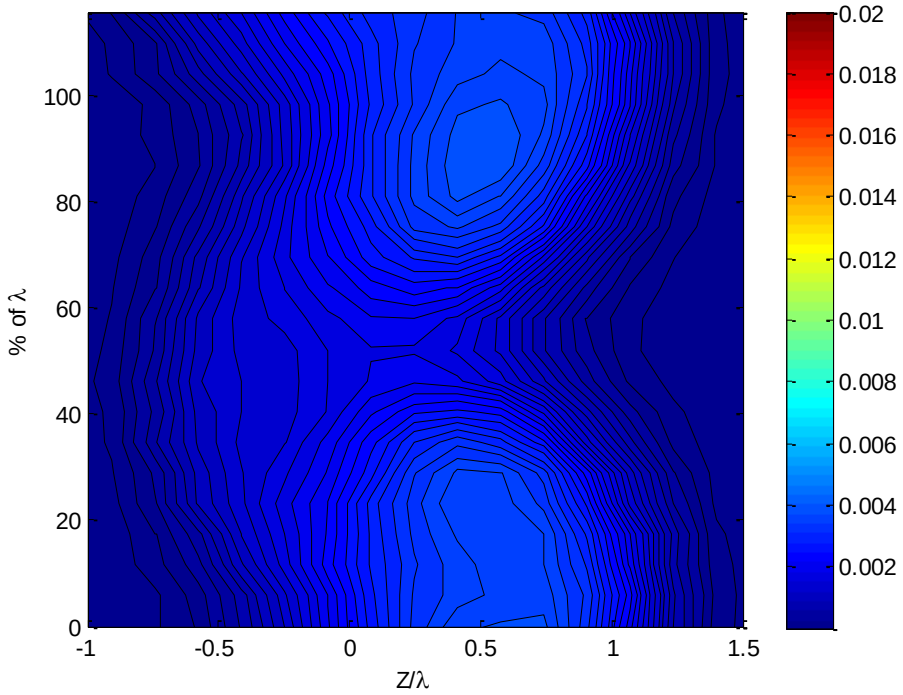

Figure 3.94 Mean Turbulence Kinetic Energy Profile of TE-8 at 1.18 Axial Chords Downstream

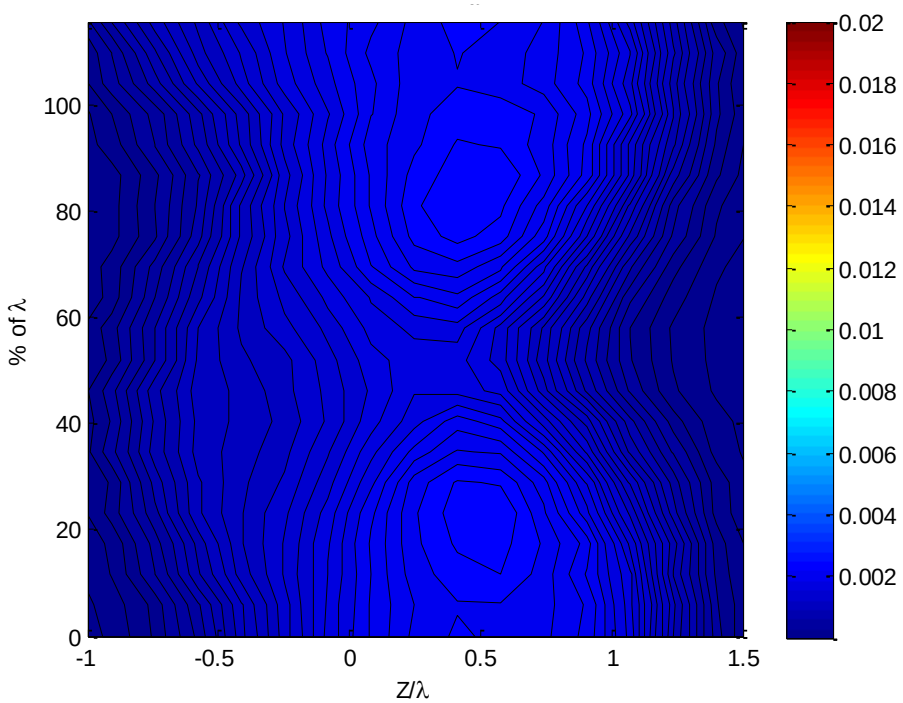

Figure 3.95 Mean Turbulence Kinetic Energy Profile of TE-8 at 1.6 Axial Chords Downstream

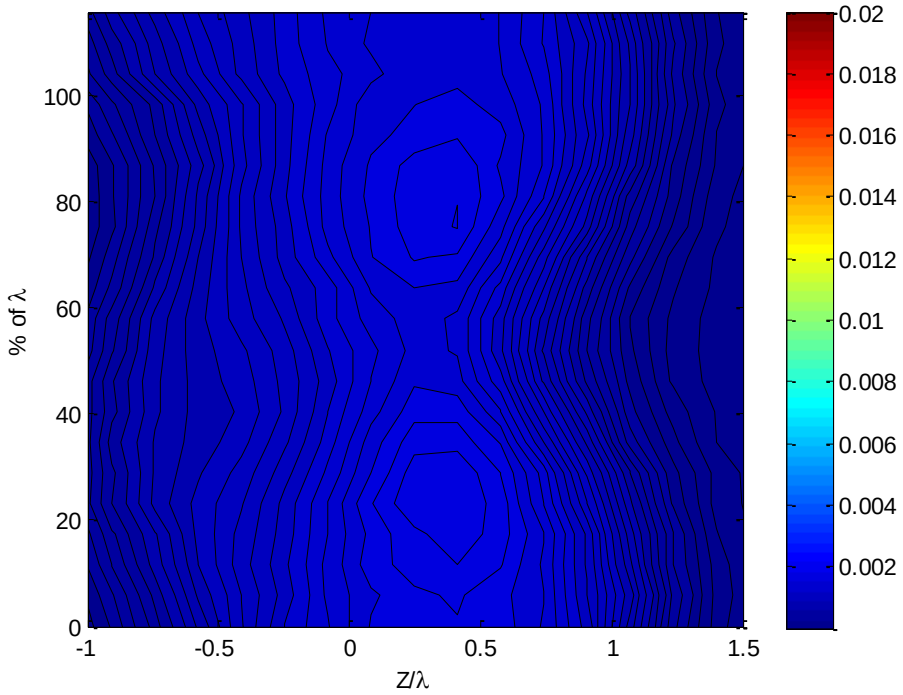

Figure 3.96 Mean Turbulence Kinetic Energy Profile of TE-8 at 1.88 Axial Chords Downstream

3.4 Comparison of Trailing Edge Designs

The following section will directly compare the data measured for each of the three trailing edges TE-1, TE-7, and TE-8. The data used for these comparisons is extracted from the results presented in Section 3.2 and Section 0 of this report. The baseline data was obtained using midspan quadwire measurements taken previously by Derek Geiger at locations of 0.6, 1.2, 1.8, and 2.4 axial chords downstream of the baseline trailing edge. These measurements were performed at the midspan region of the baseline trailing edge. The values obtained at the midspan location are assumed constant across the span of the baseline data. In order to provide direct comparison of the information required, this baseline data was interpolated using cubic splines to obtain information on the downstream locations not directly measured.

3.4.1 Streamwise Vorticity Generation Comparisons

This section will provide direct comparisons of the streamwise vorticity levels generated by each of the three trailing edge configurations measured. These comparisons will be presented for the four common downstream locations measured, which include 0.4, 0.8, 1.2, and 1.6 axial chords downstream of the baseline trailing edge. The figures presented in this section are obtained using the methods described in Section 3.2.2.2 of this report. The horizontal axes of these figures show the pitchwise location normalized on the vorticity period, λ, for each configuration. The vertical axes present the spanwise location normalized as a percentage of λ for each configuration. In order to show comparison of intensity levels for each trailing edge configuration, the contour plots are presented on the same

scale for each trailing edge configuration, using the configuration with the highest recorded streamwise vorticity levels as the basis for the color bar limits.

At 0.4 axial chords downstream (**Figure 3.97**), it can be seen that the TE-8 configuration produces the highest levels of streamwise vorticity, and reaches a maximum of 4.24 c_a/U_∞. The TE-1 and TE-8 configurations produce maximum vorticity of 2.023 c_a/U_∞ and 2.907 c_a/U_∞, respectively. Additionally, each of these trailing edges can be seen to produce regions of high vorticity paired with regions of opposing vorticity that is slightly weaker, and show the mirror image of this vorticity about the center period location. It should be noted that the TE-1 configuration produces regions of vorticity that are opposite to those produced by both the TE-7 and TE-8 configurations.

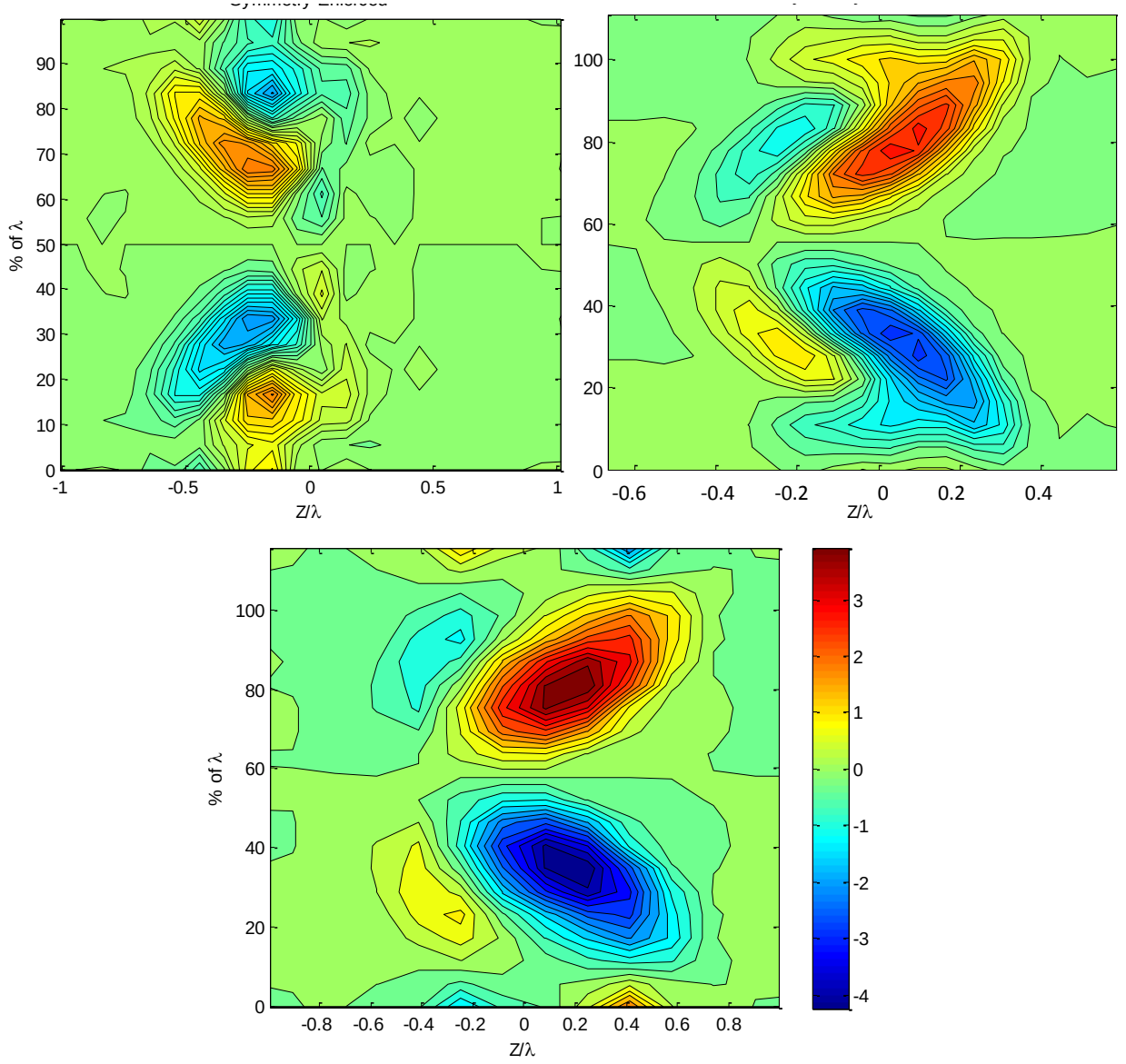

Figure 3.97 Comparison of streamwise vorticity at 0.4 axial chords downstream (TE-1: top left, TE-7: top right, TE-8: bottom). Symmetry enforced

As the wake convects further downstream to 0.8 axial chords (**Figure 3.98**), the decline in vorticity across all three trailing edge configurations can be seen. The TE-8 configuration, which maintains the highest levels, drops to a peak vorticity of 1.96 c_a/U_∞. The TE-1 and TE-7 configurations show a peak vorticity level of 0.985 c_a/U_∞ and 1.575 c_a/U_∞, respectively. At this downstream locations, the vorticity of each trailing edge configurations maintain the same structure as seen further upstream.

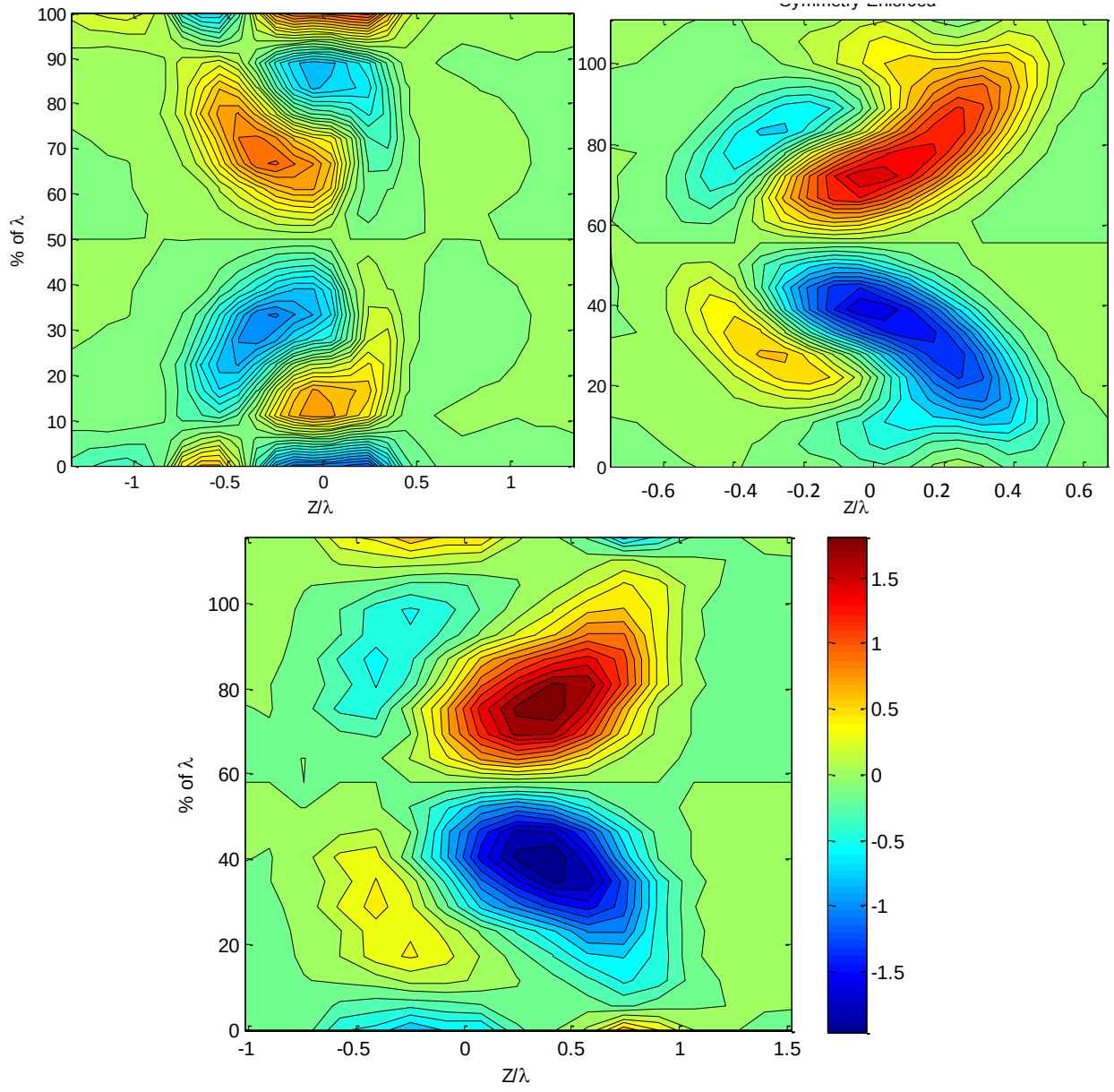

Figure 3.98 Comparison of streamwise vorticity at 0.8 axial chords downstream (TE-1: top left, TE-7: top right, TE-8: bottom). Symmetry enforced.

Once the wake propagates to 1.2 axial chords downstream of the baseline trailing edge, it can be seen that the observed vorticity levels begin to show a smaller variance between each trailing edge configuration (**Figure 3.99**). Additionally, the TE-8 configuration no longer shows the highest level of

peak streamwise vorticity, but instead TE-7 shows the highest peak level. At 1.2c_a downstream, TE-7 has a peak vorticity of 1.22 c_a/U_∞, TE-8 has a peak streamwise vorticity of 1.20 c_a/U_∞, and TE-1 produces a noticeably lower peak streamwise vorticity of 0.73 c_a/U_∞. It can also be seen that, although TE-8 produces a lower peak level of vorticity, the area appears to be somewhat broader.

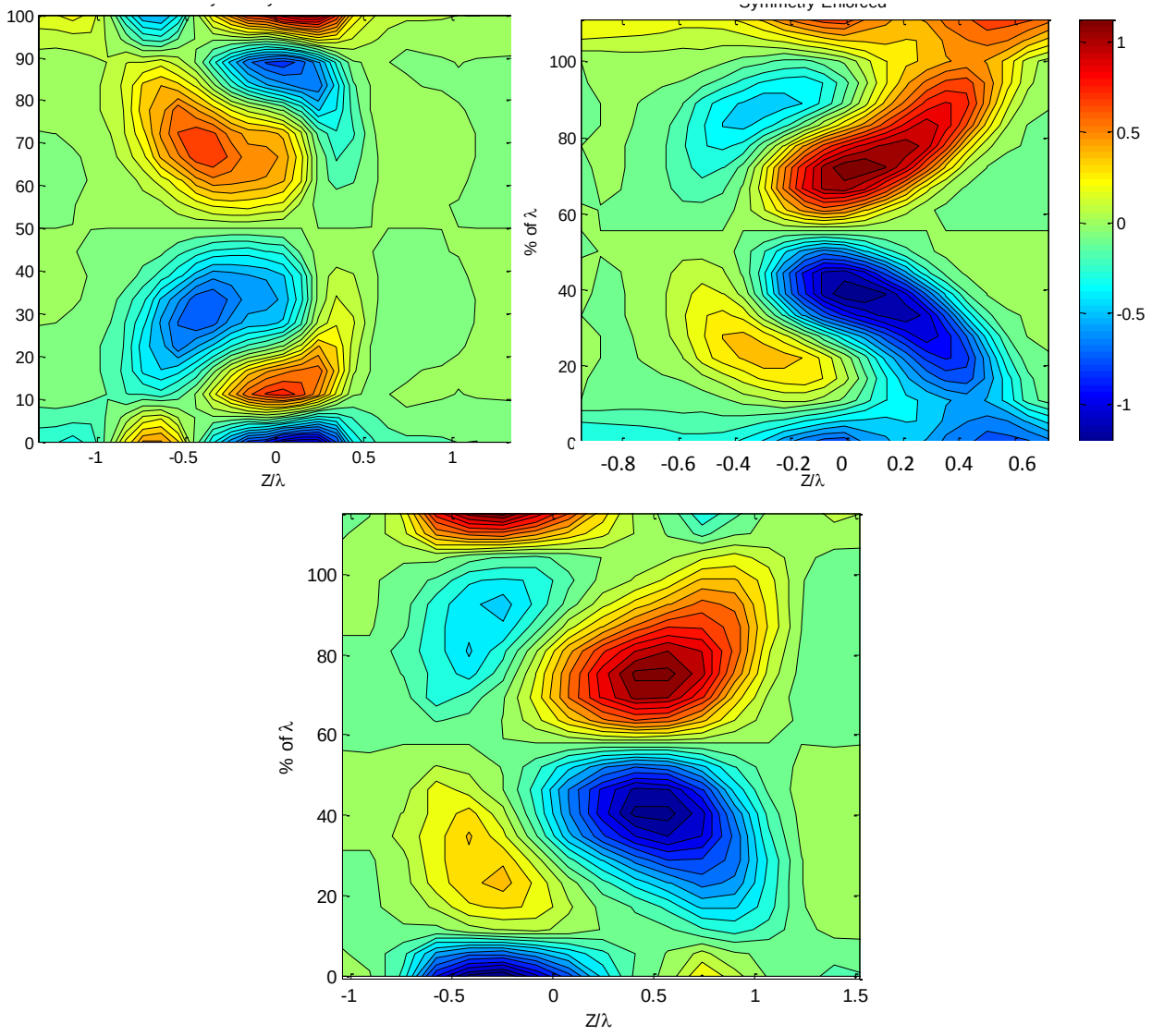

Figure 3.99 Comparison of streamwise vorticity at 1.2 axial chords downstream (TE-1: top left, TE-7: top right, TE-8: bottom). Symmetry enforced

Once the wake reaches the furthest downstream location analyzed for all three trailing edges (x/c_a = 1.6), some key differences in the trailing edge configurations can be further identified (**Figure 3.100**). At 1.6 axial chords downstream, the maximum streamwise vorticity of TE-1, TE-7, and TE-8 is 0.608 c_a/U_∞, 0.978 c_a/U_∞, and 0.794 c_a/U_∞, respectively. However, at 0.4 axial chords downstream (**Figure 3.97**), the maximum streamwise vorticity measured with TE-8 was nearly over 30% *higher* than that observed for TE-7. Thus, the TE-8 configuration starts significantly higher than the other trailing

edge configurations, but shows a significantly faster decline in peak vorticity levels when compared to the other configurations.

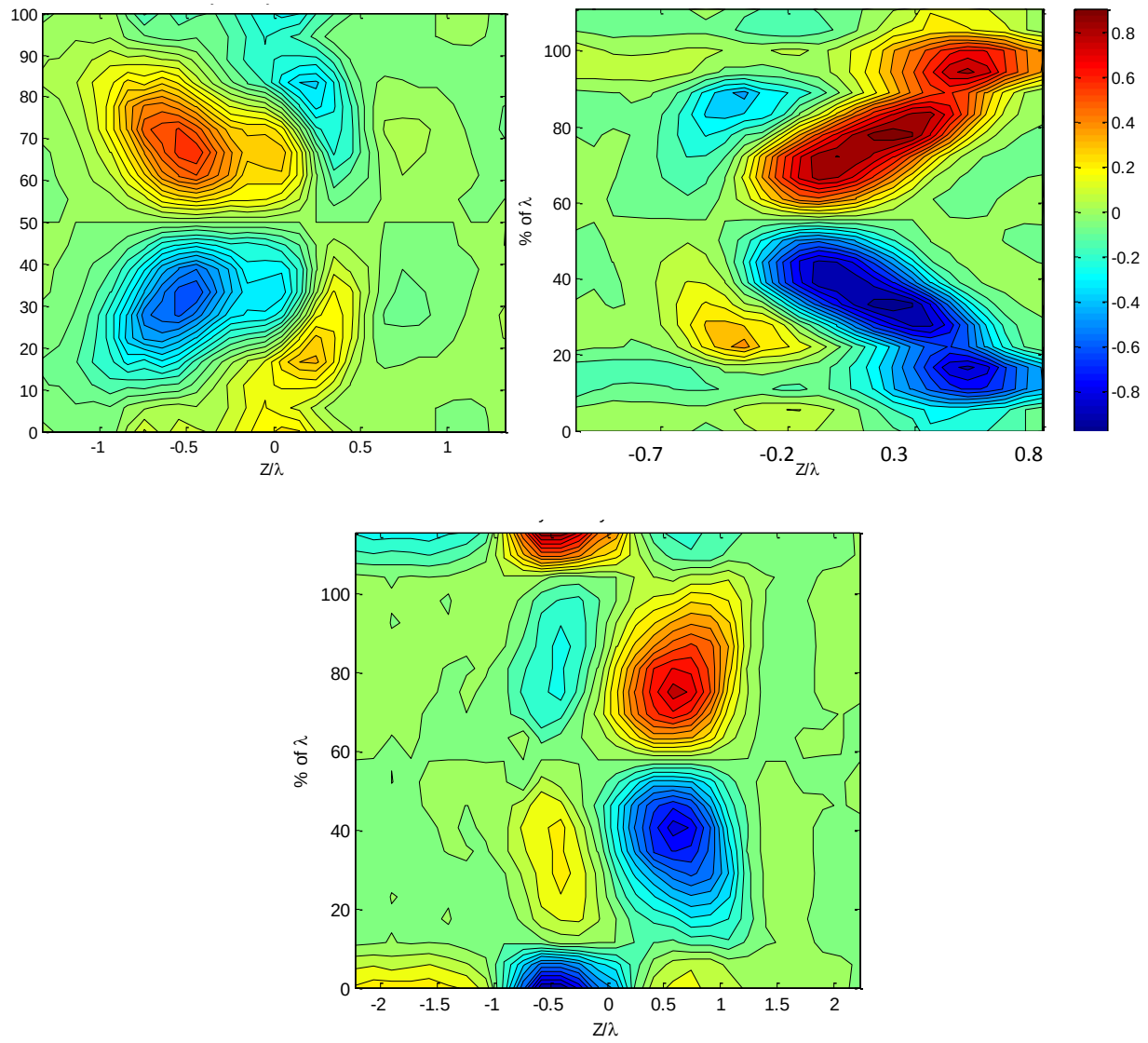

Figure 3.100 Comparison of streamwise vorticity at 1.6 axial chords downstream (TE-1: top left, TE-7: top right, TE-8: bottom). Symmetry enforced.

Throughout all downstream locations, it can be seen that the TE-1 configuration is less effective at producing streamwise vorticity when compared to both the TE-7 and TE-8 configurations. At the $1.6c_a$ downstream location, the TE-1 streamwise vorticity strength is 30% of that measured at the $0.4c_a$ downstream location. The TE-7 configuration shows a similar decline in streamwise vorticity which measures 33.6% of the originally measured intensity at these two downstream locations. In contrast, however, the TE-8 configuration shows a significantly higher decline in vorticity intensity as the wake propagates downstream. At the furthest location of $1.6c_a$, the peak streamwise vorticity produced by TE-8 drops to 18.7% of the vorticity observed at 0.4 axial chords downstream. The axial variation of peak

streamwise vorticity is shown in **Figure 3.101**. The TE-8 configuration initially shows the highest levels of peak TKE, but the magnitude drops below the vorticity levels observed in TE-7 at approximately 1.2 axial chords downstream of the trailing edge. Furthermore, at approximately 1.7 axial chords downstream it can be seen that the vorticity levels of TE-8 drop below the expected peak values of TE-1, which showed consistently lower peak magnitude at all previous downstream locations.

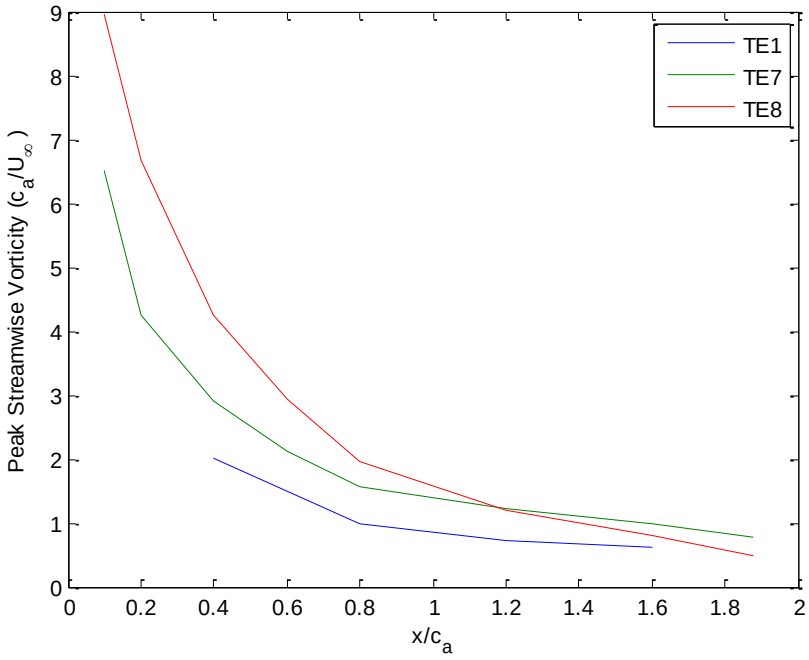

Figure 3.101 Axial Decay of Peak Streamwise Vorticity Compared for Each Trailing Edge Configuration

It should be noted that at some downstream locations, regions of vorticity appear at the top and bottom of the period of vorticity injection. These regions, such as those seen in TE-8 contour of **Figure 3.100**, are a byproduct of imperfect measurement techniques that resulted in measuring slightly more than one complete period. These regions of alternating vorticity are negligible and not a characteristic of the flow.

3.4.2 Spanwise Variation of Peak Turbulence Kinetic Energy

The turbulence kinetic energy (TKE) produced by each of the trailing edge configurations studied was measured and recorded using four sensor hotwire anemometry as described in Section 3.2.2.3 of this report. Each of the following plots presents the maximum TKE levels observed at each spanwise location traversed behind the trailing edge configurations. The horizontal axis shows the spanwise location as a percentage of λ for each individual configuration. The numerical value of λ is different for each trailing edge configuration, so normalizing as a percentage of λ gives a means for direct comparison among each of the three trailing edges considered. The vertical axis on these plots shows the maximum TKE values observed pitchwise across the wake for each spanwise location measured.

The first location measured for comparison of these trailing edge configurations is located at 0.4 axial chords downstream of the baseline trailing edge, and can be seen in **Figure 3.102**. The periodic nature of the three trailing edge configurations can be seen. The TE-1 configuration, which consists of surface mounted vortex generators, shows the highest value of peak TKE at the center of the spanwise period, but appears to show a lower value of peak TKE at the outside regions of λ (0% and 100%). This suggests that the TE-1 vortex generator configuration is not as effective at producing a spanwise change in the peak TKE levels. In contrast, the TE-7 and TE-8 configurations are able to show a stronger variation across the period of λ, with TE-8 showing the lowest peak TKE values observed for all three configurations. It is interesting to note that all three trailing edge configurations analyzed show regions of peak TKE that are actually lower than the baseline observed peak TKE. This suggests that although the introduction of vorticity into the flow increases peak TKE at some locations, it actually serves to reduce the level of peak TKE around the center period of vorticity.

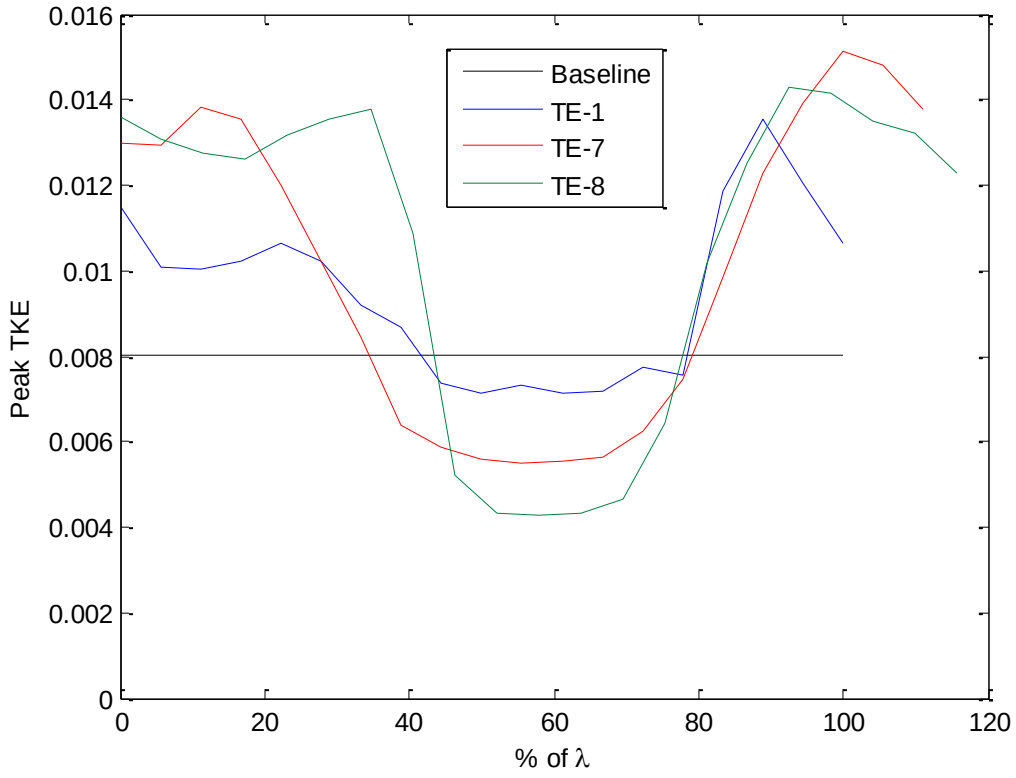

Figure 3.102 Comparison of spanwise variation of peak TKE values for each trailing edge configuration, measured at 0.4 axial chords downstream

As we progress to the next downstream location of 0.8 axial chords behind the baseline trailing edge, the values of peak TKE can be seen to be lower than those observed at 0.4 axial chords downstream. As **Figure 3.103** shows, the baseline peak TKE has reduced to $0.0052U_\infty^2$, which is 65% of the baseline peak TKE values measured at 0.4 axial chords downstream. At this downstream location, the same general pattern of TKE variance across the span of each trailing edge remains similar to those observed at 0.4 axial chords downstream. It is interesting to note that at this downstream location,

both TE-1 and TE-7 show very similar minimum values of peak TKE (at the centerspan), but TE-1 shows lower levels of TKE at the extremes of λ. Additionally, the TE-8 configuration once again shows the minimum levels of peak TKE among the three trailing edges, and appears to show a more rapid decline in peak TKE around the outside regions of λ when compared to TE-7.

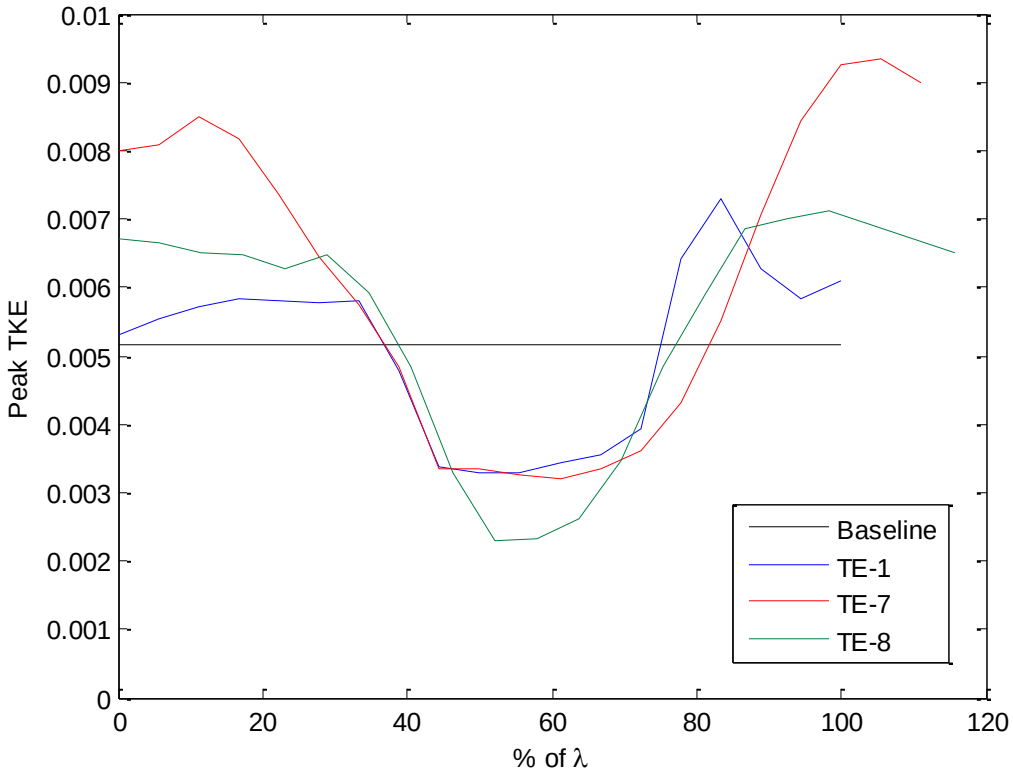

Figure 3.103 Comparison of spanwise variation of peak TKE values for each trailing edge configuration, measured at 0.84 axial chords downstream

At 1.2 axial chords downstream, the trends of variation in peak TKE continue (**Figure 3.104**). At this downstream location, the baseline peak TKE has reduced to $0.0037U_\infty^2$. At this distance downstream, the spanwise variation of peak TKE for the TE-1 and TE-8 configuration appear to be very comparable across the entire span. Although the TE-7 configuration shows minimum peak TKE levels similar to those observed for TE-1 and TE-8, the maximum observed values of peak TKE across the span are significantly higher for TE-7. This suggests that the TE-8 configuration is more effective at causing a decrease in the maximum values of TKE observed. Although the initial peak TKE values for TE-7 and TE-8 are similar, TE-7 shows a significantly faster decline in these values. It is also interesting to note that the vorticity produced by TE-1 and TE-8 observed at this downstream locations seem to cause the peak TKE values observed to never increase significantly higher than the baseline values. For the TE-1 configuration at 1.2 axial chords downstream, the mean TKE value across the span is 0.003438 U_∞^2, in comparison to 0.003389 U_∞^2 for the TE-8 configuration. Thus, the average peak TKE values across the span of TE-7 and TE-8 are actually lower than the average peak TKE of $0.0037U_\infty^2$ observed for the

baseline case. In contrast, the average value of peak TKE across the span of the TE-7 configuration is 0.004397 U_∞^2, which remains higher than the baseline case at this downstream location.

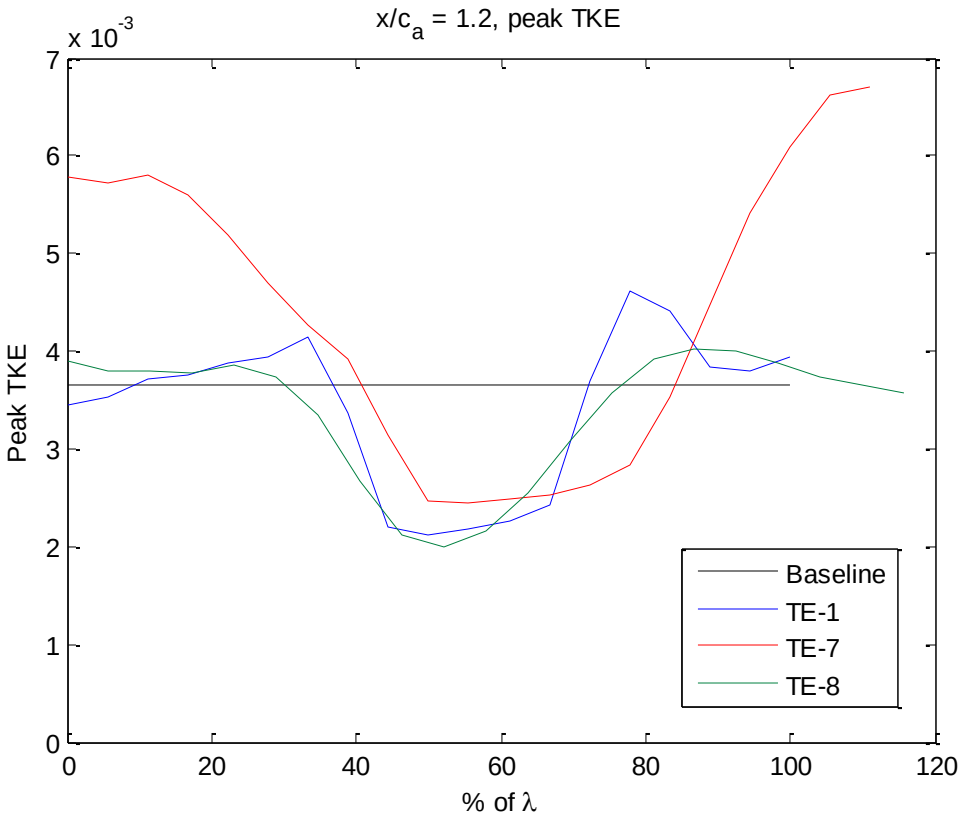

Figure 3.104 Comparison of spanwise variation of peak TKE values for each trailing edge configuration, measured at 1.2 axial chords downstream

Once the flow reaches the farthest downstream location measured (1.6 axial chords), **Figure 3.105** shows the development of the wake for each trailing edge configuration. At this station downstream, the peak TKE for the baseline blade configuration reaches its lowest observed value of 0.0029 U_∞^2. Each of the three trailing edge configurations tested continues to show the same general shape across the span of the blade that is seen at each of the previous streamwise positions measured. As with the previous cases, the maximum peak TKE values of TE-7 across the span continue to remain higher than the peak TKE values observed for the baseline case, with a mean TKE value of 0.00305 U_∞^2 across λ_{TE7}. The most interesting cases are observed for the TE-1 and TE-8 configurations, in that nearly the entire period of λ for both of these configurations is lower than the baseline TKE values observed. Although the TE-1 configuration shows small spanwise locations where the peak TKE is above the baseline (at approximately 28% λ and 78% λ), the TE-8 configuration peak TKE is consistently lower than the baseline across the entire period. The mean peak TKE across the period of TE-1 is 0.002453 U_∞^2, and is calculated as 0.002237 U_∞^2 for TE-8. Thus, the mean peak TKE values for TE-1 and TE-8 across the period are 84.6% and 77.1%, respectively, of the peak TKE values observed for the baseline case at 1.6 axial chords downstream.This suggests that proper introduction of streamwise vorticity can actually

cause a faster decline in the peak TKE values, resulting in less turbulence downstream when compared to the baseline blade. The axial decay of peak TKE Values are presented in **Figure 3.106**. This shows that the peak TKE levels observed in TE-7 are consistently higher than those observed in either TE-1 or TE-8. Additionally, the slopes of the curves in **Figure 3.106** appear to be approximately comparable, which indicates that the rate of axial decay of vorticity (**Figure 3.101**), is not a major factor in the axial decay of peak TKE.

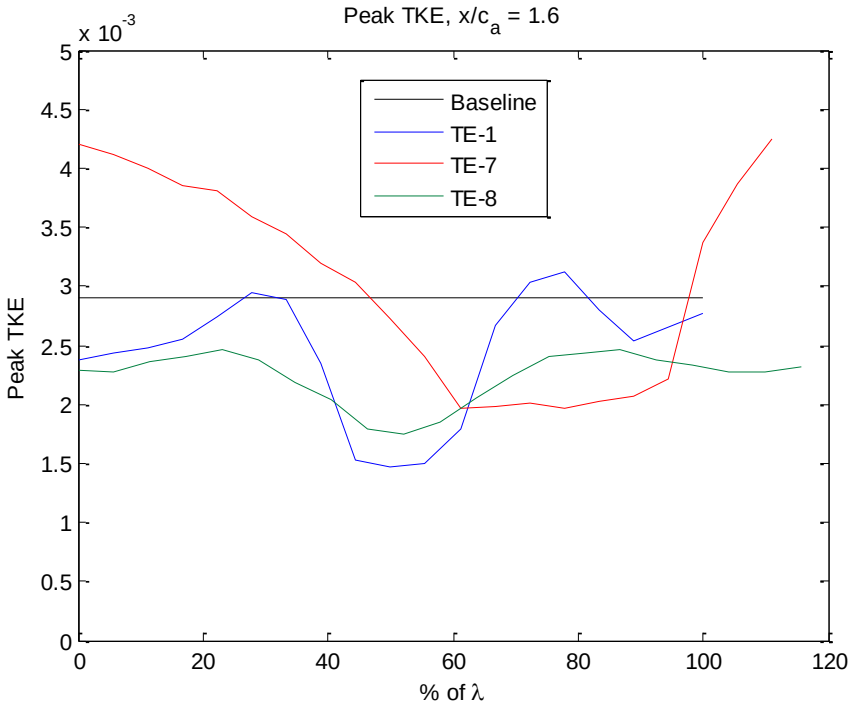

Figure 3.105 Comparison of spanwise variation of peak TKE values for each trailing edge configuration, measured at 1.6 axial chords downstream

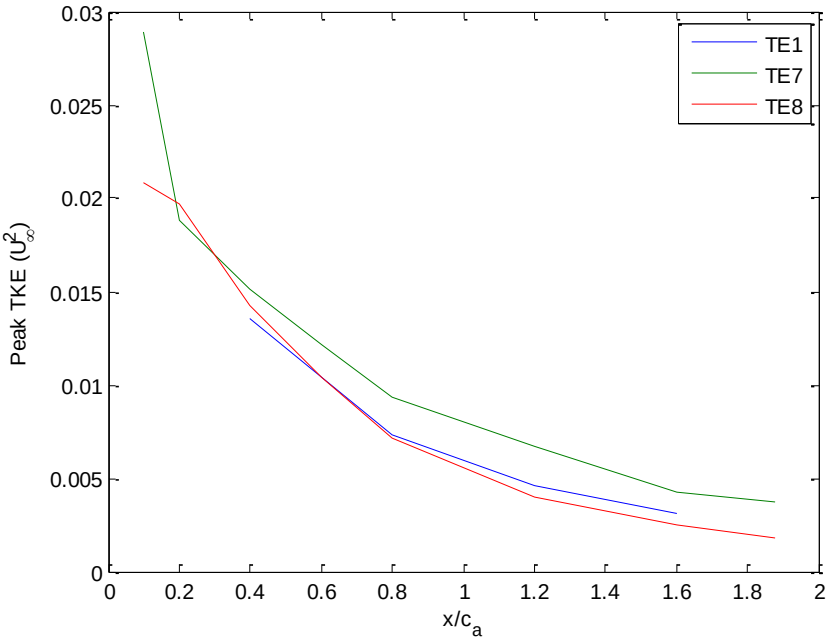

Figure 3.106 Axial Decay of Peak TKE Compared for Each Trailing Edge Configuration

The TKE values for each trailing edge configuration were plotted based on a logarithmic scale in order to gain further insight into the decay of TKE. To obtain the turbulence kinetic energy scaled in decibels, 10 times the $\log_{10}$ of the TKE was calculated, or

$$TKE_{dB} = 10 \log_{10}(TKE), \quad \textbf{(3-5)}$$

where TKE is the turbulence kinetic energy value calculated using Equation $\boldsymbol{TKE = \frac{\overline{u}^2 + \overline{v}^2 + \overline{w}^2}{2}}$. (3-3. The turbulence kinetic energy in decibels is presented in **Figure 3.107** and **Figure 3.108**, at 0.4 and 1.6 axial chords downstream of the trailing edge. The decibel levels at the peak TKE region (corresponding to 100% λ), and the minimum TKE regions (corresponding to 50% λ) are presented in **Table 3-2** and **Table 3-3**.

Table 3-2 TKE Values for Each Trailing Edge Configuration at 0.4 Axial Chords Downstream

Configuration	Peak TKE Region (100% λ) (dB)	Min TKE Region (50% λ) (db)	Variation (Peak TKE – Min TKE) (dB)
TE-1	-18.7	-21.4	-2.75
TE-7	-18.6	-22.6	-4.033
TE-8	-18.7	-23.6	-4.95

Table 3-3 TKE Values for Each Trailing Edge Configuration at 1.6 Axial Chords Downstream

Configuration	Peak TKE Region (100% λ) (dB)	Min TKE Region (50% λ) (db)	Variation (Peak TKE – Min TKE) (dB)
TE-1	-26.3	-29.8	-3.47
TE-7	-23.8	-27.0	-3.14
TE-8	-26.4	-27.6	-1.23

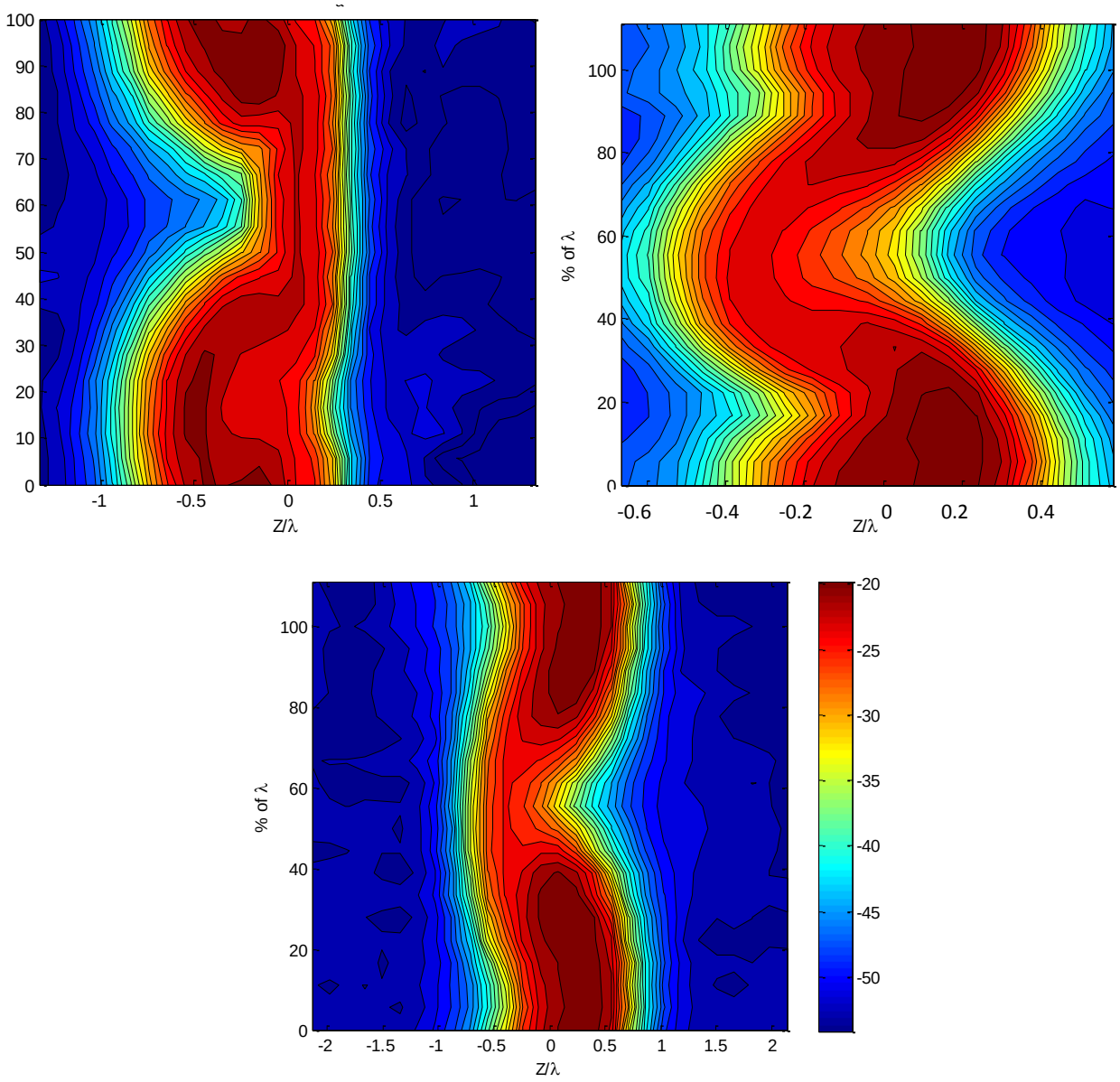

Figure 3.107 Comparison of TKE at 0.4 axial chords downstream (TE-1: top left, TE-7: top right, TE-8: bottom). Measured in decibels.

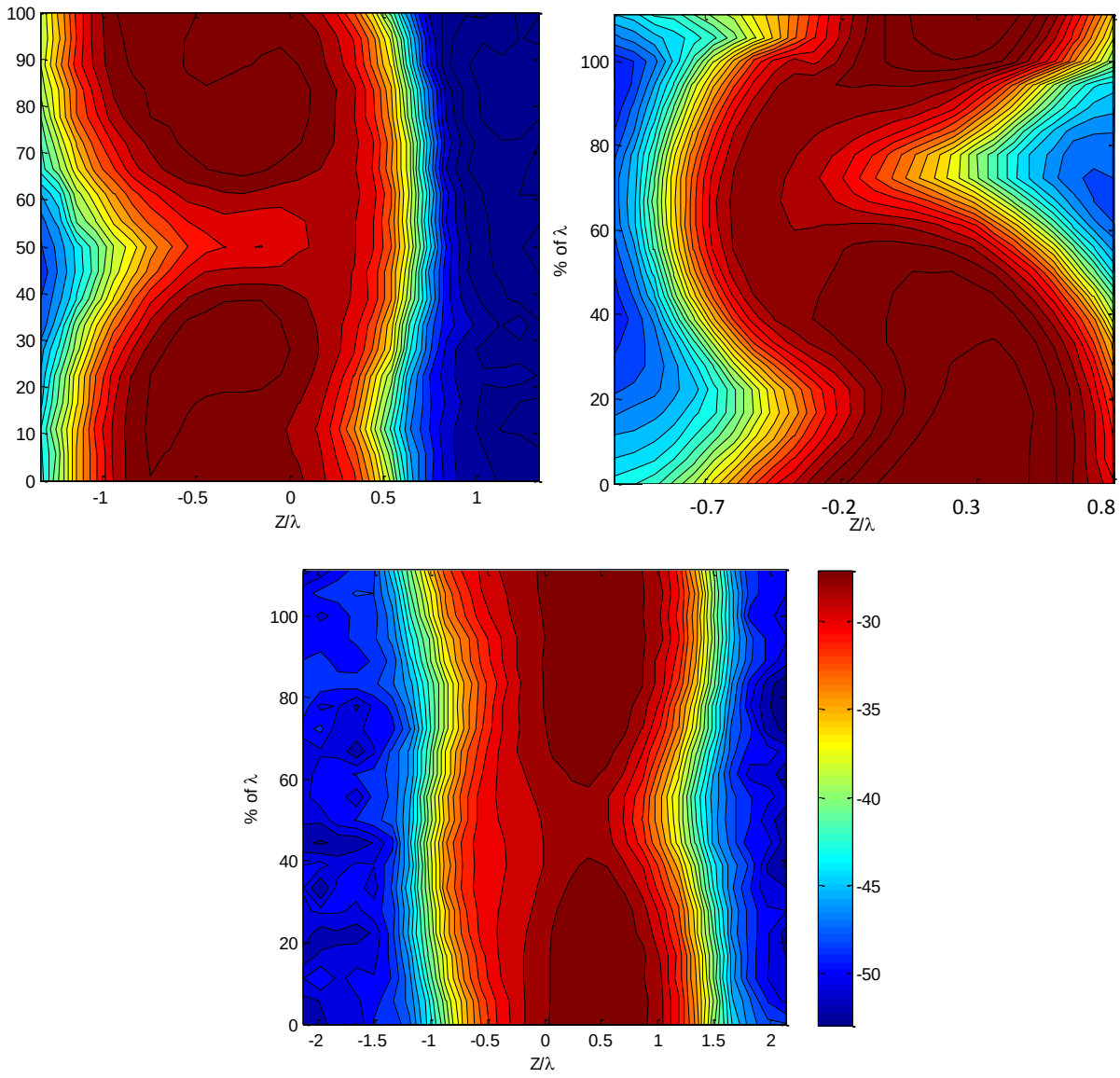

Figure 3.108 Comparison of TKE at 1.6 axial chords downstream (TE-1: top left, TE-7: top right, TE-8: bottom). Measured in decibels.

3.4.3 Wake Width Comparisons

The spanwise average wake velocity profiles were calculated for each trailing edge configuration as described in Section 3.2.2.4 of this report. This allowed for a direct comparison of the half wake widths resulting from each trailing edge configuration. For the direct comparison between each trailing edge, the half wake widths are presented normalized on the spanwise period of vorticity injection for each trailing edge. As seen in **Figure 3.109**, the TE-8 configuration is the most efficient at widening the average wake profile behind the blade. The TE-8 configuration is nearly 30% more effective at increasing the half wake width behind the blade than the second most effective TE-1 configuration. The least effective configuration at producing a large half wake width is the TE-7 configuration, which still is significantly wider than the baseline case (not presented for direct comparison in this figure). The

spanwise average profile seen in **Figure 3.109** also sheds significant insight into the average velocity deficit produced by each trailing edge configuration. It can be seen that the TE-7 and TE-8 configuration produce a noticeably shallower wake than TE-1, indicating a potential for lower drag levels for these two configurations.

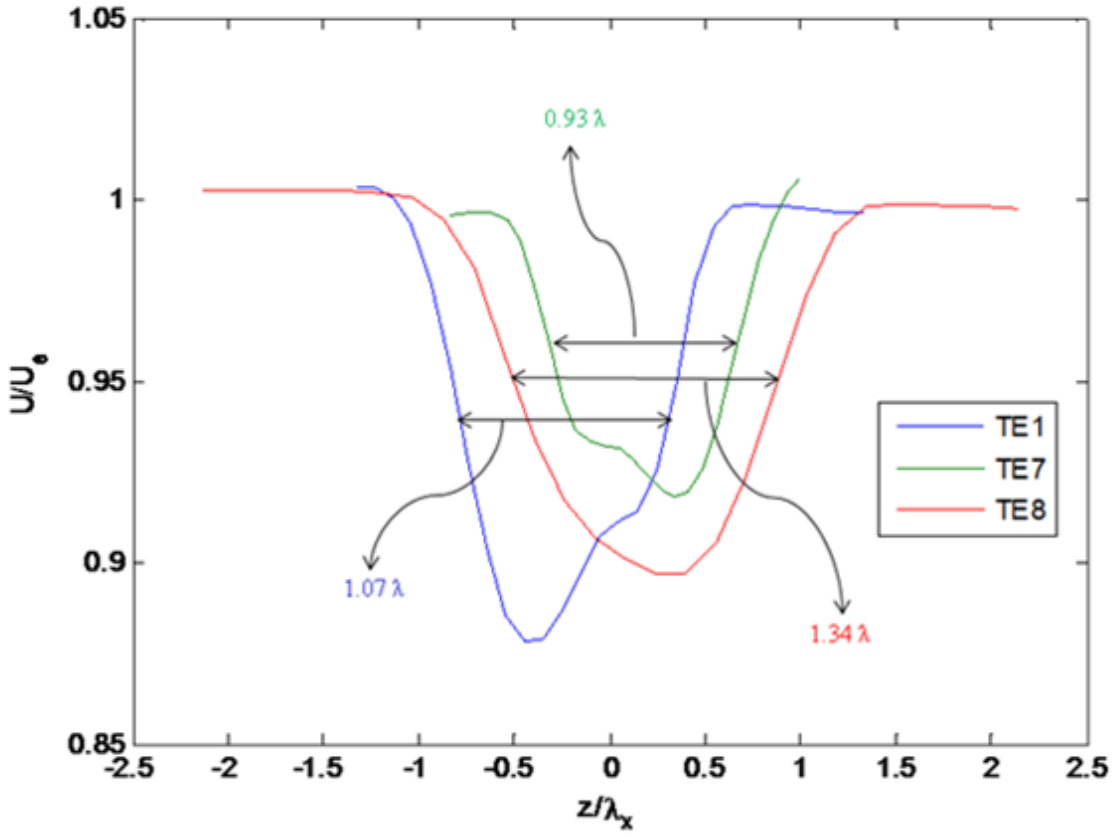

Figure 3.109 Spanwise Average Velocity Profile for TE-1, TE-7, and TE-8 at 1.6 Axial Chords Downstream

The half wake width of the spanwise average velocity field was calculated for each trailing edge at several axial locations downstream. This information is presented normalized on λ for each individual configuration. As can be seen in **Figure 3.110**, the half wake width of the spanwise average velocity is the largest for the TE-8 configuration. The TE-7 configuration is the least efficient wake widening-configuration. It is also interesting to note that, in addition to having a larger half wake width across all downstream locations, the TE-8 configuration appears to have the fastest increase in half wake width as the wake propagates downstream.

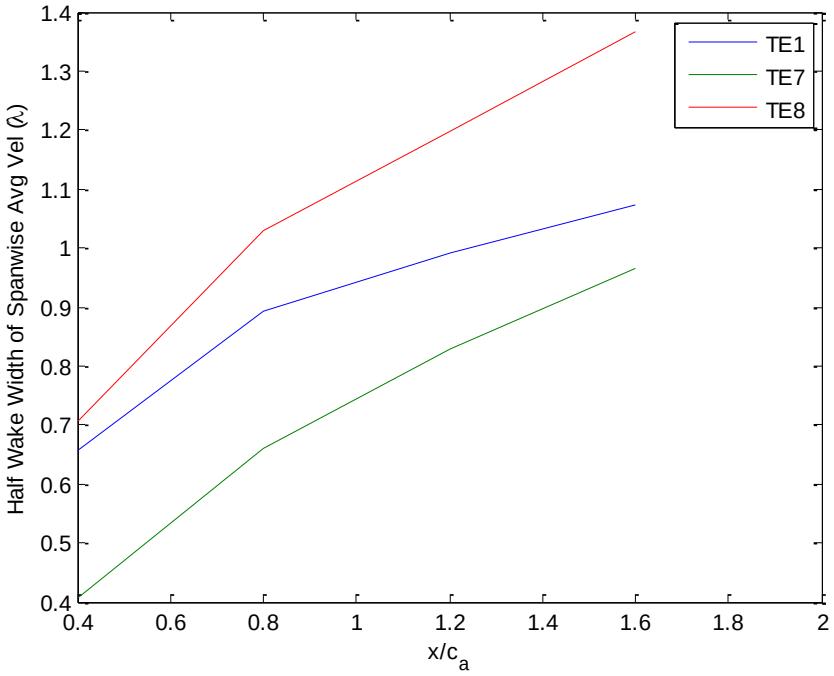

Figure 3.110 Axial Variation of the Half Wake Width of the Spanwise Average Velocity Field

3.4.4 Momentum Thickness Comparisons

In order to obtain a comparison of the drag created by each of the trailing edges, the momentum thickness was calculated based upon the wake profiles measured at 0.4, 0.84, 1.2, and 1.6 axial chords downstream. The momentum thickness values were normalized on the freestream velocity, U_∞, and the baseline blade axial chord, c_a. For each downstream location and trailing edge, the momentum thickness was obtained by integrating the velocity deficit both pitchwise and spanwise across the wake of the trailing edge. The velocity deficit was normalized on the edge velocity, U_e, for each of the individual cases analyzed. The momentum thickness of the wake is calculated using the equation

$$Momentum\ Thickness = \int \int \frac{(U_e - U_i)U_i}{U_e^2} dZdY. \quad \textbf{(3-6)}$$

To evaluate these integrals, the trapezoidal method was utilized. Performing the first integral in the pitchwise direction provides the spanwise variation in momentum thickness across the wake of each trailing edge. To obtain the overall momentum thickness, the average of the spanwise values was taken for each downstream location between 0.4 and 1.6 axial chords downstream.

The spanwise variation in momentum thickness is presented in **Figure 3.111** for each of the three trailing edge configurations. The horizontal axis on this graph presents the momentum thickness of each trailing edge, and the vertical axis shows the spanwise location as a percentage of λ for each configuration. All three of these trailing edge configurations show a periodic spanwise variation in momentum thickness across the span of the trailing edge. A minimum value of momentum thickness

can be seen surrounding the 50% λ location for each trailing edge configuration. The momentum thickness then increases from this minimum value where it reaches a maximum at the 0% and 100% λ locations. Although the TE-1 configuration shows significantly higher momentum thickness at the edge of the vorticity period, the minimum momentum thickness value at the 50% λ location is comparable to the values produced by TE-7 and TE-8.

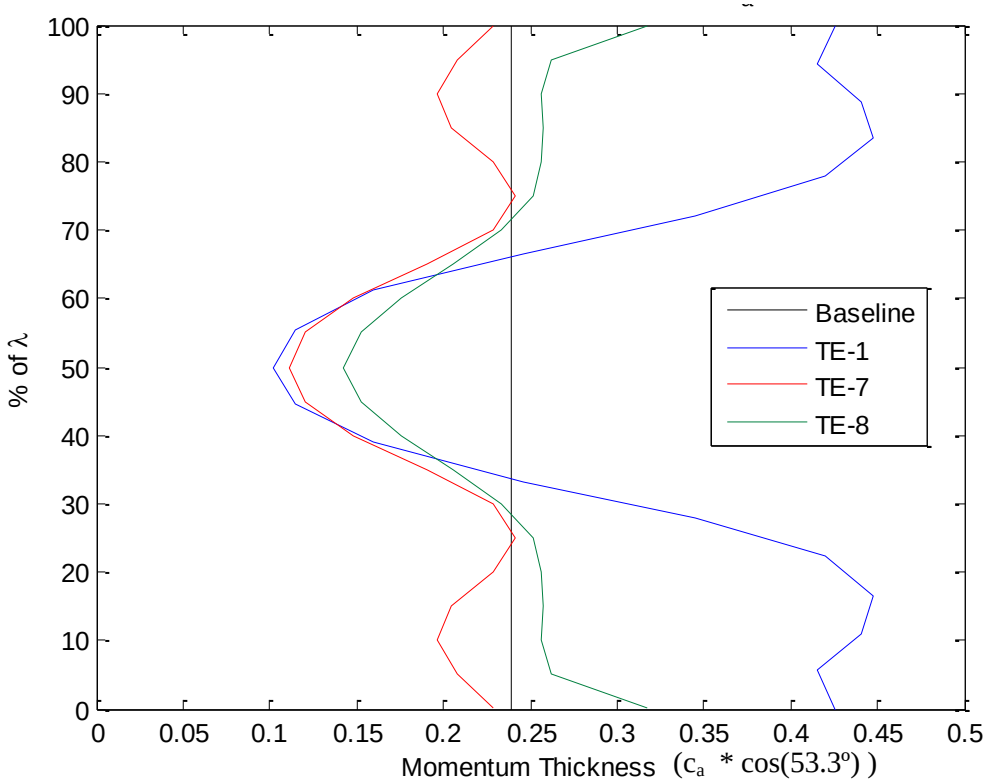

Figure 3.111 Spanwise variation of Momentum Thickness at 1.2 axial chords downstream

The momentum thickness of each trailing edge configuration was calculated at the four measured downstream stations (see **Figure 3.112** through **Figure 3.114**). To obtain a single value for the momentum thickness of each trailing edge configurations, the calculated values at each of these downstream stations was averaged. This average value of momentum thickness gives a value that is proportional to the drag produced by each configuration. The results of this analysis can be seen in **Table 3-4**. This data suggests that the TE-7 configuration produces the smallest value of momentum thickness of all configurations tested. Additionally, the TE-1 configuration shows values of momentum thickness that is over 50% higher than that observed for the TE-7 configuration. In contrast, the TE-8 configuration shows an average momentum thickness value that is only 13.3% higher than those seen with TE-7.

Table 3-4 Average Momentum Thickness Values for each Trailing Edge Configuration

Configuration	Average Momentum Thickness (c_a * cos(53.3º))	Difference from Baseline (%)
TE-1	0.3289	39
TE-7	0.2136	-9.72
TE-8	0.2419	2.2
Baseline	0.2366	--

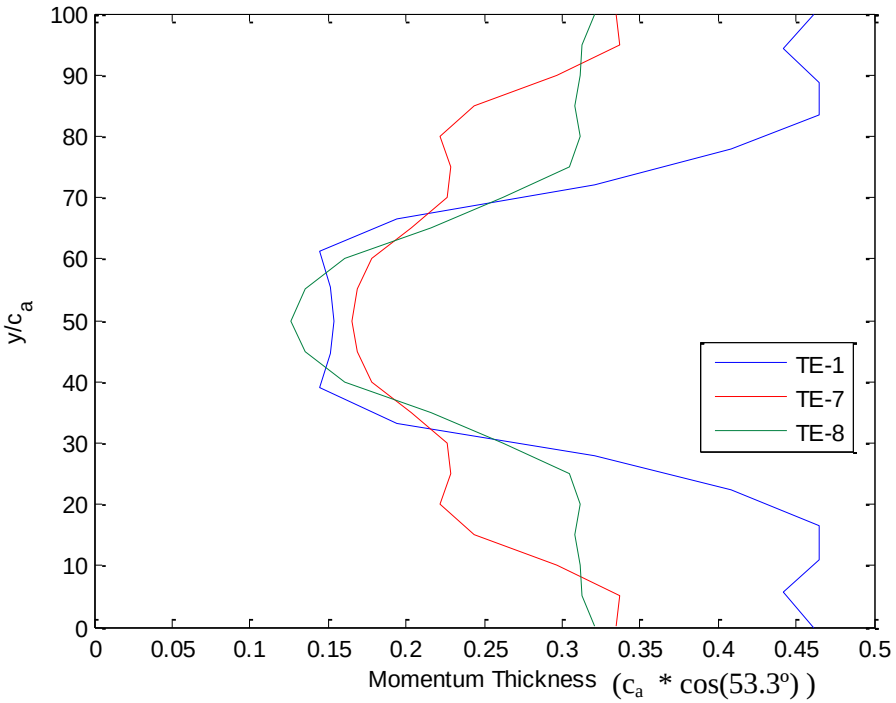

Figure 3.112 Momentum Thickness at 0.4 axial chords downstream

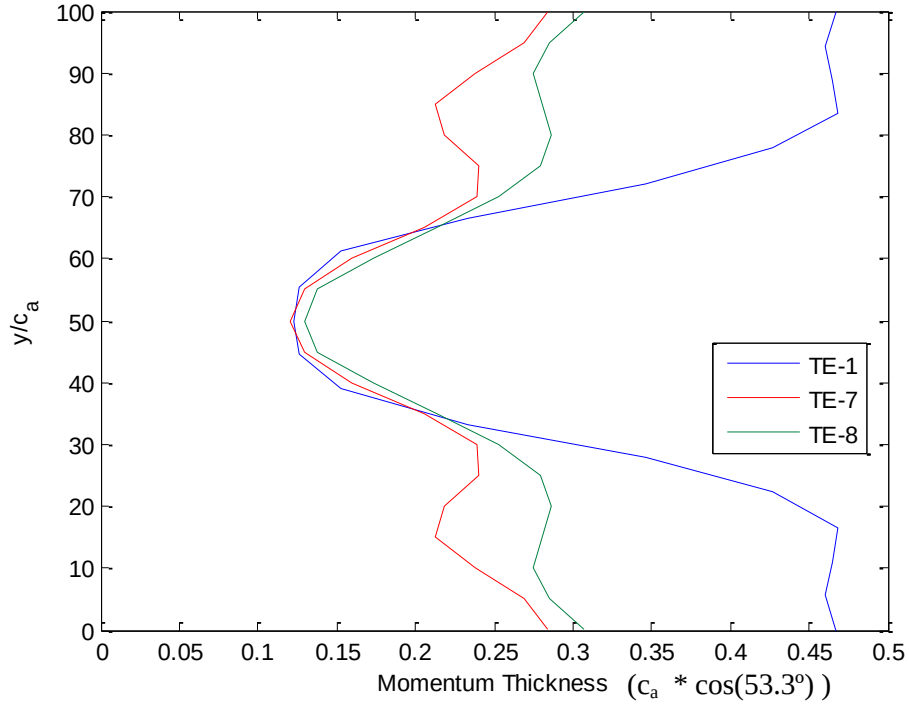

Figure 3.113 Momentum Thickness at 0.8 axial chords downstream

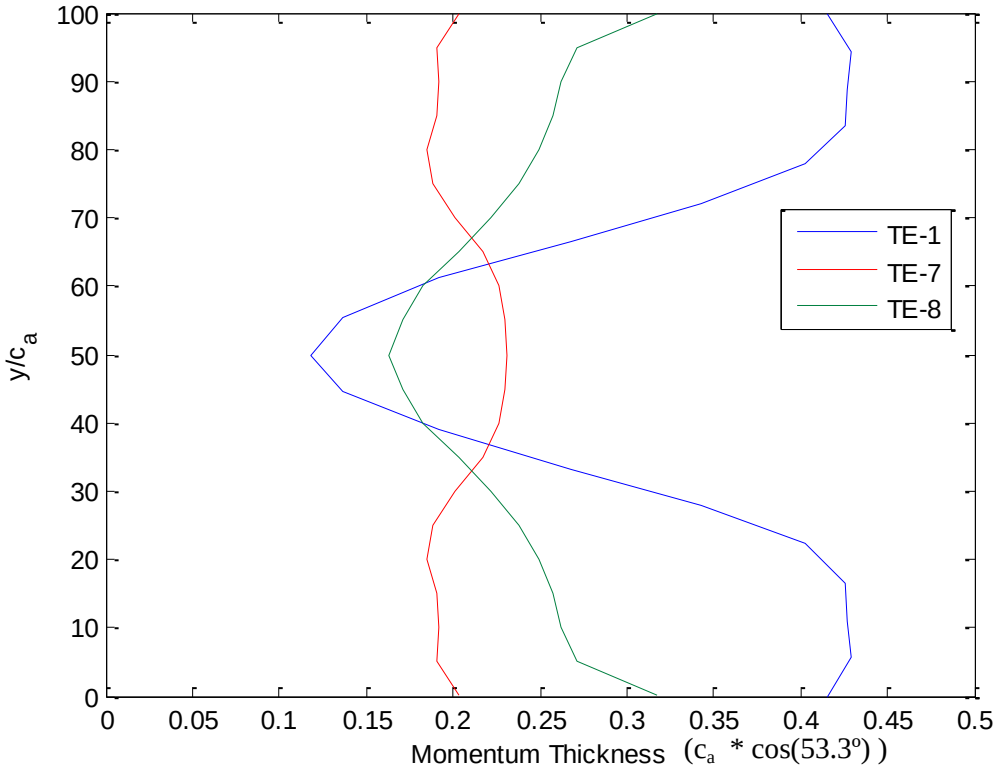

Figure 3.114 Momentum Thickness at 1.6 axial chords downstream

4 Conclusions

The flow downstream of cascade blades designed to simulate compressor blades were measured and analyzed for three trailing edge configurations. Each trailing edge configuration was developed using varying techniques to impart streamwise vorticity into the flow. The initial trailing edge configuration (TE-1) involved placement of small vortex generators periodically across the suction side of the blade at the 80% chord location. The remaining trailing edges considered were developed using a proprietary design, and were labeled TE-7 and TE-8. Pitot-static and four-sensor hotwire measurements were made behind the blades in their wakes inside the test section of a linear cascade wind tunnel. These measurements were then used to compare the performance of each of these trailing edge configurations, and their differences from the baseline blade trailing edge configuration.

All three of these trailing edge designs were effective at imparting streamwise vorticity into the downstream flow. At the closest downstream locations measured, the TE-8 configuration was the most effective at imparting streamwise vorticity. The TE-8 configuration showed peak vorticity levels nearly twice as high as those observed with the TE-1 configuration. Despite this initially higher intensity, the TE-8 configuration was unique in that it also showed the fastest rate of decay of streamwise vorticity levels measured.

As a result of the vorticity imparted on the flow, the streamwise velocity cross-sections of each of these trailing edge configurations show some unique characteristics. The introduction of vorticity effectively stretches the wake behind the trailing edge, giving it the effect of showing corrugation in the pitchwise direction. Additionally, the vorticity seems to impart lobes of higher velocity deficit adjacent to a center region of decreased streamwise velocity deficit.

Additionally, the vorticity produced by each of these trailing edge configurations was shown to be quite effective at broadening the wake profile which interacts with the downstream stator. The spanwise-averaged pitchwise velocity profiles showed that each trailing edge configuration produced a significantly larger half-wake width when compared to the baseline trailing edge. Thus, generation of streamwise vorticity is a very effective means to passively diffuse the wake downstream of an airfoil.

The analysis of the Turbulence Kinetic Energy for each trailing edge showed that introduction of streamwise vorticity can actually decrease the observed peak TKE levels compared to the baseline at certain locations across the period of vorticity injection. For the three trailing edges tested, the TE-8 configuration showed the greatest potential for decreasing the overall TKE levels observed at downstream locations. For this trailing edge configuration, the peak TKE levels were actually lower than the baseline across the entire span once the flow reached 1.6 axial chords downstream. Even at 1.2 axial chords downstream, the TE-8 configuration showed peak TKE levels that were below the baseline at the center period location, and were at a comparable level at the outermost regions of peak TKE.

The momentum thickness changes resulting from the trailing edge configurations tested suggest potential for drag reduction with properly designed vorticity generation. The standard surface mounted vortex generators utilized for TE-1 showed an increased momentum thickness when compared to the

baseline trailing edge configuration. Additionally, the TE-8 configuration showed a slightly increased momentum thickness value. However, the TE-7 configuration actually showed *decreased* momentum thickness when compared to the baseline trailing edge.

All of the modifications to the wake characteristics as a result of the trailing edge designs tested suggest the potential for tremendous acoustic and aerodynamic improvement resulting from proper application of streamwise vorticity. This flow characteristic can be utilized to not only broaden, but also decrease the depth of the velocity deficit profile behind the blade. Furthermore, the enhanced mixing that results from imparting streamwise vorticity can effectively reduce the levels of turbulence kinetic energy and fluctuations that are present downstream of the airfoil. Thus, streamwise vorticity when applied properly can be used as a simple effective means for decreasing rotor-stator interaction noise without causing any aerodynamic penalties.

References

Ashcroft and Schultz. "Numerical Modeling of Wake-Jet Interaction with Application to Active Noise Control in Turbomachinery". 2004

Borgoltz, Aurelien. "Modifications of Coherent Structures in Fan Blade Wakes for Broadband Noise Reduction". Virginia Tech PhD Dissertation. 2007.

Borgoltz and Devenport. "trailing Edge Flows of Serrated Blades". Technical Report to GE. 2007

Bourgoyne et al. "Time-averaged flow over a hydrofoil at high Reynolds number". 2003.

Brookfield. "Turbofan Rotor/Stator Interaction Noise Reduction through Trailing Edge Blowing". MIT Master's Thesis. 1998.

Craig, Margaret Elizabeth. "Trailing-Edge Blowing of Model Fan Blades for Wake Management". Virginia Tech Master's Thesis. 2006.

Doty et al. "Turbulent Flow Field Measurements of Separate Flow Round and Chevron Nozzles with Pylon Interaction Using Particle Image Velocimetry". 2004.

Geiger, Derek. "Comparative Analysis of Serrated Trailing Edge Designs on Idealized Aircraft Engine Fan Blades for Noise Reduction". Virginia Tech Master's Thesis. 2004.

Guidati et al. "Prediction and Reduction of Wind Turbine Noise, An Overview of Research Activities in Europe". 2000.

Halasz et al. "Fan Flow Control for Noise Reduction Part 1: Advanced Trailing Edge Blowing Concepts". 2005.

Henderson et al. "The Impact of Fluidic Chevrons on Jet Noise". 2005.

Howe, M.S. "Noise Produced by a Sawtooth Trailing Edge". 1990.

Langford et al. "Fan Flow Control for Noise Reduction Part 2: Investigation of Wake-Filling Techniques". 2005.

Langford et al. "Fan Flow Control for Noise Reduction Part 3: Rig Testing of Optimal Design". 2005.

Lilley. "THE PREDICTION OF AIRFRAME NOISE AND COMPARISON WITH EXPERIMENT". 2002.

Selby et al. "Effect of passive devices on low-speed wake flow for unswept and swept blunt trailing-edge airfoil models". 1990.

Sell. "Cascade testing to assess the effectiveness of mass addition/removal wake management strategies for reduction of rotor-stator interaction noise". MIT Masters Thesis. 1997.

Sutliff et al. “LOW-SPEED FAN NOISE REDUCTION WITH TRAILING EDGE BLOWING”. 2002

Sutliff. “BROADBAND NOISE REDUCTION of a LOW-SPEED FAN NOISE USING TRAILING EDGE BLOWING”. 2005.

Weygandt and Mehta. “Effects of Streamwise Vorticity Injection on a Plane Turbulent Wake”. 1995.

Winkler et al. “Airfoil Trailing-Edge Blowing: Broadband Noise Prediction from Large-Eddy Simulation”. 2009.

Wittmer et al. “A four-sensor hot-wire probe system for three-component velocity measurement”. Experiments in Fluids. 1998.

Yu and Yip. “Experimental investigation of two-stream mixing flows with streamwise and normal vorticity”. 1997.

Yu et al. “Velocity Measurements Downstream of a Lobed-Forced Mixer with Different Trailing-Edge Configurations”. 1995.